3. Source composition of Ultra Heavy Cosmic Rays with $Z \geqslant 65$ under a simple Leaky Box Propagation Model

The ability to reduce everything
to simple fundamental laws
does not imply
the ability to start from those laws
and reconstruct the Universe

PHILIP W. ANDERSON

3.1. Introduction

The building up of heavy elements from lighter ones is carried out in different stellar environenments in which different nuclear reactions are taken place. It will be helpful to trace the life of star from its burning phases until its death through intermediate stages, in order to describe the stellar environenments were nucleosynthesis takes place.

3.1.1. Stellar evolution

During their lifetimes, stars evolve in a way that can be related to their position on the Hertzprung-Russell Diagram (HRD) which consists on a graph of luminosity versus

temperature for all types of stars for which these magnitudes can be measured. There are four main evolutionary stages in the life of a star: **protostar**, **pre-main sequence**, **main sequence** and **post-main sequence**. Stellar evolution is concerned with the slow changes in a star's size, luminosity and surface temperature with time, and the relationship between these and its chemical composition.

The process by which stars form and begin to shine can be summarised as follows: interstellar clouds contract under gravity and gravitational potential energy is converted into thermal and radiative energy. Eventually the core of the cloud becomes hot enough allowing to begin nuclear fusion reactions. While the star is still in free-fall collapse it is called a protostar. From this stage until nuclear ignition it is called pre-main sequence star, internal pressure retards the collapse and it becomes hot enough to be faintly luminous. There are exceptions to the progression, however. If a protostar reaches a mass less than ~ 0.08 $M_\odot$ (where $M_\odot$ is the solar mass), then the gravitational contraction will be insufficient for nuclear reactions to start and, hence, the star will never reach the main sequence. Such an object is called a **brown dwarf** and is more like an enormous planet than a star. The only energy source for brown dwarfs is gravitational potential energy and in consequence they are cool and have low luminosities. Stellar models show that an object is classified as a planet if its mass is less than 0.002 $M_\odot$, thus,a brown dwarf mass will be between 0.002 $M_\odot$ and 0.08 $M_\odot$, and a star capable of hydrogen burning has an initial mass exceeding 0.08 $M_\odot$.

The path describing the progress of a star on the HRD is called its **evolutionary track**. A star in the pre-main sequence stage shrinks. The Kelvin-Helmholtz contraction causes that a star in the pre-main sequence stage to glow with a low surface temperature and luminosity, and, hence, an evolutionary track begins in the lower right-hand corner of he HRD (point A in figure 3.1). As the star continues to contract, its core temperature increases to the point where nuclear reactions start and supply the energy to make it shine. Hydrostatic equilibrium is now established, and the star begins its useful working life. It is now called a zero-age main sequence (ZAMS) star (point B on figure 3.1). At this point, it commences the longest stage in its career, burning hydrogen into helium over many million of years. This era is know as the main sequence phase. How long the star spends on the main sequence depends on its mass (the Sun has a main sequence lifetime of roughly 10^{10} years).

As the hydrogen in the core is used up, hydrostatic equilibrium causes the interior temperature to gradually increase as well as the density. This ensures that the rate of nuclear reactions in the core are maintained. The star contracts slightly, increasing its luminosity due to a greater flow of energy to its surface. On the HRD the evolutionary track moves along the main sequence until it reaches point C, where it starts to veer over to the right and the star is now ready to enter the next stage of its evolution, called post-main sequence.

While on the main sequence, a star uses up less than 10% of its hydrogen reserves

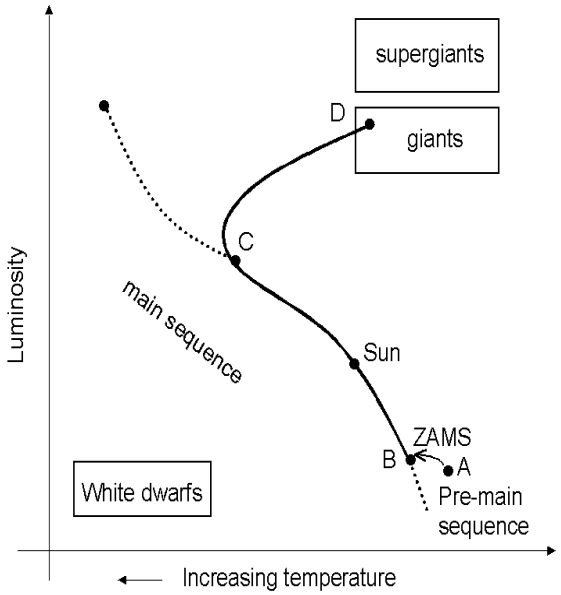

Figure 3.1. Evolutionary track on the Hertzprung-Russell Diagram

and so does not appreciably change its mass. However, in its core, where the nuclear reactions take place, the composition changes as hydrogen is converted into helium, forcing the star to radically alter its structure and appearance.

When all the hydrogen in the core is exhausted, the thermonuclear reactions stop and gravity compress the core to a smaller size. However, surrounding the core, which is now mainly helium, there is a shell of hydrogen which is heated by the gravitational contraction, so hydrogen burning continues in the shell. This fact produces an outward pressure which prevents the star from collapsing and makes it to expand to several hundred times its former size. It has now become a **red giant** with a lower surface temperature and higher temperature (point D in figure 3.1, also called red giant branch or RGB). A few stars are both more luminous and larger than typical red giants and are called **supergiants**.

At this point, the evolution of the central regions of a star is made of successive "controlled" thermonuclear burning stages and of phases of gravitational contraction as schematically illustrated in figure 3.2. In this figure, a schematic representation of the evolution of the internal structure of a spherically-symmetric massive star ($M \approx 25$ M$_\odot$) is illustrated. The shaded zones correspond to nuclear burning phases. A given burning phase starts in the central regions (the central temperatures T_c and densities ρ_c are indicated at the bottom of the figure). In between the central nuclear burning phases, episodes of gravitational contraction occurs (downward arrows). The chemical symbols in the figure represent the most abundant nuclear species left after each nuclear-burning mode ("Fe"

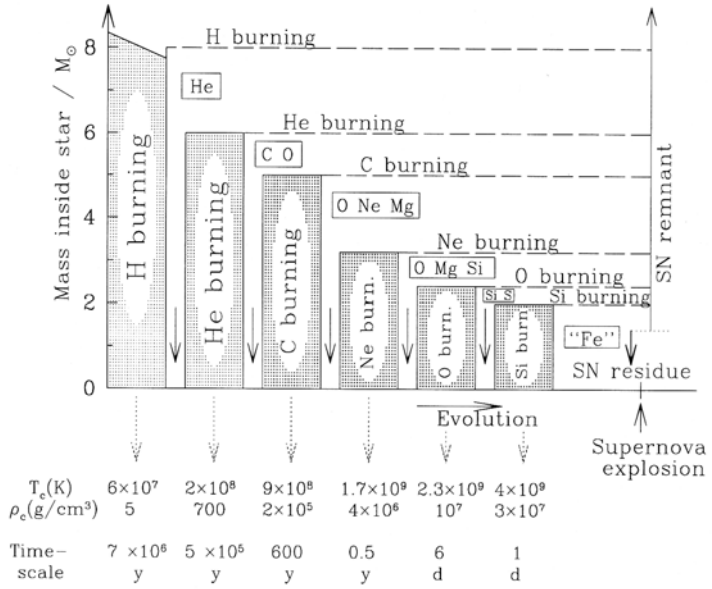

Figure 3.2. Schematic representation of the evolution of the internal structure of a spherically.symmetric massive ($M \approx 25\ M_\odot$) star. The shaded zones correspond to nuclear burning stages [Arn99].

symbolises the iron peak nuclei with $50 \lesssim A \lesssim 60$). The latter phases are responsible for a temperature increase, while the former ones produce nuclear energy through charged-particles induced reactions. Of course, composition changes also result from these very same reactions, as well as, at some stages at least, from neutron-induced reactions, which in contrast do not play any significant role in the stellar energy budget. The successive nuclear-burning stages are developed in time with nuclear fuels of increasing charge number and at temperatures increasing from several tens of 10^6 K to about $4{\cdot}10^9$ K. In addition, the duration of each burning phase decreases in a dramatic way. This situation results from the combination of a decreasing energy production when going from H burning to the later burning stages and an increasing neutrino production, and the consequent energy losses, with temperatures exceeding $\sim 5{\cdot}10^8$ K. Figure 3.2 also depicts schematically that a nuclear burning phase, once completed in the core of the star, migrates into a thin peripheral shell. As a consequence the deep stellar regions look like an onion with various "skins" of different compositions.

It is quite important to notice that all stars do not necessarily experience all the burning phases displayed in figure 3.2: while massive stars ($M \gtrsim 10\ M_\odot$) go through all those burning episodes, low and intermediate-mass stars ($M \lesssim 8\ M_\odot$) end their nuclear history without proceeding through the carbon and heavier elements burning phases. Stars in the $8\ M_\odot \lesssim M \lesssim 10\ M_\odot$ range represent complicated intermediate cases.

Although is only a brief phase compared to the overall stellar lifetime, most stars will pass through the **Asymptotic Giant Branch** (AGB) phase. The AGB phase is the last phase of evolution for low and intermediate mass stars with 1 $M_\odot \lesssim M \lesssim 8$ $M_\odot$. The ascent of the RGB in the HRD is terminated by ignition of the central helium supply. The subsequent evolution is characterised by helium burning in a convective core and a steadily advancing hydrogen burning shell. Eventually, the helium supply is totally consumed, leaving a core of carbon and oxygen (the exact proportions of which depend on the infamously uncertain rate for the $^{12}C(\alpha,\gamma)^{16}O$ reaction). In any event, following the exhaustion of central helium the star begins to ascent the giant branch again. It is now called the "second" or "asymptotic" giant branch, because of the way the evolutionary tracks seem to approach the (first) giant branch asymptotically.

There are only three possible destinies of stellar evolution: white dwarfs, neutron stars and back holes.

After helium burning is complete, in a low mass star with $M \lesssim 4$ $M_\odot$, the temperature in the core is not high enough for starting the fusion of carbon and oxygen which are the helium burning's ashes, the star's temperature drops and its luminosity decreases. As a result a **white dwarf** is formed in which high density of matter $10^8 - 10^9$ kg/m^3 is achieved. On the HRD, the evolutionary track of a low mass star crosses over the main sequence and then turns sharply downwards towards the white dwarf region (see figure 3.1).

On the other hand, the death of stars with mass $M \gtrsim 4$ $M_\odot$ is carried on by means of a different way. After heaving experienced all the burning phases depicted in figure 3.2, these stars develop an Fe core which cannot be used as nuclear fuel for further burning stages due to any transformation of the strongly-bound Fe nuclei is endothermic. Actually, this core becomes dynamically unstable and implodes as a result of free-electron captures and Fe photodisintegration. Through a very complex chain of physical events the implosion can turn into catastrophic supernova explosion known as **Type-II supernova** (SNII). In this sequence of events, neutrino production and diffusion through the SN core material play a key role. These processes crucially help the generation and powering of a shock wave propagating outward through most of the SN layers. This shock wave compress the various traversed layers, heats them up before pushing the outward until their injection into the interstellar medium (ISM). In this SN scenario not the whole of the stellar mass is returned to the ISM, thus, leaving a "legacy" which reminds the tragedy of the just death star. As a result, the inner parts survive to the SN explosion as a castaway in the cosmic ocean, which may be a **neutron star** (observable as a pulsar if it is magnetized and rapidly rotated) or even a **black hole**, depending on the main sequence mass star value.

3.1.2. Nucleosynthesis

The natural abundances of the elements heavier than carbon shown in figure 3.3 are thought to have their origins in the various phases of stellar nucleosynthesis, either under hydrostatic as well as under explosive conditions. During these phases, nuclei up

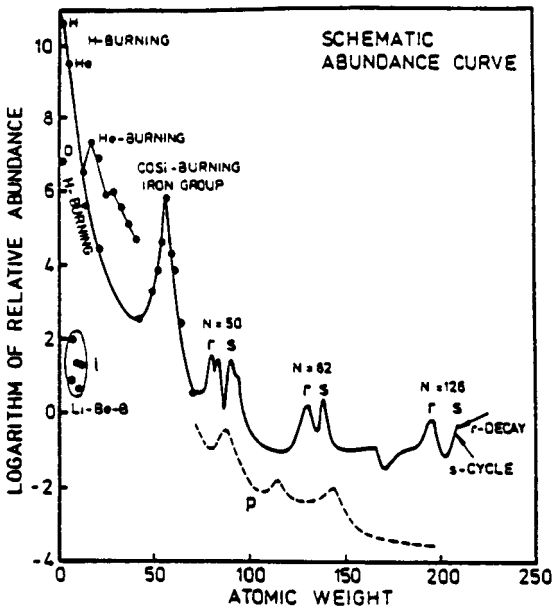

Figure 3.3. Schematic curve of the cosmic abundances of the nuclides. The various nucleosynthetic processes are also indicated. The peaks at the abundances of nuclei with "magic" neutron numbers are clearly seen [Pra89a]

to iron peak are produced from lighter ones by charged particle reactions, as originally proposed by Hoyle in 1946. Nuclei heavier than the iron peak (A $>$ 60) which are known as heavy nuclei, cannot be significantly produced by charged particle reactions due to the high temperatures required to overcome the high Coulomb barriers ($T \gtrsim 5 \cdot 10^9$ K), photodisintegration reactions become dominant, favouring, hence, the formation of iron peak nuclei.

Nature, however, has found another mechanism: neutron captures on seed nuclei are though to be responsible for the formation of the bulk of the heavier elements as neutrons are not bound by Coulomb barriers allowing to transport through stellar interiors. The idea for stellar neutron capture nucleosynthesis were proposed in the monumental paper of E.M. Burbridge, G.R: Burbridge, W.A. Fowler and F. Hoyle in 1957 (frequently named B^2FH in the nuclear astrophysics literature) as well as the paper of G.W. Cameron, also in 1957 [Cam57]. In those pioneering works it was recognized for the first time that the peaks in the abundances of the heavy isotopes can be naturally explained by the nuclear physics aspects of the neutron capture processes, thus, the enhanced stability of nuclei with "magic" neutron numbers ($N = 50, 82, 126$) can explain their high natural abundances (it should be reminded that a nuclei with magic neutron number in nuclear physics, conceptually, plays the same role as a noble gas in atomic physics; both present a complete nuclear or atomic shell, respectively).

Since these pioneering works [B^2FH] & [Cam57], nucleosynthesis studies are being worried in clarifying (*i*) the abundances of the nuclides in the solar system, (*ii*) which deviations from them in other stars, gas and galaxies are real and are to be attributed to nuclear processes, (*iii*) which are the dominant nuclear reactions and their cross sections, and (*iv*) the sites where it occurs. Intermediate progress reports on general aspects of nucleosynthesis can be found in several works: [Tru73], [Tri75], [Tri91], [Thi98], [Arn99] and [Thi01].

Primordial nucleosynthesis

The question of the origin of light elements, which include H, He, Li, Be and B (and their isotopes), occupies a very special place in the theory of nucleosynthesis. The inability of stars to produce the required amounts of light nuclei by thermonuclear reactions results from the "fragility" of those elements in stellar interiors. More specifically, their lifetimes against destruction by proton induced reactions are much shorter than the typical stellar evolutionary lifetimes at the temperatures and densities prevailing in most stellar locations. In such conditions and generally speaking, stars appear to be efficient destructors, rather than producers of light nuclei (mainly D, Li, Be, B). The situation concerning He is different as He is, after H, the most abundant nuclide in the visible Universe in general, and in the Solar System in particular. In fact is it well known that ^{4}He is produced abundantly by Hydrogen burning stages in stars but detailed calculations indicate that the stellar ^{4}He yields returned to the interstellar medium cannot account for the observed ^{4}He abundances.

In view of the difficulties encountered when trying to explain the bulk galactic and Solar-system light nuclei abundances in terms of stellar thermonuclear reactions, various other models have been developed, like the production by non-thermal reactions, that consist on the fragmentation of the cosmic radiation heavier elements when interacting with the interstellar medium, integrated over the history of the galaxy or thermonuclear production during Big Bang explosion. Big Bang nucleosynthesis, also known as primordial nucleosynthesis, was firstly suggested in the famous paper of R.A. Alpher, H. Bethe and G. Gamow in 1948 (strategically named as $\alpha\beta\gamma$) in which was recognized the significance that a hot Big Bang model of the Universe should have for the origin of the elements. The first numerical calculation of the relic abundances of light elements in a hot big bang universe were performed in the decade of sixties [Pee66], [Wag67]. After these former works, several attempts have been made in order to justify the observed abundances of light elements applying hot Big Bang nucleosynthesis models as described in [Mat93a] and [Pag00] for the case of ^{4}He, and [Pra93], [Van00] and [Hob00] for the Li, Be, and B elements, and also in some general reports [Wag73], [Sch77], [Boe85], [Esm91] and [Oli00].

Non-explosive stellar nucleosynthesis

The main hydrostatic burning stages with the concomitant reactions that occur in a massive star, can be summarised as:

Hydrogen burning: there are two sequences of reactions, the three pp-chains which convert ^{1}H into ^{4}He, and the CNO cycle which converts ^{1}H into ^{4}He by a sequence of (p,γ), β^{+}-decays and (p,α) reactions on C, N and O isotopes and subsequent beta decays.

Helium burning: the main reactions in this stellar stage are the triple-alpha reaction $^{4}\mathrm{He}(2\alpha,\gamma)^{12}\mathrm{C}$ and $^{12}\mathrm{C}(\alpha,\gamma)^{16}\mathrm{O}$ which has a very special importance for the theories of stellar evolution and nucleosynthesis [Wos88], [Thi90].and [Wea93]

Carbon burning: the main reaction are $^{12}\mathrm{C}(^{12}\mathrm{C},\alpha)^{20}\mathrm{Ne}$ and $^{12}\mathrm{C}(^{12}\mathrm{C},p)^{23}\mathrm{Na}$. Most of the ^{23}Na nuclei will react with the free protons via $^{23}\mathrm{Na}(p,\alpha)^{20}\mathrm{Ne}$.

Neon burning: This phase is initiated by the reaction $^{20}\mathrm{Ne}(\gamma,\alpha)^{16}\mathrm{O}$, the first major energetically significant photodisintegration reaction experienced by the star. The other two main reactions are $^{20}\mathrm{Ne}(\alpha,\gamma)^{24}\mathrm{Mg}$ and ,$^{24}\mathrm{Mg}(\alpha,\gamma)^{28}\mathrm{Si}$.

Oxygen burning: The main product during this burning stage is ^{28}Si by means of the nuclear reaction $^{16}\mathrm{O}(^{16}\mathrm{O},\alpha)^{28}\mathrm{Si}$. On the other hand, the production of ^{28}Si can be carried on by another channel: $^{16}\mathrm{O}(^{16}\mathrm{O},p)^{31}\mathrm{P}$ and $^{16}\mathrm{O}(^{16}\mathrm{O},n)^{31}\mathrm{S}(\beta^{+})^{31}\mathrm{P}$, most of ^{31}P is destroyed by a (p,α) reaction to ^{28}Si.

Silicon burning: Si burning is initiated like Ne burning by photodisintegration reactions which the provide the particles for capture reactions. It ends in an equilibrium abundance distribution around Fe.

s-process: This is a neutron capture process, responsible of the formation of neutron rich nuclei heavier than Fe [B^{2}FH], [Cam57], [See65], [All71], [Mat85], [Mat93b] & [Arn99], which takes place under non-explosive conditions.

The s-process

The slow neutron capture process (see [Kap89] for a general review) relies on the assumption that pre-existing nuclei, which are known as "seed" nuclei, are exposed to a flux of neutrons that is weak enough for allowing a β-unstable nuclei produced by a (n,γ) reaction to decay promptly, except perhaps for very long lived isotopes which may instead capture a neutron. Consequently, the s-process path in the Z-N plane is developed in the close vicinity of the line of β-stability. This definition does not make any reference to the origin of the required neutrons or to a specific astrophysical site. Nevertheless, the competition between neutron captures processes (whose rates depend on temperature and neutron density) and β-decays (which are mainly temperature dependant) is incorporated in semi-empirical analyses of s-process abundances in order to impose some constraints, particularly on neutron density and temperature for the s-process.

Two different neutron sources with its corresponding stellar scenarios are required in order to reproduce the solar system abundances of those nuclei synthesised by an s-

process [Pra89a], [Kap89], [Tra99]. Ultra heavy s-nuclei, below the Sr peak which is called the *weak component* ($A \leqslant 90$), are formed in central regions of massive stars ($M \gtrsim 8$ $M_\odot$) near the end of the core helium burning with $^{22}Ne(\alpha, n)^{25}Mg$ as the main neutron source [Cou74], [Lam77], [Arn85], [Bus85], [Pra87], [Lan89], [Rai92], [Bar92], [Thi98] & [Tra99]. A different site for the production of s-nuclei, from Sr to Pb which are known as the *main component* ($A \geqslant 90$) are synthesised in thermally pulsing shells of hydrogen and helium burning during the AGB phase of low and intermediate mass stars with $^{13}C(\alpha, n)^{16}O$ as the dominant neutron source. Thermal pulses and their associated dredge-up allow the contact between the hydrogen rich envelope and the carbon rich intershell zone. Then, as the star contracts, proton captures on ^{12}C are allowed and, thus, ^{13}C is produced. During the interpulse phase this reaction is followed by $^{13}C(\alpha, n)^{16}O$ which releases enough available neutrons to initiate the s-process on Fe seed nuclei [Ibe82a], [Ibe82b], [Hol88], [Hol89], [Gal93], [Mow97], [Lat98], [Arl99], [The00], [Bus01], [Abi02] & [Lug03].

Explosive stellar nucleosynthesis

Many of the hydrostatic burning process discussed above can also occur also under explosive conditions at much higher temperature and on shorter timescales. The bulk reactions remain still the same in many cases, but often the β-decay half-lives of unstable products are longer than the timescales of the explosive processes. Due to the very short timescale of explosive processing (from a fraction of a second up to several seconds), only few β-decays can take place during explosive nucleosynthesis events, resulting in heavier nuclei [Tri91], [Arn95], [Thi98] & [Arn00]. Explosive burning stages produces intermediate to heavy nuclei, depending on the temperature of the nucleosynthesis sites. The feature which distinguishes these explosive processes is the peak temperature achieved rather than the available fuel.

Explosive hydrogen burning: The burning is described by proton captures and β^+-decays on unstable proton rich nuclei, usually referred as the rp-process (rapid proton capture process) [Rem97], [Thi98] & [Thi01]. In addition alpha induced reactions, which are known as αp-process, can provide synthesised nuclei which are taken as seed nuclei by the rp-process [Arn99]. As in the hydrostatic version of this burning stage, two "hot" burning modes are involved: the hot p-p mode, and the hot CNO and NeNa-MgAl chains. For instance, the cold (hydrostatic) CNO cycle, in which the β-decay of ^{13}N occurs, switches to the hot CNO mode (also named HCNO) when $^{13}N(p,\gamma)^{14}N$ becomes faster than the ^{13}N β-decay (see [Cha92] for detailed description of such cycle).There are several astrophysical environments suggested where the rp-process can take place, but the most prominent ones are novae [Her01a] and X.ray burst [Thi01], [Her01b].

Explosive helium burning: The explosive combustion of He is characterised by the same reactions as its hydrostatic version, producing ^{12}C and ^{16}O. Neutron sources for the s-process in hydrostatic burning stages like $^{22}Ne(\alpha, n)^{25}Mg$ or $^{13}C(\alpha, n)^{16}O$ release a large neutron flux under explosive conditions, for instance, during the passage of a supernova

shockfront through the He-burning zones of a massive star, although for such astrophysical condition the amount of He burned would be negligible due to the temperature achieved is not high enough [Thi98].

Explosive carbon and neon burning: When temperatures which allow the hot C-burning, are achieved ($T_9 \sim 2$), the explosive Ne-burning is also activated. Both processes supply many nuclei in the mass range $20 < A < 30$ in solar proportions. Photodisintegration reactions of pre-existing more neutron-rich nuclei with a combination of radiative proton capture processes can produce proton rich stable isotopes, which are so-called p-nuclei (see discussion of the proton capture process or p-process in [Woo78], [Pra89b], [How91], [How93], [Ray93] & [Ray95]).

Explosive oxygen burning: At slightly higher temperatures ($T_9 \sim 3.3$) the hot O-burning will reproduce the main products in the mass range $28 < A < 45$ [Tru70]. In other zones with temperatures close to $T_9 \sim 4.0$, there exists some contamination by several Fe-group nuclei [Thi98].

Explosive silicon burning: For temperatures exceeding $T_9 \gtrsim 4.0 - 5.0$ essentially all Coulomb barriers can be overcome and a nuclear statistical equilibrium is established, leading to a complete Si-exhaustion, and Fe-group nuclei are produced.

r-process: Together with the s-process, this is the other neutron capture process responsible for the formation of neutron rich nuclei heavier than Fe which occurs under explosive conditions [B^{2}FH], [Cam57], [See65], [All71], [Mat85], [Mat93b] & [Arn99].

The r-process

In contrast to the s-process, the "rapid" neutron capture process, called r-process, is based on the assumption that the neutron flux is high enough to allow that neutron captures be always faster than β-decays. The seed nuclei are converted by successive neutron captures into very neutron rich nuclei until the inverse (γ, n) reactions take place efficiently, due to the low neutron separation energies (S_n), and thus, impede further progression.

In the simplest picture of the r-process, an $(n, \gamma) \rightleftharpoons (\gamma, n)$ equilibrium is reached in each isotopic chain starting at iron ($Z = 26$) seed nuclei. In such conditions, the isotopic abundance distribution for a given charge Z is independent of the (n, γ) and (γ, n) cross sections, depending mainly on S_n, temperature and neutron density. Once distributed in such way, the isotopes then "wait" for β-decay to occur (this is known as the *waiting point approximation*). Beta decays, thus, governs the speed of the nuclear flow (the r-process path in the $N - Z$ plane). If the r-process path reaches the trans-actinide region, neutron induced (or β-delayed) fissions could interrupt the flow to higher Z values and could be responsible for a cycling-back of the material to lower mass nuclei.

Some simple models for the nuclear physics of the r-process assume that the neutron flux and the temperature go abruptly to zero after a neutron irradiation exposure in opposition to the classical models in which these magnitudes are taken as constant [Fre99]. As a result, the very neutron rich unstable nuclides on the r-process path start to cascade

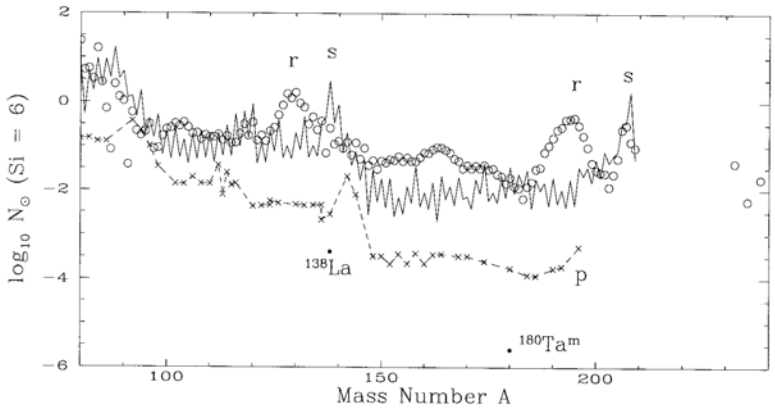

Figure 3.4. Decomposition of the solar abundances of heavy nuclides into an s-process (*solid line*), an r-process (*open circles*) and a p-process (*crosses*) contributions [Arn99].

through β-decays back to the line of stability in the (N, Z) plane. This cascade may be complicated by β-delayed fission or neutron emissions.

The fundamental r-process theory of [B^{2}FH] & [Cam57] successfully explains the gross features of the solar r-process abundance distribution, such as the existence of abundance peaks at $A \sim 80, 130$ and 195. A quantitative modelling of the s and r-process allows to study the contribution of each process to the solar system composition. Figure 3.4 shows the solar abundance curve, beyond the Fe peak region, splitted into an s- and r- component, the contribution of the p-process is also included [Kap89], [Tak95].

The study of astrophysical sites for the r-process still remains as an open question despite the fact that many possibilities have been suggested since the classical works by [B^{2}FH], [Cam57] & [See65]. In all such r-process sites, an excess of neutrons over protons is required in order to ensure a large neutron-to-seed nucleus abundance ratio (10-150 n/seed-nucleus, [Thi01]), nevertheless, high ratio values can also be achieved without assuming neutron rich environments [Mey02].

The conditions required for the r-process have been examined in terms of the electron fraction, the entropy per baryon, and the dynamic timescale for adiabatic expansion from high temperature and density. This parametrization of the astrophysical environment treats the determination of the neutron-to-seed ratio, the r-process, and the freeze-out in a smooth sequence and is more realistic than the traditional parametrization using a set of neutron number density, temperature, and neutron irradiation time [Qia03].

The quest for possible astrophysical scenarios of the r-process is a question not yet solved. The classical works pointed out to explosive models related to type II supernovae as the most realistic site for the r-process (see [Cow91], [Wal97] & [Arn99] for a more up-to-date review). Nevertheless, in the latest decade a great progress has been realised and, in consequence, many new models have been proposed as promising r-process sites

[Thi98], [Thi01] & [Qia03]. The bulk of these models can be classified into core collapse supernovae models [Sne96], [Hil02] & [Cow02] and neutron stars merger models [Sch82], [Mey89], [Ruf97], [Fre99] & [Sum98].

Core collapse supernova models can be divided into three categories: (*i*) Neutrino wind models in which the free nucleons accelerated by the intense neutrino flux near the neutrino sphere of a core collapse supernova assemble to heavier nuclei [Woo94], [Ots00] & [Wan01]. (*ii*) An alternative explosion mechanism is the prompt mechanism in which the bounce of the inner core upon reaching nuclear density launches an energetic shock which then drive a successful explosion [Bet90]. This mechanism might work for the collapse of a O-Ne-Mg cores of 8-10 $M_{\odot}$ stars [Whe98] & [Wan03] and maybe some low-mass Fe cores [Sum01]. (*iii*) Another supernova mechanism relies on the formation of magnetohydrodynamic jets following the core collapse [Leb70], [Kho99] & [Cam01]. Although this scenario was suggested some time ago, a new scenario has been proposed in which jets are associated to the formation of an accretion disk around a protoneutron star [Cam01].

On the other hand, neutron star merger models are splitted into two versions: Two neutron stars mergers [Phi91], [Arz99] & [Bel02], and neutron star-Black hole mergers [Lat74] & [Lat76].

In addition, recent spectroscopic studies of extremely metal-poor stars in the Galactic halo indicate that the observed abundances patterns of the lighter (Z<56) and heavier (Z>56) neutron-capture elements cannot be explained by a single astrophysical site, there must exist at least two different r-process sites [Cow99], [Qia00] [Ish00], [Qia01], [Thi01], [Joh02] & [Sne03].

3.2. The propagation of Cosmic Rays

Once the Cosmic Rays are synthesised in their sources and are ejected to the interstellar medium, they move through interstellar space varying their intensity, chemical composition and energy spectrum when compared with the corresponding characteristics in the sources. This changes are caused by the interaction with the interstellar gas and with the magnetic fields encountered by the cosmic rays during their travel into the propagation region. In order to connect these properties of cosmic rays measured near the Earth and their properties in the source, a transfer equation has to be formulated which also allows quantitative analysis.

3.2.1. General transfer equation for Cosmic Rays

The general equation for the concentration, $N_i(E, \overrightarrow{r}, t)$, which describes the transport of particles of kind i, is deduced from the continuity equation in the phase space allowing for collisions. This equation includes several effects on the traveling particles such as spatial diffusion, energy losses, re-acceleration and transformation of the chemical composition in the interstellar medium (ISM). The general transfer equation can be written in

the form [Gin64]:

$$\frac{\partial N_i}{\partial t} - \overrightarrow{\nabla} \cdot (D_i \overrightarrow{\nabla} N_i) + \frac{\partial}{\partial E}(b_i N_i) - \frac{1}{2}\frac{\partial^2}{\partial E^2}(d_i N_i) = \tag{3.1}$$

$$= q_i(E, \overrightarrow{r}, t) - P_i N_i + \sum_{j \neq i} \int P_i^j(E', E) N_j(E', \overrightarrow{r}, t) dE'$$

Let us detail the meaning of each term in the above equation:

- $\frac{\partial N_i}{\partial t}$ shows the variation in time of the concentration of particles of type i.
- $\overrightarrow{\nabla} \cdot (D_i \overrightarrow{\nabla} N_i)$ describes the spatial diffusion of particles with a diffusion coefficient $D_i = D_i(E, \overrightarrow{r}, t)$ which in the general case depends on the type of particle, energy, position and time. In the case of considering systematic motion of the medium, *i.e.* expansion or compression, an extra term $\overrightarrow{\nabla}(N_i \overrightarrow{u})$, where $\overrightarrow{u}$ is the velocity of the systematic large-scale motion, has to be added to the left hand side of equation 3.1.
- $\frac{\partial}{\partial E}(b_i N_i)$ characterises the systematic energy variation due to the action of the energy gain mechanisms (re-acceleration) and energy loss mechanisms (collisions, ionisation). In this case, the coefficient $b_i = b_i(E)$ is the mean energy increment of the particle per unit of time: $b_i = \frac{dE}{dt}$.
- $\frac{1}{2}\frac{\partial^2}{\partial E^2}(d_i N_i)$ includes the fluctuations in the continuous variation in energy described in previous term. In the general case, the coefficient $d_i = d_i(E)$ is equal to the mean square of the energy increment per unit of time:

$$d_i(E) = \frac{d}{dt}(\overline{\triangle E})^2$$

- $q_i(E, \overrightarrow{r}, t)$ corresponds to the intensity of the cosmic ray sources. $q_i(E, \overrightarrow{r}, t) dE \cdot d\overrightarrow{r} \cdot dt$ is the number of particles of type i supplied by the sources during the time dt in an element of volume $d\overrightarrow{r} = dxdydz$ in the energy range $(E, E + dE)$.
- $P_i N_i$ allows for "catastrophic" energy losses and also the appearance of new particles when the considered particles of type i interact with the ISM. In this context, "catastrophic" means that the particles as such, disappears. Spallation of nuclei by means of collisions with ISM particles is an example of such processes. In this case P_i is the probability per unit of time of such a process for particles of type i and $P_i N_i$ is the number of disappeared particles.

$$P_i = \frac{1}{\tau_i} = n v \sigma_i$$

where τ_i is the mean life with respect of the corresponding "catastrophic" process, σ_i is the associated effective cross section, n i the particle concentration of the medium and v is the speed of the particles.

- $\sum_{j \neq i} \int P_i^j(E', E) N_j(E', \overrightarrow{r}, t) dE'$ describes the influx of particles as a result of catastrophic processes. $P_i^j(E', E)$ is the probability per unit of time and unit of energy of catastrophic process of a particle of type j with an energy E' yielding a particle of type i having energy E.

Equation 3.1 is applicable to the description of the behaviour of cosmic rays not only in the Galaxy but also in the supernova shells, radio galaxies, intergalactic space and so on. It will be only necessary to parametrise, in the transfer equation, the associated conditions and parameters of the considered situation.

To find a solution of equation 3.1 becomes an extremely difficult task due to its general character, and consequently several simplifying hypothesis have to be assumed. Different propagation models are generated depending on the simplifications considered.

The time and position dependence of the diffusion coefficient, D_i, as well as the remaining coefficients in equation 3.1 may be caused by the change in the structure and scales of the magnetic field inhomogeneities and also by a change in the concentration and composition o of the interstellar gas in different parts of the propagation region and during its evolution. However, position-dependence can be ignored due to the homogeneity of the propagation volume under such changes. Time-dependence can also be neglected because of the life of the cosmic rays in the propagation volume is far less than its age.

More simplifications concerning to energy as a variable can also be made. In the "laboratory" reference frame associated to the propagation region, the fragmented particles move at the same velocity as the original relativistic ones. Therefore, the energy per nucleon $\varepsilon \equiv \frac{E}{A}$ (where A is the mass number of the nucleus) is identical for both, i.e. the original and the formed nucleus which follow an spallation process. Consequently,

$$P_i^j(\varepsilon', \varepsilon) = p_i^j \delta(\varepsilon' - \varepsilon)$$

and hence, equation 3.1 can be rewritten as:

$$\frac{\partial N_i}{\partial t} - \overrightarrow{\nabla} \cdot (D_i \overrightarrow{\nabla} N_i) + \frac{\partial}{\partial \varepsilon}(b_i N_i) - \frac{1}{2}\frac{\partial^2}{\partial \varepsilon^2}(d_i N_i) = q_i(\varepsilon, \overrightarrow{r}, t) - P_i N_i + \sum_{j<i} p_i^j N_j \qquad (3.2)$$

where $i = 1$ corresponds to the heaviest nuclei considered. So, $j < i$ means that it has been assumed that nuclei of a given type i, only can be formed from heavier nuclei of kind j.

Next simplification assumes that the particles are not accelerated in the ISM during the propagation travel, so that, the forth term in left hand of equation 3.2 has to be neglected, and consequently, the b_i coefficient only accounts for energy losses (in particular,

ionisation energy loss). Two different kinds of "catastrophic" processes are taken into account: radioactive decay processes and fragmentation processes. As a result, each of the two terms describing such catastrophic processes (i.e. second and third terms in right hand of equation 3.2) are splitted into two new terms. So, equation 3.2 is converted to:

$$\frac{\partial N_i}{\partial t} - \overrightarrow{\nabla} \cdot (D_i \overrightarrow{\nabla} N_i) + \frac{\partial}{\partial \varepsilon}(b_i N_i) + nv\sigma_i N_i + \frac{1}{\tau_i} N_i = q_i(\varepsilon, \overrightarrow{r}, t) + \sum_{j<i} nv\sigma_{ij} N_j + \sum_{j<i} \frac{1}{\tau_{ij}} N_j \quad (3.3)$$

where n is the concentration of interstellar gas, v is the velocity of the propagating particles, $\sigma_i = \sigma_i(\varepsilon)$ is the total interaction cross section of a nucleus of type i colliding with particles of the interstellar gas. σ_{ij} is the partial inelastic cross section for the production of nuclei of type i from the break up of heavier nuclei of type j. τ_i is the lifetime of the nuclei of kind i with respect to radioactive decay and the last term of equation 3.3 describes the formation of nuclei of type i due to decays of other nuclei.

The generic equation 3.3 corresponds to the transport equation for the diffusion model which describes the propagation process of cosmic rays. A general method of solving a set of diffusion equations with additional simplifying assumptions can be found in [Ber90].

3.2.2. The Leaky Box model

The Leaky Box Model (LBM) for the propagation of Cosmic Rays was firstly proposed by Cowsik *et al.* [Cow67] and has been widely used in propagation studies due to its simplicity. In a certain sense, the LBM can be considered as an extremely simplified version of the diffusion model. This simplification consist on assuming that diffusion takes place rather rapidly and, therefore, the density of cosmic rays in the whole propagation region remains constant. As the system considered includes the cosmic rays sources, it is necessary to allow for a certain escape time of these cosmic rays from the propagation volume in order to keep constant the density of cosmic rays inside. Thus, the LBM assumes that there is a strong reflection of the particles at the boundaries of the propagation region but allows a little leakage of particles from that region [Glo69], [Gin76]. As a result, the motion of particles inside the region of propagation may not be diffusion, but can be of another type, for instance, free motion. In this sense, the diffusion model and the LBM should be considered as independent propagation models. Under such conditions the terms $\frac{\partial N_i}{\partial t} - \overrightarrow{\nabla} \cdot (D_i \overrightarrow{\nabla} N_i)$ in equation 3.3 may be replaced by $\frac{\partial N_i}{\partial t} + \frac{1}{\tau_{esc}} N_i$, where τ_{esc} is a parameter, with the dimension of time, which characterises the escape of cosmic rays from the propagation volume. So that equation 3.3 is transformed to:

$$\frac{\partial N_i}{\partial t} + \frac{1}{\tau_{esc}} N_i + \frac{\partial}{\partial \varepsilon}(\overline{b}_i N_i) + \overline{n} v \sigma_i N_i + \frac{1}{\tau_i} N_i = \overline{q}_i + \sum_{j<i} \overline{n} v \sigma_{ij} N_j + \sum_{j<i} \frac{1}{\tau_{ij}} N_j \quad (3.4)$$

In equation 3.4 several quantities have been averaged over the volume of the propagation region, such as the power of the sources $\overline{Q}_i$, the density of the interstellar gas $\overline{n}$ and the rate of energy loss $\overline{b}_i$.

Assuming the stationary case (*i.e.* $\frac{\partial N_i}{\partial t} = 0$), and neglecting ionisation energy losses (*i.e.* $\overline{b}_i = 0$), the final transport equation for the simplest LBM is:

$$\frac{1}{\tau_{esc}} N_i + \overline{n} v \sigma_i N_i + \frac{1}{\tau_i} N_i = \overline{q}_i + \sum_{j<i} \overline{n} v \sigma_{ij} N_j + \sum_{j<i} \frac{1}{\tau_{ij}} N_j \tag{3.5}$$

Thus, a system of algebraic equations in which each equation correspond to a nucleus of type i is obtained. Equation 3.5 can be expressed in a simpler manner as:

$$N_i \left(\frac{1}{\lambda_{esc}} + \frac{1}{\lambda^i_{int}} + \frac{1}{\lambda^i_{dec}} \right) = \overline{Q}_i + \sum_{j<i} N_j \left(\frac{1}{\lambda^{j\to i}_{spall}} + \frac{1}{\lambda^{j\to i}_{dec}} \right) \tag{3.6}$$

where $\overline{Q}_i = \frac{\overline{q}_i}{\overline{\rho}\beta c\gamma}$, λ^i_{dec} and $\lambda^{j\to i}_{dec}$ (in g/cm^2) are, respectively, the mean free paths for decay of a nuclei of type i and for radioactive decay of nuclides of type j to lighter nuclei of type i, that can be obtained by means of:

$$\lambda_{dec} = \overline{\rho}\beta c\gamma\tau_{dec} \tag{3.7}$$

with $\overline{\rho}$ the mean density of the ISM which is equal to $\overline{\rho} = m_{ISM}\overline{n}$, being m_{ISM} the mass (in g) of the ISM gas. γ is the Lorentz factor, $\gamma = \frac{1}{\sqrt{1-\beta^2}}$ with $\beta = v/c$, and c is the speed of light.

The spallation and nuclear interaction mean free paths, λ^i_{int} and $\lambda^{j\to i}_{spall}$ can be obtained from:

$$\frac{1}{\lambda^i_{int}} = \frac{\sigma_i}{m_{ISM}} \qquad\qquad \frac{1}{\lambda^{j\to i}_{spall}} = \frac{\sigma_{ij}}{m_{ISM}} \tag{3.8}$$

The escape mean free path is determined from the following relationship:

$$\lambda_{esc} = \overline{\rho}\beta c\gamma\tau_{esc} \tag{3.9}$$

The system of equations for the LBM 3.6, can be easily solved in order to express the densities N_i in terms of the source contribution $\overline{Q}_i$ or vice versa depending on the input data.

3.3. Parameters on the Leaky Box Model

In this section, the values and expressions corresponding to all parameters which have been used to solve the leaky box transport equation are detailed.

3.3.1. Total interaction cross section

The total interaction cross section is used to determine which fraction of a certain nuclei remains after passing through a material medium. As hydrogen is the main component of ISM, total inelastic cross section for the proton-nuclei reactions are employed in order to calculate the interaction mean free path λ_{int}^{i} using expression 3.8.

In the present work, energy dependent expressions of the total inelastic cross section have been adopted [Let83]:

$$\sigma_i(\varepsilon) = \sigma_i(\varepsilon \to \infty) \cdot \left[1 - 0.62 \exp\left(-\frac{\varepsilon}{200}\right) \sin\left(10.9\varepsilon^{-0.28}\right)\right] \tag{3.10}$$

with ε in units of MeV/n, and cross section in mb. $\sigma_{int}(\varepsilon \to \infty)$ is the limiting value of the cross section which is independent of the energy and can be calculated by means of the following expression [Sil90a]:

$$\sigma_i(\varepsilon \to \infty) = 45 \cdot A_P^{0.7} \cdot [1 + 0.016 \sin(5.3 - 2.63 \ln A_P)] \tag{3.11}$$

where A_P is the mass number of the projectile particle in the reaction: Projectile+proton$\longrightarrow$Fragment.

3.3.2. Partial inelastic cross sections

The partial inelastic cross sections specify the probabilities of production of nuclides of type i from the break up of heavier nuclides of type j. In order to calculate the fragmentation charge-changing cross sections, several sets of predictions can be used. In our case, the semiempirical fit expressions provided by R. Silberberg & C.H. Tsao and successively improved have been adopted for the propagation calculation [Sil73a], [Sil73b], [Sil77a], [Sil77b], [Tsa79], [Sil85a], [Sil85b], [Sil89], [Sil90a] & [Sil90b].

It has to be mentioned that the expressions of the bulk of the parameters appearing in the formulae of the charge changing partial inelastic cross sections for spallation in proton-nucleus reactions, depend on the energy of the projectile nuclei considered. In consequence, only those expressions corresponding to an energy over $\sim 3GeV/n$ are given below.

Different expressions for the charge changing cross sections have to be adopted depending on the conditions of fragmentation for the generic reaction Projectile+proton$\longrightarrow$Fragment.

(i) The general formula in which $\Delta A > 4$ (where ΔA is the difference in the projectile and fragment mass numbers) can be written as:

$$\sigma_{ij} = \sigma_0 \cdot f(A_F) \cdot f(E) \cdot e^{-P\Delta A} \cdot e^{-\left(R \cdot \left|Z_F - SA_F + TA_F^2 + UA_F^3\right|^{\nu}\right)} \cdot \Omega \cdot \eta \cdot \xi \tag{3.12}$$

where Z_F, A_F are, respectively, the charge and the mass number of the fragment nucleus, and E is the energy which is the same for both fragment and projectile nuclei. The values of the parameters in equation 3.12 can be calculated as:

$$\sigma_0 = \frac{144 f_1 f_2 P A_P^{0.367}}{1 - \left(\frac{0.3}{PA_P}\right) - \left(0.7 - \frac{0.3}{PA_P}\right) e^{-PA_P}}$$

with $f_1 = 1.05$, $f_2 = 1$, and $P = 1.97 A_P^{-0.9}$. The correction factors $f(A_F)$ and $f(E)$ are taken as:

$$f(A_F) = 1$$

$$f(E) = 1$$

the remaining parameters are:

$$R = 11.8 A_F^{-0.45}$$

$$S = 0.482 - 0.07 \frac{(A_P - \overline{A_P})}{Z_P}$$

where $\overline{A_P} = 2Z_P + 0.015 Z_P^{1.8}$

$$T = 0.00028$$

$$U = 3 \cdot 10^{-7}$$

$$\nu = \begin{cases} 1.3 & Z^* < -1 \\ 1.5 & -1 \leq Z^* \leq 1 \\ 1.75 & Z^* > 1 \end{cases}$$

where $Z^* \equiv Z_F - S A_F + T A_F^2 + U A_F^3$

$$\Omega = 1$$

$$\xi = 1$$

$$\eta = \begin{cases} 1.25 & Z_F \text{ even, } N_F \text{ even} \\ 0.9 & Z_F \text{ even, } N_F \text{ odd} \\ 1 & Z_F \text{ odd, } N_F \text{ even} \\ 0.85 & Z_F \text{ odd, } N_F \text{ odd} \end{cases}$$

where N_F in the number of neutrons of the fragment nuclei.

(*ii*) When peripherical reactions in which $\Delta A \leq 4$, are considered, σ_{ij} is calculated using the following new expression:

$$\sigma_{ij}(peripherical) = \sigma\left(E_0\right) \cdot H(E) \cdot Y(Z_P, A_P) \cdot \varphi(A_P, E) \tag{3.13}$$

where the complete expressions of the functions appearing in equation 3.13 can be evaluated using:

$$\sigma\left(E_0\right) = 21$$

$$\begin{aligned} H(E) \;=\; & \left\{1 - \exp\left[-\left(\frac{E}{230}\right)^2\right] + 2.2\exp\left[-\frac{E}{75}\right] + 0.33\exp\left[-\left(\frac{E-900}{500}\right)^2\right]\right\} \\ & \cdot\left\{1 - \exp\left[-\left(\frac{E}{25}\right)^4\right]\right\} \end{aligned} \tag{3.14}$$

$$\varphi(A_P, E) = 1 - 0.01(A_P - 157) \tag{3.15}$$

$$Y(Z_P, A_P) = \exp\left[\frac{d\left(A_P - \overline{A_P}\right)}{Z_P}\right]$$

with $d\left(A_P - \overline{A_P}\right) = -3$.

(*iii*) Peripherical reactions for the case of the Uranium nuclei require a special treatment, so, different expressions, instead of 3.13, have to be used:

$$\sigma_{ij}(U, peripherical) = \sigma\left(E_0\right) \cdot H(E) \cdot \varphi(A_P, E) \tag{3.16}$$

where $H(E)$ and $\varphi(A_P, E)$ can be respectively calculated by means of equations 3.14 and 3.15. $\sigma(E_0)$ has a different expression:

$$\sigma\left(E_0\right) = \begin{cases} 1.2\exp\left[-0.7\left(A_F - 224\right)\right] & Z_F = 88 \\ 1.6\exp\left[-0.15\left(A_F - 224\right)\right] & Z_F = 89 \\ 8.0\exp\left[-0.25\left(A_F - 233\right)\right] & Z_F = 90 \\ 18.5\exp\left[-0.55\left(A_F - 234\right)\right] & Z_F = 91 \\ 55.0\exp\left[-0.8\left(A_F - 237\right)\right] & Z_F = 92 \end{cases}$$

3.3.3. Escape probability

The probability that a particle abandons the confining region is expressed in terms of an escape length which estimates how easily a given particle escapes from observation. The larger the scape length, the lower the probability that the particle could escape from the storage region. There are several formulae available for the escape mean free path (λ_{esc}) which are energy dependent, usually expressed in terms of magnetic rigidity.

The first expression is derived from studies of light nuclei, and has the form [Orm78], [Pro81] & [Koc81]:

$$\lambda_{esc} = \begin{cases} \lambda_{e0} & R \leq 7.6 \text{ GV} \\ \lambda_{e0} \left(\frac{7.6Gv}{R}\right)^{\delta} & R > 7.6 \text{ GV} \end{cases} \tag{3.17}$$

where R is the magnetic rigidity ($R = \frac{pc}{Ze}$, with p the lineal momentum of the particle, and e the electron charge) of the particle in units of GV, λ_{e0} and δ are adjustable parameters which take the values of $\lambda_{e0} = 5.5$ g/cm^2 and $\delta = 0.4 \pm 0.1$ [Orm78]. For the most ultra heavy nuclei with energies about 3 GeV/n, the escape length is a constant of λ_{e0}.

The second expression proposed is obtained from ultraheavy cosmic rays data [Eng81] & [Bou82] can be written as [Wad85] & [Bre85]:

$$\lambda_{esc} = \begin{cases} 26.9 \left[1 + \left(\frac{1.88}{R}\right)^2\right]^{3/2} & R < 11.4 \text{ GV} \\ 25.8 R^{-0.7} & R \geq 11.4 \text{ GV} \end{cases} \tag{3.18}$$

which returns a value of $\lambda_{esc} = 6.0$ g/cm^2 for particles with an energy of $\simeq 5$ GeV/n.

In our propagation calculation, an escape mean free path value of $\lambda_{esc} = 5.5$ g/cm^2, which is compatible with both expressions 3.17 & 3.18 as well as that given by other authors [Mar86], has been adopted.

3.3.4. Decay parameters

Although the transport equations have to be applied for each nuclear species in the charge region considered, only the most abundant isotope of each element has been taken as a first approach to the propagation problem. In the ultra heavy charge range with $Z \gtrsim 65$, the most abundant isotopes coincide with those having a larger life for alpha decay and, therefore, with the most stable ones.

The only possible radioactive decay, in the charge range considered is alpha decay, in which $\Delta Z = 2$. Therefore, all those nuclei with half life time for α-decay larger than 10^7years can be treated as stable and consequently the radioactive decay term should be neglected from the leaky box transport equation 3.6 (i.e. $\frac{1}{\lambda^i_{dec}} = 0$ and $\frac{1}{\lambda^{j\to i}_{dec}} = 0$). On the other hand, for the nuclei with half-life time for α-decay shorter than 10^7years, relationship 3.7 has to be applied in order to evaluate the mean free path for radioactive decay (λ^i_{dec} and $\lambda^{j\to i}_{dec}$).

In order to calculate the value of the confinement time of cosmic rays in the propagation region expression 3.9 has been used assuming that cosmic rays have an energy of ~ 3 GeV/n, thus $\beta \simeq 0.98$ and $\gamma \simeq 5$. As mentioned above $\lambda_{esc} = 5.5$ g/cm^2, the mean density of the ISM, $\overline{\rho} = \overline{n} m_{ISM}$ is calculated assuming that $\overline{n} = 0.3$ atoms/cm^3 [Wie80] & [Gar81] and the interstellar mass is equal to the proton mass (i.e. $m_{ISM} = m_p = 1.6726231 \times 10^{-24}$ g) because the ISM is considered to be formed only by hydrogen atoms although it is known that 90% if ISM is hydrogen and the remaining consists on Helium

atoms. The obtained value of $\tau_{esc} \simeq 10^7$years is in agreement with the age of cosmic rays in the Galaxy using secondary stable nuclei with diffusion propagation models [Ber90].

3.4. Application of the Leaky Box model

A set of computer codes, based on the leaky box propagation model have been set up in order to determine the source abundances of cosmic rays from the abundances experimentally registered at the top of the Earth's atmosphere, solving a set of transport equations which can be easily be written as:

$$\overline{Q}_i = N_i \left(\frac{1}{\lambda_{esc}} + \frac{1}{\lambda^i_{int}} + \frac{1}{\lambda^i_{dec}} \right) - \sum_{j<i} N_j \left(\frac{1}{\lambda^{j\to i}_{spall}} + \frac{1}{\lambda^{j\to i}_{dec}} \right) \tag{3.19}$$

This model has been applied for estimating the source abundances of cosmic rays inferred from the abundances measured in the *Ultra Heavy Cosmic Ray Experiment* (UHCRE). Because of the geomagnetic cut-off corresponding to the orbits followed by the *Long Duration Exposure Facility* (LDEF) satellite which boarded the UHCRE experience, only cosmic rays with an energy over $\simeq 2$ GeV/n can be recorded. In addition, due to the recording threshold of the solid state nuclear track detectors used in the UHCRE and taking into account the above energy threshold, only ultra heavy cosmic ray nuclei with charge over $Z \gtrsim 65$ can be registered. As a result, the propagation code has been applied to the 28 stable isotopes, from Tb ($Z = 65$) to U ($Z = 92$) considering that all of such nuclei have an energy over $\simeq 4$ GeV/n which is compatible with the assumption of taking the Galaxy as the propagation region.

3.4.1. Test for the propagation model

The codes which are depicted in detail in [Font94], have been tested taking known propagated abundances results at the top of the Earth's atmosphere obtained by other authors, and trying to reproduce their sources row data by propagating back from the Earth by means of the code developed based on equation 3.19. For this test, results provided by Letaw *et al.* [Let84] which are illustrated in figure 3.5, have been chosen. In their work, Letaw *et al.* studied the propagation of UH ($65 \leqslant Z \leqslant 82$) cosmic rays assuming, as source abundances, the Cameron cosmic ray solar system (SS) abundances [Cam82] with a First Ionization Potential (FIP) correction [Let84], which accounts for preferential acceleration of cosmic-ray species with low FIP at the sites of injection, and propagating them to the Earth vicinity. The propagation was carried out at an energy of 5 GeV/n and considering an exponential Path Length Distribution with a mean value of $\lambda_{esc} = 6$ g/cm^2. Nuclei involved in this transport calculation are grouped in couples instead of be treated individually, due to the charge uncertainty associated to the Ariel VI and HEAO-3 experiments, which results are used to be compared with the propagated abundances.

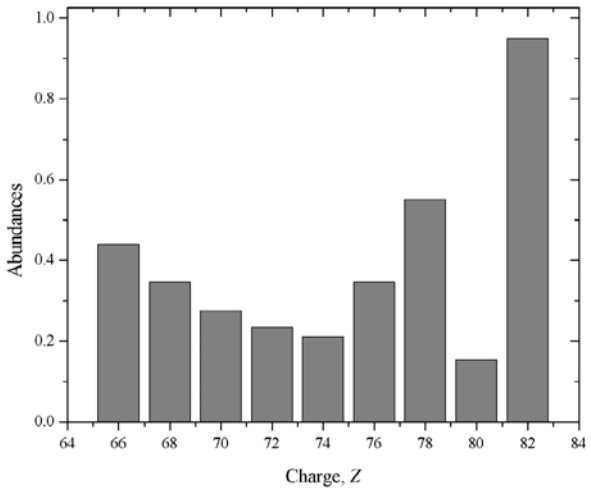

Figure 3.5. Propagated abundances through 6 g/cm^2 of ISM at 5 GeV/n assuming Cameron Solar System abundances with FIP correcion obtained by [Let84], which have been taken as input data for the test of propagation codes.

If the Letaw et al. [Let84] propagated abundances shown in figure 3.5 are taken as input for our calculation codes and are propagated back to the sources, the Cameron SS abundances corrected with the FIP effect should be reproduced. In order to use the results obtained by Letaw *et al.* a deconvolution based on natural proportions of elements has been applied to each couple of elements, as our propagation calculation requires taking individually all elements of a given charge range. Figure 3.6 shows the SS abundances corrected by FIP, together with the results of our propagation of the Letaw et al. results from the Earth to the sources [Font95].

In Figure 3.6 two different charge regions can be distinguished as a function of the results obtained. In the lower charge region $65 \leqslant Z \leqslant 76$, our propagation results (solid diamond in figure 3.6) display an overabundance of the even charge elements with respect to the Cameron SS abundances, achieving a factor $\lesssim 2$, whereas the results of our calculation agree with the SS+FIP source abundances in the $65 \leqslant Z \leqslant 76$ charge region.

3.4.2. Application to the UHCRE results

The transport equation 3.19 allowed the straightforward calculation of the term $\overline{Q}_i$, related to the source production of nuclei of type i, if the abundances in Earth's neighborhood are known. One such equation for each type of cosmic ray nuclei involved in the propagation could be written, and therefore a set of coupled equations could be solved to calculate the source abundances. In the present work we were interested in the resolution of

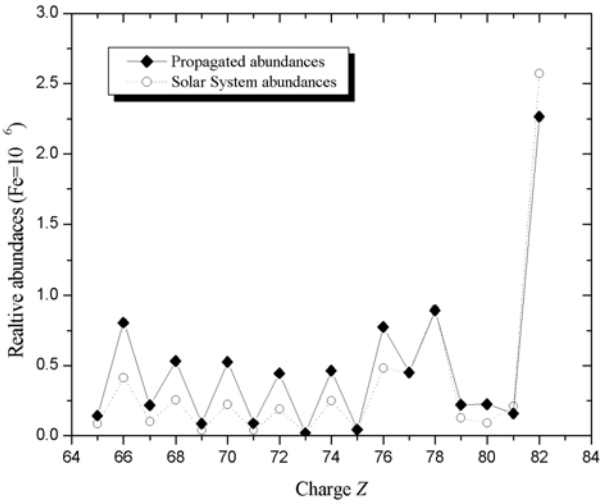

Figure 3.6. Cameron Solar System abundances (relative to iron = 10^6) [Cam82] corrected with FIP effect (open circles) and source abundances obtained by our calculation codes from the Letaw et al. reaults [Let84] (solid diamonds).

the propagation equations for the Cosmic Ray Ultra Heavy elements (from Tb, $Z = 65$, to U, $Z = 92$). The approximation of taking only the most stable/abundant isotope for each element has been used for propagation calculation, although the strict application of the model would establish one equation of type 3.19 for each isotope in the given charge range, resulting in a set of more than 100 simultaneous equations. The equations were numbered from i=1 for U ($Z = 92$) to i=28 for Tb ($Z = 65$).

Source abundances of the 28 elements with charge $65 \leqslant Z \leqslant 92$, represented by the terms $\overline{Q}_i$ of equation 3.19, have been calculated using computer codes developed for this purpose [Dom96]. The propagation took the abundances of UH elements registered in the UHCRE, shown in figure 3.7, as starting point, and considered an escape mean free path $\lambda_{esc} = 5.5$ g/cm^2, for particles with kinetic energy of 4 GeV/n. At this energy, effects of solar modulation on the traveling cosmic rays can be neglected.

It is known that in the charge region $65 \leqslant Z \leqslant 92$ there are two main peaks of UH cosmic ray abundances:

(i) The Platinum group peak centered at $Z = 78$, that corresponds to elements synthesized predominantly by the r-process.

(ii) The Lead group peak centered at $Z = 82$, that corresponds to elements synthesized by the s-process.

In addition, a third less important peak in the actinides region ($Z \geqslant 87$), corresponds to elements synthesized by the r-process. The UH source abundances propagated

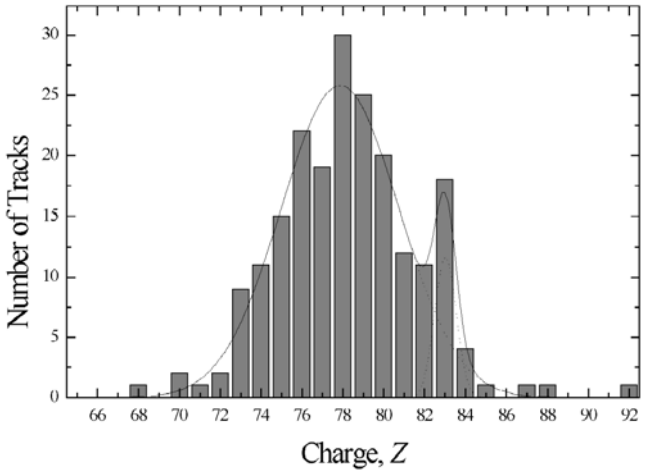

Figure 3.7. Charge histogram corresponding to the 206 ultra heavy nuclei with $Z \geqslant 65$ obtained from the UHCRE. The double gaussian fit to the Platinum and Lead peaks are also displayed.

from the UHCRE results are compared with several source compositions, such as the Solar System abundances given by Cameron [Cam82] in figure 3.8, the solar system abundances reported by Anders and Ebihara [And82] in figure 3.9 and an r-type source abundances in figure 3.10.

Abundances given in figures 3.8, 3.9 & 3.10 are normalized to unity area in order to make them comparable, allowing to visualize easily the relative importance of the Lead and Platinum peaks in each case. Elemental abundances of every couple of contiguous elements (odd-even) obtained from the UHCRE have been grouped, and individual odd and even element abundances have been calculated assuming an odd/even abundance ratio equal to that of the Solar System (according to [Cam82]) as the charge uncertainty of UH events recorded in the UHCRE (1.5 to 2 charge units) did not allow to separate individual elements.

3.5. Discussion and conclusions

The leaky box propagation equations have been solved numerically by means of a computer code which has been tested by reproducing the propagation results using the same model obtained by other authors [Let84] also using the LBM. Figure 3.6 illustrates the result of this test imposed to the propagation code.

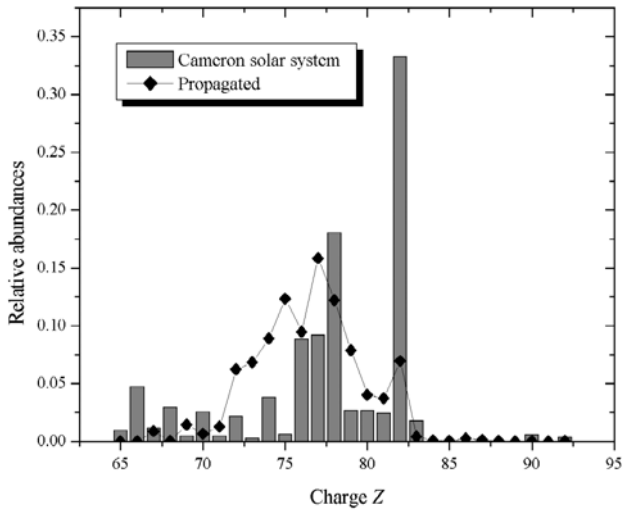

Figure 3.8. Charge histogram showing the source abundances (normalized to an area equals to unity) obtained from propagation of UHCRE results, together with the Solar System abundances given by Cameron [Cam82].

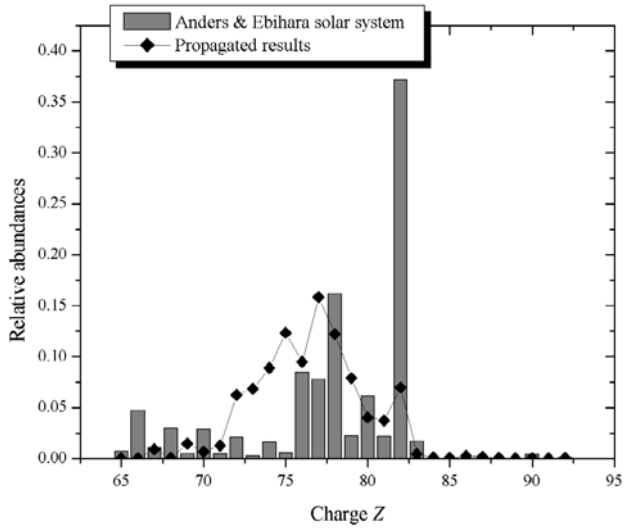

Figure 3.9. Charge histogram showing the source abundances (normalized to an area equals to unity) obtained from propagation of UHCRE results, together with the Solar System abundances given by Anders & Ebihara [And82].

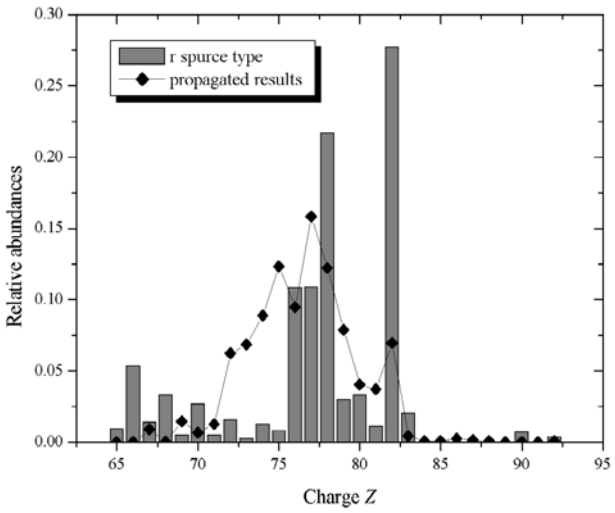

Figure 3.10. Charge histogram showing the source abundances (normalized to an area equals to unity) obtained from propagation of UHCRE results, together with an r type source abundances.

Our propagation displays an overabundance of the even charge elements in the $65 \leqslant Z \leqslant 76$ charge region, whereas the results of our calculation agree with the SS+FIP source abundances in the $77 \leqslant Z \leqslant 82$ charge region. The differences that appear in the first region may be explained by the fragmentation process that takes place during propagation, together with the fact that we have oversimplified our calculation by propagating only the most stable isotope of each element. In fact, Letaw *et al.* [Let84] propagate over 100 isotopes in the $65 \leqslant Z \leqslant 76$ region. Our calculation propagates only the most stable isotope of each element, so that we have neglected the contribution to the term $\frac{1}{\lambda_{spall}^{j\to i}}$ of isotopes lighter and heavier than the most stable one. It is inferred, from the spallation cross section calculations applying the Silberberg & Tsao formulae, that $\frac{1}{\lambda_{spall}^{j\to i}}$ decreases when the isotope mass number increases (see table 3.1). Therefore, neglecting isotopes heavier than the most stable one is irrelevant as their contribution to $\frac{1}{\lambda_{spall}^{j\to i}}$ is small in front of the most stable isotope contribution; but neglecting isotopes lighter than the most stable one implies that $\frac{1}{\lambda_{spall}^{j\to i}}$ is underestimated. This underestimation leads, according to equation 3.19, to an overestimation of $\overline{Q}_i$ in our calculation. This effect is more relevant for even-charge elements, as they have a higher number of possible lighter stable isotopes than odd-charge elements. The agreement of the results in the region ($77 \leqslant Z \leqslant 82$) is explained because our calculation, like the Letaw *et al.* [Let84] one, does not consider the propagation of elements with $Z > 82$. Hence, nuclides in that region can not be originated

Table 3.1. Fragmentation cross sections (in mb) of $^{208}_{82}$Pb, $^{195}_{78}$Pt and $^{197}_{79}$Au for production of lighter nuclei at 5 GeV/n. The isotopes marked with $^{\checkmark}$ have used in our calculation. Note that fragmentation to lighter isotopes implies larger cross sections.

Product	Fragmented nucleus		
	Pb^{208}_{82}	Pt^{195}_{78}	Au^{197}_{79}
$^{\checkmark}Os^{192}_{72}$	0.05	0.037	0.02
Os^{191}_{72}	0.19	0.14	0.1
Os^{190}_{72}	0.27	0.2	0.15
$^{\checkmark}W^{184}_{74}$	0.19	0.14	0.1
W^{183}_{74}	0.26	0.2	0.16
W^{182}_{74}	0.71	0.55	0.32
$^{\checkmark}Hf^{180}_{72}$	2.4	0.034	0.024
Hf^{179}_{72}	3.0	0.052	0.041
Hf^{178}_{72}	7.16	0.14	0.086

from fragmentation of heavier elements, and the contribution to the summation term in equation 3.19 is very similar in our calculation as in the Letaw one.

The results obtained in this chapter allow to conclude that the propagation of all isotopes is needed for a precise determination of the UH element source abundances; but that a simple model, based on the propagation of only the most abundant isotope of each element, is enough in order to obtain a rough estimation of the order of magnitude of such source abundances. In any case, the non-validity of the cross section expressions in the charge and energy range of the ions involved is, probably, the main source of error in this calculation and hence, the effect of considering only the most abundant isotope of each element could become irrelevant.

It has to be emphasised that the transport equations based on a simplified LBM which has been used to propagate the abundances provided in the UHCRE (illustrated in figure 3.7), has to be understood as a first approach to the problem of the determination of the source composition of ultra heavy cosmic rays with $Z \geqslant 65$. Figures 3.8, 3.9 & 3.10 show the propagation result compared with several source abundances (respectively,. Cameron solar system, Anders & ebihara solar system and r source type abundances).

From these figures it is inferred that Solar System abundances display a prominent peak in the Lead region and a relatively less important peak in the Platinum region. In contrast, the Platinum group peak was obviously the main one for the UHCRE abundances propagated back to the sources while the Lead peak was clearly less important. This Pt-Pb peak inversion has also been found by other authors when experimental data from Ariel VI and HEAO-3 experiments are compared to the propagation calculation results using different transport models. Figures 3.11, 3.12 and 3.13 show that other authors have found similar

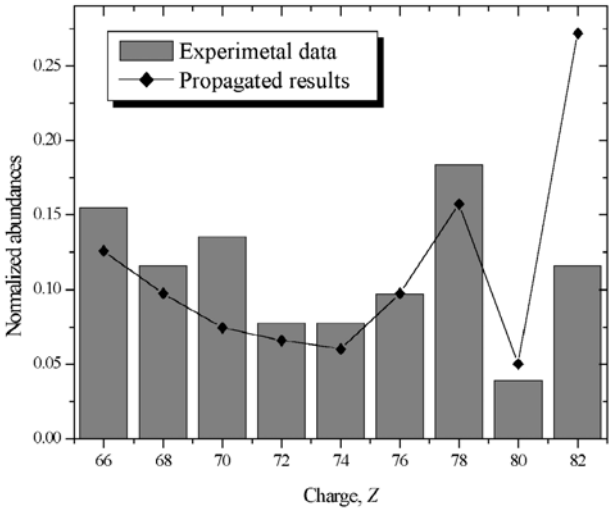

Figure 3.11. Comparison between experimental data from Ariel VI and HEAO-3 experiments and propagated abundances through 6 g/cm^2 of ISM at 5 GeV/n taking Cameron solar system abundances [Cam82] with FIP correction as source composition [Let84].

results for the Pt-Pb peak inversion when comparing their experimental results with the propagated abundances assuming different source compositions of solar system type. (see captions for details). This fact indicated an enhancement of the r-process nucleosynthesis in the cosmic ray sources and, therefore, that the source abundances were deficient in s-process elements. Consequently, nucleosynthesis of UH cosmic rays seemed to take place in explosive environments of the Galaxy, such as core collapse supernovae models or neutron stars merger models, in which the extreme conditions needed to activate the r-process were reached. In any case, it seemed evident that UH elements are synthesized in sources having completely different nucleosynthesis conditions than those that have originated the Solar System material. In opposition to these results, Margolis & Blake [Mar85] suggested a solar system type source abundances because their propagation results are in agreement with the experimental data when solar system abundances are taken as source composition of ultra heavy cosmic rays. This result is illustrated in figure 3.14.

Although the propagation result obtained taking UHCRE data seems to agree with former studies where LBM has been employed, but with different assumptions which thus lead to a transport equations different from 3.6 [Bre83], [Let84] & [Bin89], it would be more convenient to apply a weighted slab technique based on the LBM as it provides a suitable framework to study the effects of several parameters on this propagation model, because the propagation model used in this case should be considered as a first approximation to the

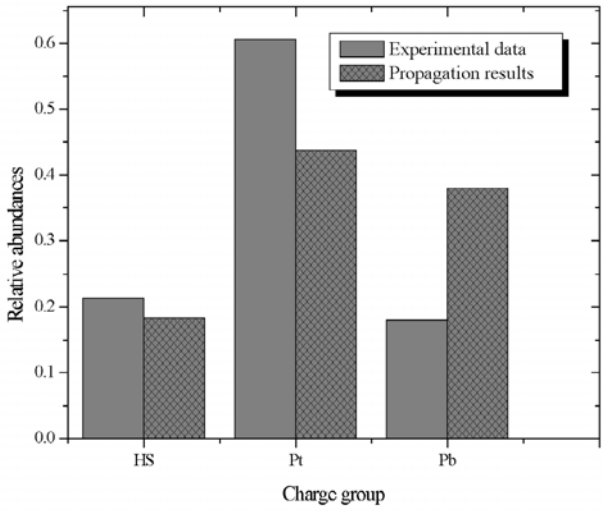

Figure 3.12. Comparison between experimental data provided by HEAO-3 esperiment and propagated abundances using rigidity-dependent mean free path at 2.1 GeV/n assuming Anders & Ebihara solar system abundances [And82] including FIP effect as source composition [Bin89].

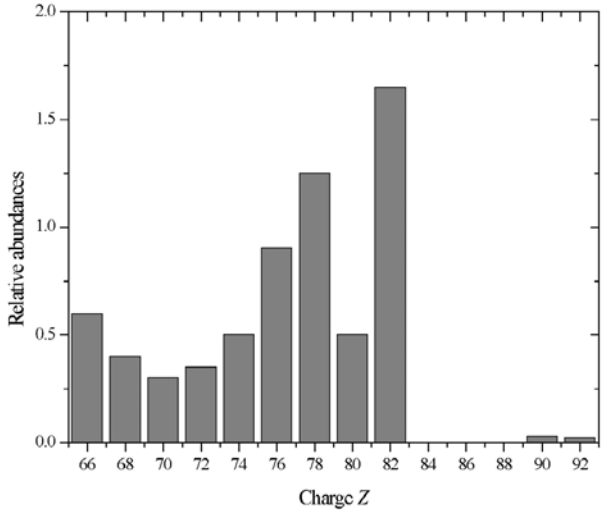

Figure 3.13. Propagated abundances assuming Cameron solar system source abundances [Cam82] with a mean free path of 5.5 g/cm^2 at an energy of 2.3 GeV/n. Odd charges have been shared equally between adjacent even charges [Bre83]

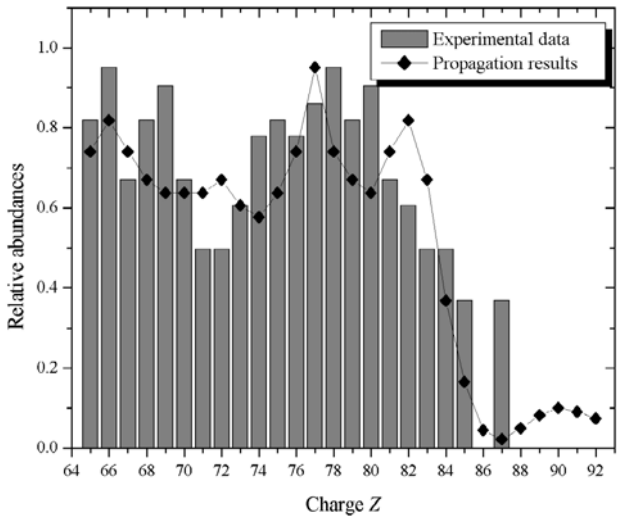

Figure 3.14. Comparison between experimental data from HEAO-3 and propagation rsults through a 7 g/cm^2 of ISM taking Anders & Ebihara solar system abundances [And82] as source composition [Mar85].

LBM. The weighted slab approximation, described in detail in chapter 4, allows to reproduce exact solutions for the LBM transport equation, as well as for the diffusion model equations [Ptu96].

The propagation calculation results illustrated in figures 3.8, 3.9 and 3.10 could significativelly vary when different parameters values are changed. For instance, spallation cross sections play a significant role in the propagation of ultra heavy cosmic rays [Let84] & [Cli93], so that, the estimated source abundances may be affected if different expressions to calculate these cross sections are used. The influence of this parameter and other ones such as the scape length or the energy of cosmic rays, in the propagation calculation will be studied in next chapter where a different procedure to solve the LBM transport equation is utilized.

References

[Abi02] C. Abia *et al.*, astro-ph/0207245.

[All71] B.J. Allen *et al.*, Adv. Nucl. Phys. **4** (1971) 205.

[And82] E. Anders & M. Ebihara, Geochim et Cosmochim. Acta, **46** (1982) 2363.

[Arl99] C. Arlandini *et al.*, Astrophys. J. **525** (1999) 886.

[Arn85] W.D. Arnett & F.K. Thielemann, Astrophys. J. **295** (1985) 589.

[Arn95] W.D. Arnett, Ann. Rev. Astron. Astrophys. **33** (1995) 115.

[Arn99] M. Arnould & K. Takahashi, Rep. Prog. Phys. **62** (1999) 395.

[Arn00] W.D. Arnett, Phys. Rep. **333-334** (2000) 109.

[Arz99] Z. Arzoumanian *et al.*, Astrophys. J., **520** (1999) 696.

[B^2FH] E.M. Burbridge, G.R. Burbridge, W.A. Fowler & F. Hoyle, Rev. Mod. Phys. **29** (1957) 547.

[Bar92] I. Baraffe *et al.*, Astron. Astrophys. **258** (1992) 357.

[Bel02] K. Belczynski *et al.*, Astrophys. J., **571** (2001) L147.

[Ber90] V.S. Berezinskii *et al.*, Astrophysics of Cosmic Rays. V.L. Ginzburg ed. (North Holland, 1990) pg. 45.

[Bet90] H.A. Bethe, Rev. Mod. Phys. **62** (1990) 801.

[Bin89] W.R. Binns et al., Astrophys. J., **346** (1989) 997.

[Boe85] A.M. Boesgaard & G. Steigman, Ann Rev. Astron. Astrophys., **23** (1985) 319.

[Bou82] M. Boufard et al., Astrophys. Spa. Sci. **84** (1982) 3.

[Bre83] N.R. Brewster et al., Astrophys. J., **264** (1983) 324.

[Bre85] N.R. Brewster et al., Astrophys. J., **294** (1985) 419.

[Bus85] M. Busso & R. Gallino, Astron. Astrophys. **151** (1985) 205.

[Bus01] M. Busso *et al.*, Astrophys. J. **557** (2001) 802.

[Cam57] A.G.W. Cameron, Chalk River Report **CLR-41** (1957).

[Cam82] A.G.W. Cameron, Essays in nuclear astrophysics, C.A. Barnes et al. eds. (Cambridge university press, 1982) pg 23.

[Cam01] A.G.W. Cameron, Astrophys. J., **562** (2001) 456.

[Cha92] A.E. Champagne & M. Weischer, Annu. Rev. Nucl. Part. Sci. **42** (1992) 39.

[Cli93] R.R. Clinton & C.J. Waddington, Astrophys. J., **403** (1993) 644.

[Cou74] R.H. Couch *et al.*, Astrophys. J. **190** (1974) 95.

[Cow67] R. Cowsik *et al.*, Phys. Rev. **158** (1967) 1238.

[Cow91] J.J. Cowan *et al.*, Phys. Rep. **208** (1991) 267.

[Cow99] J.J. Cowan *et al.*, Astrophys. J., **521** (1999) 194.

[Cow02] J.J. Cowan *et al.*, Astrophys. J., **572** (2002) 861.

[Dom96] C. Domingo et al., Rad. Meas., **26** (1996) 825.

[Eng81] J.J. Engelmann et al., Proc. 17th ICRC (Paris) **9** (1981) 97.

[Esm91] R. Esmailzadeh *et al.*, Astrophys. J., **378** (1991) 504.

[Font94] J. Font, Master in Science Thesis (Universitat Autònoma de Barcelona, 1994).

[Font95] J. Font et al., Proc. 21st ICRC (Rome) **3** (1995) 144.

[Fre99] C. Freiburghaus *et al.*, Astrophys J., **516** (1999) 381.

[Gal93] R. Gallino *et al.*, Nuclei in the cosmos, F. Käppeler & K. Wisshak eds. (IOP Publishing Ltd, 1993) p. 509.

[Gar81] M. Garcia-Muñoz et al., Proc. 17th ICRC (Paris) **2** (1981) 72.

[Gin64] V.L. Ginzburg & S.I. Syrovatskii, The origin of Cosmic Rays. D. Ter Haar ed. (Pergamon press, 1964) pg 283.

[Gin76] V.L. Ginzburg & V.S. Ptuskin, Rev. Mod. Phys. **48** (1976) 161.

[Glo69] G. Gloecker & J.R. Jokipii, Phys. Rev. Lett. **22** (1969) 1448.

[Her01a] M. Hernanz *et al.*, Proc. "Cosmic evolution" (Paris, 2000) (astro-ph/0101343).

[Her01b] M. Hernanz, Invited paper 4th INTEGRAL Workshop (Alicant, Spain, 2000) (astro-ph/0103418).

[Hil02] V. Hill *et al.*, Astronom et Astrophys., **387** (2002) 560.

[Hob00] L.M. Hobbs, Phys. Rep. **333-334** (2000) 449.

[Hol88] D. Hollowell & I. Iben, Astrophys. J. **333** (1988) L25.

[Hol89] D. Hollowell & I. Iben, Astrophys. J. **340** (1989) 966.

[How91] W.M. Howard *et al.*, Astrophys. J., **373** (1991) L5.

[How93] W.M. Howard *et al.*, Nuclei in the cosmos, F. Käppeler & K. Wisshak eds. (IOP Publishing Ltd, 1993) p. 575.

[Ibe82a] I. Iben & A. Renzini, Astrophys. J. **259** (1982) L79.

[Ibe82b] I. Iben & A. Renzini, Astrophys. J. **263** (1982) L23.

[Ish00] Y. Ishimaru & S. Wanajo, Fisrt stars, A. Weiss et al., eds (Springer-Verlag, Berlin 2000) p. 189.

[Joh02] J.A. Johnson & M. Bolte, Astrophys. J., **579** (2002) 616.

[Kap89] F. Käppeler *et al.*, Rep. Prog. Phys. **52** (1989) 945.

[Kho99] A.M. Khokhlov *et al.*, Astrophys. J., **524** (1999) L107.

[Koc81] L. Koch-Miramond et al., Proc. 17th ICRC (Paris) **2** (1981) 18.

[Lam77] S.A. Lamb *et al.*, Astrophys. J. **217** (1977) 213.

[Lan89] N. Langer *et al.*, Astron. Astrophys. **210** (1989) 187.

[Lat74] J.M. Lattimer & D.N. Schramm, Astrophys. J., **192** (1974) L145.

[Lat76] J.M. Lattimer & D.N. Schramm, Astrophys. J., **210** (1976) 549.

[Lat98] J.C. Lattanzio, Invited review in "Nuclei in the Cosmos V" (Volos, 1998).

[Leb70] J.M. LeBlanc & J.R. Wilson, Astrophys. J., **161** (1970) 541.

[Let83] J.R. Letaw *et. al.*, Astrophys. J. Suppl., **51** (1983) 271.

[Let84] J.R. Letaw et al., Astrophys. J., **279** (1984) 144.

[Lug03] M. Lugaro *et al.*, Astrophys. J., **586** (2003) 1305.

[Mac01] A.I. MacFadyen *et al.*, Astrophys. J., **550** (2001) L11.

[Mat85] G.J. Mathews & R.A. Ward, Rep. Prog. Phys. **48** (1985) 1371.

[Mat93a] G.J. Mathews *et al.*, Astrophys. J. **403** (1993) 65.

[Mat93b] G.J. Mathews *et al.*, Phys. Rep. **1** (1993) 175.

[Mar85] S.H. Margolis & J.B. Blake, Astrophys. J., **299** (1985) 334.

[Mar86] S:H. Margolis, Astrophys. J., **300** (1986) 20.

[Mey89] B.S. Meyer, Astrophys. J., **343** (1989) 254.

[Mey02] B.S. Meyer, astro-ph/0207227.

[Mow97] N. Mowlavi, Tours Symposium on Nucl. Phys., H. Utsunomiya ed. (AIP, 1997).

[Oli00] K. A. Olive *et al.*, Phys. Rep. **333-334** (2000) 389.

[Orm78] J.F. Ormes & P. Freier, Astrophys. J., **222** (1978) 471.

[Ots00] K. Otsuki et al., Astrophys J. **533** (2000) 424.

[Pag00] B.E.J. Pagel, Phys. Rep. **333-334** (2000) 433.

[Pee66] P.J.E. Peebles, Astrophys. J. **146** (1966) 542.

[Phi91] E.S. Phinney, Astrophys. J., **380** (1991) L17.

[Pra87] N.Prantzos *et al.*, Astrophys. J. **315** (1987) 209.

[Pra89a] N. Prantzos, Nuclear Astrophysics, M. Lozano *et al.* eds. (Springer-Verlag, 1989) pg 1.

[Pra89b] N. Prantzos, Nuclear Astrophysics, M. Lozano *et al.* eds. (Springer-Verlag, 1989) p. 18.

[Pra93] N. Prantzos, Nuclei in the cosmos, F. Käppeler & K. Wisshak eds. (IOP Publishing Ltd, 1993) p. 471.

[Pro81] R.J. Protheroe et al., Astrophys. J., **247** (1981) 362.

[Ptu96] V. Ptuskin et al., Astrophys. J., **465** (1996) 972.

[Qia00] Y.Z. Qian & G.J. Wasserburg, Phys. Rep., **333-334** (2000) 77.

[Qia01] Y.Z. Qian & G.J. Wasserburg, Astrophys. J., **559** (2001) 925.

[Qia03] Y. Z. Qian, Prog. Part. Nucl. Phys. **50** (2003) 153.

[Rai92] C.M. Raiteri *et al.*, Astrophys. J. **387** (1992) 263.

[Ray95] M. Rayet *et al.*, Astron & Astrophys. **298** (1995) 517.

[Ray93] M. Rayet *et al.*, Nuclei in the cosmos, F. Käppeler & K. Wisshak eds. (IOP Publishing Ltd, 1993) p. 613.

[Rem97] F. Rembges *et al.*, Astrophys. J. **484** (1997) 412.

[Ruf97] M. Ruffert *et al.*, Astron. & Astrophys., **310** (1997) 122.

[Sch77] D.N. Schramm & R.V. Wagoner, Ann. Rev. Nucl. Sci. **27** (1977) 37.

[Sch82] D.N. Schramm, Essays in nuclear Astrophysics. C. A. Barnes et al. eds. (Cambridge univ. press, 1982) p. 325.

[See65] P.A. Seeger *et al.*, Astrophys. J. Suppl **11** (1965) 121.

[Sil73a] R. Silberberg & C.H. Tsao, Astrophys. J. Suppl., **25** (1973) 315.

[Sil73b] R. Silberberg & C.H. Tsao, Astrophys. J. Suppl., **25** (1973) 335.

[Sil77a] R. Silberberg & C.H. Tsao, Proc. 15th ICRC (Plovdiv) **2** (1977) 84.

[Sil77b] R. Silberberg & C.H. Tsao, Proc. 15th ICRC (Plovdiv) **2** (1977) 89.

[Sil85a] R. Silberberg et al., Composition and origin of cosmic rays. M.M. Shapiro, ed. (D. Reidel Publishing Company, 1985) pg 321.

[Sil85b] R. Silberberg et al., Astrophys. J. Suppl., **58** (1985) 873.

[Sil88] R. Silberberg et al., Genesis and propagation of cosmic rays. M.M. Shapiro & J.P. Wefel eds. (D. Reidel Publishing Company, 1988) pg 357.

[Sil90a] R. Silberberg & C.H. Tsao, Phys. Rep., **191** (1990) 351.

[Sil90b] R. Silberberg & C.H. Tsao, Proc. 21st ICRC (Adelaide) **8** (1990) 424.

[Sne96] C. Sneden *et al.*, Astrophys. J., **467** (1996) 819.

[Sne03] C. Sneden & J.J. Cowan, Science **299** (2003) 70.

[Sum98] K. Sumiyoshi *et al.*, Astron. & Astrophys., **334** (1998) 159.

[Sum01] K. Sumiyoshi *et al.*, Astrophys. J., **562** (2001) 880.

[Tak95] K. Takahashi, Neutrons and their appications, G. Vourvopoulos & T. Paradellis eds. (SPIE 2339,1995) p. 20.

[The00] L.S. The *et al.*, Astrophys. J. **533** (2000) 998.

[Thi98] F.K. Thielemann *et al.*, Nuclear and particle astrophysiscs, J. Hirsch & D. Page eds. (Cambridge University Press, 1998) p. 27.

[Thi01] F.K. Thielemann *et al.*, Prog. Part. Nucl. Phys. **46** (2001) 5.

[Thi90] F.K. Thielemann *et al.,* Astrophys. J. **349** (1990) 222.

[Tra99] C. Travaglio *et al.*, Astrophys. J. **521** (1999) 691.

[Tri75] V. Triemble, Rev. Mod. Phys. **47** (1975) 877.

[Tri91] V. Triemble, Astron. Astrophys. Rev. **3** (1991) 1.

[Tru70] J.W. Truran & W.D. Arnett, Astrophys. J., **160** (1970) 181.

[Tru73] J.W. Truran, Spa. Sci. Rev. **15** (1973) 23.

[Tsa79] C.H. Tsao & R. Silberberg, Proc. 16th ICRC (Kyoto) **2** (1979) 202.

[Van00] E. Vangioni-Flam *et al.*, Phys. Rep. **333-334** (2000) 365.

[Wad85] C.J. Waddington et al., Proc. 19th ICRC (La Jolla) **3** (1985) 1.

[Wag67] R.V. Wagoner *et al.*, Astrophys. J. **148** (1967) 3.

[Wag73] R.V. Wagoner, Astrophys. J. **179** (1973) 243.

[Wal97] G. Wallerstein *et al.*, Rev. Mod. Phys. **69** (1997) 995.

[Wan01] S. Wanajo *et al.*, Astrophys J. **554** (2001) 578.

[Wan03] S. Wanajo *et al.*, Astrophys J. **593** (2003) 968.

[Wea93] T. Weaver & S.E. Woosley., Phys. Rep. **227** (1993) 65.

[Whe98] J.C. Wheeler *et al.*, Astrophys. J., **493** (1998) L101.

[Wie80] M.E. Wiedenbeck & D.E. Greiner, Astrophys. J., **239** (1980) L-139.

[Woo78] S.E. Woosley & W.M. Howard, Astrophys. J. Suppl., **36** (1978) 285.

[Woo94] S.E. Woosley *et al.*, Astrophys. J., **433** (1994) 229.

[Wos88] S.E. Woosley et al., Proc. Astron. Soc. Aust. **7** (1988) 355.

4. Study of the Leaky Box Model on different parameters using the Weighted Slab Technique

An expert is a man who
has made all the mistakes
which can be made
in a very narrow field

NIELS BOHR

4.1. Introduction

Several processes affecting cosmic rays particles in terms of composition and energy spectrum come out during their "adventure" which begins with the building up of the cosmic ray elements in their nucleosynthesis factories (sources) and ends when they reach the vicinity of the Earth with the consequent detection. Mainly these disturbing processes are: the injection, the acceleration and the propagation processes.

Although this chapter is focused on the propagation mechanism, choosing one transport model and comparing its results with those provided by the Ultra Heavy Cosmic Ray Experiment (UHCRE), the remaining disturbing processes will be revisited in order to know their state of art and, hence, offer a wider and richer workframe for propagation purposes.

4.1.1. The acceleration mechanism

The mechanism by which cosmic ray particles are accelerated to the observed energies (up to ultrarelativistic energies) is one of the most intriguing problem in cosmic ray physics. The specific features of particle acceleration which any model for such process has to account for, are:

(i) A power law energy spectrum for particles of all types. The cosmic ray flux energy spectrum below the knee (see figure 1.18 of chapter 1) measured at the Earth has the form :

$$dN(E) \propto E^{-\beta} dE$$

where the exponent β lies in the roughly range (2.5-2.7).

(ii) The acceleration of cosmic rays up to energies $E \approx 10^{14} eV$.

(iii) The cosmic ray composition after acceleration should be consistent with the chemical abundances of the elements.

Fermi in 1949 first postulated that cosmic rays could be accelerated to high energies by means of stochastic processes which assume that particles collide with clouds in the interstellar medium (ISM). If such clouds have predominantly random directions of motion, then the frequency of "head on" collisions between particles and clouds would exceed the rate of "tail" encounters, resulting in a net acceleration that is diffusive in energy. This mechanism is known as *second order Fermi acceleration* (or *stochastic acceleration*), because according to this model the average energy gain per collision $\frac{\Delta E}{E} \propto \left(\frac{v}{c}\right)^2$ where v is the velocity of the moving cloud (and c the speed of light), so it is a very slow process due to $v \ll c$. When particles are confined, such a diffusive process naturally produces a power-law cosmic ray energy distribution, thereby modelling correctly the observations. This fact justified the success of such acceleration model which has been adopted by several workers [Osb87], [Gil87], [Ach92] & [Ost96]

Next step was the notion of the acceleration process in the presence of strong shock waves [Axf77], [Bel78] & [Bla78]. It was stated that shocks in space plasmas could also provide such diffusive acceleration in a more efficient manner tapping the dissipative potential of the flow discontinuity by transferring the shocks kinetic energy to non-thermal population both upstream and downstream of the shock, and at same time heating the downstream gas. According to this model, the average energy gain per collision $\frac{\Delta E}{E} \propto \left(\frac{v}{c}\right)$ so it was appropriately called *first order Fermi acceleration* or *regular acceleration*. In many cases, the acceleration of cosmic ray particles in astrophysical plasmas can be expressed by a Fokker-Planck type equation [Ach92] which describes particle momentum scattering with a regular acceleration term included. Taking appropriate conditions and assumed coefficients, this regular term could vanish from the Fokker-Plank equation resulting a momentum diffusion equation corresponding to a second order Fermi acceleration mechanism [Ost96].

Diffusive shock acceleration is a very attractive version of a first order Fermi acceleration mechanism in the presence of strong shock waves which could be applied to many

physical systems such as the solar system, our galaxy, and through the Universe because of its great efficiency for generating non-thermal ions. It is now believed, as reflected by a large number of papers, that galactic cosmic rays are accelerated mostly from the ISM at Supernova remnants (SNR) blast waves within our galaxy by the diffusive shock acceleration process [Axf77], [Bla78], [Bla80a], [Bla80b], [Dru83], [Mor83], [Web85], [Bla87], [Bar97], [Jon01], [Kan01], [Kan02], [Sla02], [Kan03] & [Vin03].

The diffusion shock acceleration theory provides detailed predictions consistent with observation, such as [Kan01]: (*i*) about 10% of shock energy can be transferred to cosmic ray particles in case of SNR blast waves, (*ii*) the accelerated particle distribution has a power law spectrum, and (*iii*) cosmic ray composition can also be explained to the lowest order by the acceleration of averaged ISM convolved with propagation and spallation effects.

There are several physical reasons by which SNR are the most promising acceleration sites of galactic cosmic rays:

(*i*) It has been observed from direct measurements [Ell90] & [Bar95] that particles do get accelerated at the shock. Also plasma simulations show that ions can be scattered back and forth across the shock by self-generated waves, and these scattered ions can provide a seed population of cosmic rays [Que88].

(*ii*) SNR are the most energetic engines working in our galaxy and the only candidates which explain the required energy for cosmic rays energy density [Bla94]. Taking the observed local flux at the solar system which is considered to coincide with the averaged flux in the galaxy, this leads an average required cosmic ray power input near 10^{41} erg/s [Fie00]. On the other hand, assuming a galactic supernova rate to be one SN every 30 years, and kinetic energy yield per event to be 10^{51} erg, the available power in SNR is rough 10^{42} erg/s. So, SNR-based models must be at least moderately efficient to supply the needed power ($\backsimeq 10\%$). No other known galactic source comes closer than an order of magnitude to this power supply.

(*iii*) According to the standard acceleration which assumes a spherically symmetric shock propagating into the uniform ISM and a mean magnetic field parallel to the shock and the Bohm diffusion coefficient, the maximum energy to which particles can be accelerated by a typical SNR is about 10^{14} eV for protons [Lag83]. Particles may be accelerated to even higher energies assuming additional effects, such as oblique shocks [Mel02] or non-linear effects [Ber96], [Ber99]

(*iv*) The accelerated particle spectrum at the SNR is a power law of index $\beta \backsimeq 2.1 - 2.2$ at the source [Ber94] & [Ost02]. The propagation process generally leads to a steepening of the spectrum with respect to its form at the source, by an increment $\backsim 0.5 - 0.6$ in the slope [DuV96a], such effect points to an energy dependence to the cosmic ray escape rate. Consequently, the expected spectrum at the Earth should have an index $\beta \backsimeq 2.6 - 2.8$, which is in agreement with the observed one.

There are different techniques of tackling the problem of performing numerical

studies with diffusive shock acceleration theory:

Monte Carlo Method: According to an assumed scattering law, the scattering of individual particles by the underlying flow around a one-dimensional shock, which is treated as steady-state, is followed in Monte Carlo simulations, [Bel78], [Bar97] & [Lem03].

Two-Fluid Model: Cosmic ray acceleration at SNR is simulated by two-fluid method in which the cosmic rays energy density is solved instead of the distribution function [Dor90] & [Jon92]. The main conclusion was that about 10% of the SN explosion energy can be transferred to cosmic rays with reasonable assumptions on the model parameters and injection rate.

Kinetic Simulations: This method consists on solving the diffusion-convection equation for the momentum distribution function of high energy particles in the vicinity of a strong shock [Bla78], [Bla80a], [Ber00], [Jon01], [Kan02] & [Vie03].

It has been pointed out that the efficiency of cosmic ray acceleration at strong shocks depends sensitively on the injection rate [Ber95] & [Mal99]. It becomes crucial, therefore, to incorporate the injection process in diffusive shock acceleration models as it plays a critical role. Recently, significant progress in understanding the injection process in parallel shocks has been made through self consistent, analytic and non-linear calculations [Mal98a], [Mal98b] & [Kan03]. In addition, the effect of energy loss process during the acceleration of cosmic rays should be taken into account as both processes could play together but in opposites directions.

Figure 4.1 schematically illustrates the competition between the acceleration process and the energy loss process. The energy loss curve as a function of kinetic energy is compared quantitatively to a uniform acceleration rate. As it can be seen, if the acceleration mechanism is to be effective, the particles must either be injected into the acceleration region with energies greater than those corresponding to the maximum energy loss rate, or else the initial acceleration process must be rapid enough to overcome the energy losses (the solid line illustrates the sufficient acceleration mechanism, while dotted lines account for insufficient acceleration mechanisms).

Preferential acceleration processes have been proposed, by which the thermal particles which will become traveling cosmic rays are pre-select according to the first ionisation potential [Cas78], [Bin81], [Bre83] & [Let84] or to the condensation temperature and their mass-to-charge ratio [Mey97] & [Mey98], evidencing that atomic physics plays a significant role in cosmic ray physics.

Although the standard procedure depicts the acceleration of cosmic rays and afterwards the subsequent propagation, the possibility of a *re-acceleration* or *continuous acceleration* mechanism also named *distributed acceleration* has been considered which takes place in the ISM simultaneously with the propagation of cosmic rays [Eich80], [Sim86], [Wan87], [Let87], [Gil88], [Gil89], [Let93] & [Let95]. This re-acceleration needs to be more effective for energies below $\sim$ 1 GeV/n and disappears at higher energies. Therefore, a re-acceleration term has to be added to the transport equation of traveling cosmic rays in

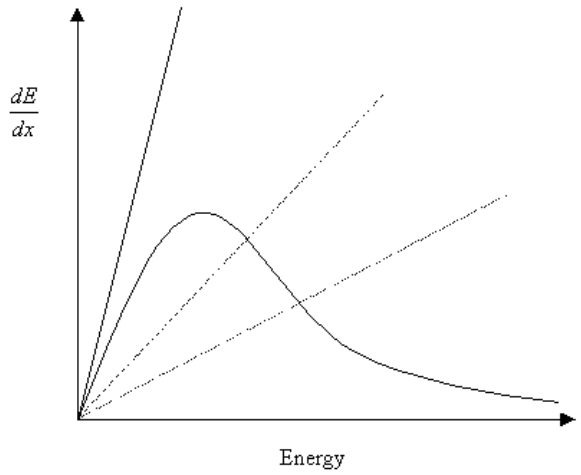

Figure 4.1. Comparison of energy loss rate by ionisation and acceleration rates. The solid line corresponds to a suffient accelation whereas dotted lines illustrate insufficient acceleration.

order to perform numerical calculations [Sil90].

4.1.2. Overview of propagation models

Cosmic ray propagation is the discipline of cosmic ray physics which perhaps has experienced the slowest evolution due to the lack of accurate experimental data related to this complex problem. Nevertheless, many different propagation models have been proposed. Any of such models should account for the following features:

(i) The cosmic ray chemical composition experimentally measured in the Earth neighbourhood.

(ii) The energy spectrum at the Earth for all types of particles which follow the known power-law $dN(E) \propto E^{-\beta}dE$ being β comprised between 2.5 and 2.7.

The propagation models that can be found in literature with a brief description of each one of them are given below.

Closed galaxy model: This model considers a complete reflection of cosmic rays at the boundaries of the confinement volume which is assumed to be the galaxy. So that, there is no escape probability from the galaxy. Resident cosmic rays inside the galaxy are eliminated by means of nuclear interaction or energy loss processes resulting in a mixture of young particles together with old ones [Ras75] & [Pet77].

Diffusion models: According to this model, motion of cosmic ray particles is gov-

erned by diffusion mechanism which is related somehow to the galactic magnetic field. The diffusion process also determines the escape of cosmic rays from the propagation region. The model also takes into account the energy loss process mainly by ionisation [Gin64] & [Gin76].

Distributed acceleration model: This model is essentially a diffusion model but including the effects of re-acceleration of cosmic rays during their propagation in the confinement region [Sim86], [Sil89], [Sil90], [Sha92], [Let93] & [Hei95].

Convection-diffusion model: It is an extension of the diffusion model in which the convection process caused by "frozen" magnetic fields is taken into account [Ber90] & [Mau01].

Halo diffusion model: This model assumes that the propagation region consists on two distinct regions: a thin galactic disc and the halo volume. According to the model, distributed sources of cosmic rays are located within the galactic disc and the escape of cosmic ray particles from the disc into the halo and finally into the intergalactic space is controlled by diffusion [Jok76], [Owe77], [Kot80], [Fre80], [Wib92], [Str97], [Str98] & [Ptu03]. The model could include convection processes in the halo while the diffusion process is bounded only to the galactic disc [Web92] & [Blo93], or both processes simultaneously [Mau01], [Mau02a] & [Mau02b].

Dynamic halo wind model: In this case, a one dimensional galaxy model is considered. Cosmic ray sources and interstellar gas are concentrated in a thin disc. The wind velocity is assumed to be constant and directed outward from the galactic plane. A cosmic ray halo where particles freely exit from the galaxy is also assumed [Jok76], [Jon79], [Blo93] & [Jone01].

Turbulent diffusion model: In this model there is no regular convective (wind) transport of cosmic rays, rather, the flow is turbulent and the motion is given in a more random manner. It is also assumed that turbulent diffusion also contributes to cosmic ray diffusion [Jone01].

Leaky Box model: In this model, the galaxy is considered as the confinement region in which sources of cosmic rays are uniformly distributed. The model also assumes that there is a partial reflection at the boundaries of the propagation region allowing an escape of particles from the galaxy. In other words, cosmic rays leak out from the box (galaxy). The transport of cosmic rays is not controlled by diffusion but by other type of motion, for instance, free motion [Cow67], [Glo69], [Gin76] & [Ber90].

Nested leaky box model: This model is based on the leaky box model, but assuming two confinement regions: sources of cosmic rays are distributed inside the inner region which is enveloped by a second region having the dimensions of the galaxy [Cow73], [Cow75] & [Sim77].

Local super-bubble model: The model considers an expanding super-bubble as confinement region in which the solar system is located. The region inside the super-bubble is of low density. Cosmic ray particles traverse the inside region relatively free, interacting

with the dense walls of the super-bubbles and, thus, accumulating grammage in repeated wall encounters [Str83] & [Str85].

Three tier model: This model combines the ideas of closed galaxy and nested leaky box models. According to this model, cosmic rays are initially confined near the source regions in an energy dependent manner and latter stored in spiral arms from which the leak out into a wider region where they are destroyed through nuclear interactions [Ste81].

Multiple cloud model: This model introduces a cloudy source region from which cosmic rays escape in the same way as described in the nested leaky box model [Sil83]

Non-equilibrium model: One of the simplest version of non-equilibrium models propose two different types of sources, on one hand a single recent relatively close source which could be a SNR, and on the other hand, uniformly distributed sources as those set out in equilibrium models [Fic68].

Among all these propagation models, the Leaky Box model and the Nested leaky box model, have been chosen in order to perform transport calculations of ultra heavy cosmic rays, so that a detailed treatment of both propagation models would be appropriate to be given before to make any propagation study with any of them.

4.2. The propagation model

In this chapter the Leaky Box propagation model will be worked with by solving the corresponding transport equation using the so-called Weighted Slab Technique. In order to understand the transport equation it would be convenient to shows the different steps of its deduction, taken into account that the leaky box equation is obtained from the diffusion transfer equation, taking several simplifying assumptions as described in detail in chapter 3. Therefore, the first step is the derivation of such equation for the diffusion model.

4.2.1. The diffusion transfer equation

One possible approach to deduce the diffusion transfer equation considers a coordinate space in which energy is along the Y-axis and a spatial coordinate along the abscissa is plotted (generalisation to three spatial coordinates is easily). Figure 4.2 illustrates this coordinate-space.

In this coordinate space, a little box is drawn which is traversed by particles moving in the X-direction by diffusion and in the Y-direction by energy gains or losses. Fluxes describing such motion are noted by ϕ_x and ϕ_E respectively. The number of particles between positions x and dx having energies comprised between E and $E + dE$, is $N(E, x, t)dEdx$. Therefore, the rate of change of particles density in this little box in coordinate space can be expressed:

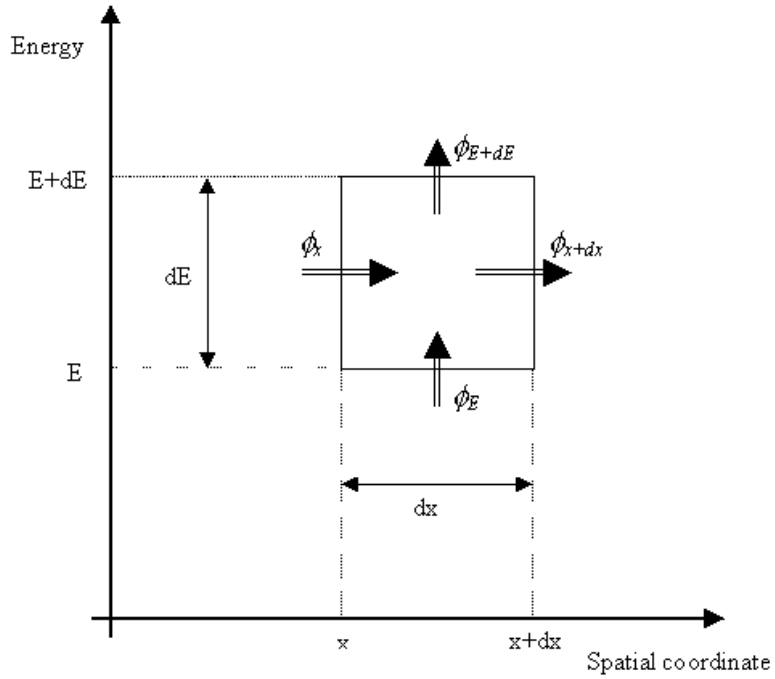

Figure 4.2. A coordinate space diagram of energy against spatial coordinates.

$$\begin{aligned}\frac{d}{dt}N(E,x,t)dEdx &= \left[\phi_x(E,x,t)-\phi_{x+dx}(E,x+dx,t)\right]dE + \\ &+ \left[\phi_E(E,x,t)-\phi_{E+dE}(E+dE,x,t)\right]dx + q(E,x,t)dEdx\end{aligned} \tag{4.1}$$

the first and second terms on right hand of equation account for the contribution of particles by diffusion and energy variations respectively, and $q(E,x,t)$ is the rate of production of particles per unit of volume of the coordinate space. Fluxes ϕ_{x+dx} and ϕ_{E+dE} could be developed performing a Taylor expansion:

$$\begin{aligned}\phi_{x+dx}(E,x+dx,t) &\simeq \phi_x(E,x,t)+\frac{\partial\phi_x}{\partial x}dx+\ldots \\ \phi_{E+dE}(E+dE,x,t) &\simeq \phi_E(E,x,t)+\frac{\partial\phi_E}{\partial E}dE+\ldots\end{aligned}$$

Thus, neglecting second and higher order terms, equation 4.1 can be written as:

$$\frac{d}{dt}N(E,x,t) = -\frac{\partial\phi_x(E,x,t)}{\partial x}-\frac{\partial\phi_E(E,x,t)}{\partial E}+q(E,x,t) \tag{4.2}$$

The flux of particles caused by diffusion through the energy interval dE at position x in space, ϕ_x, is by definition:

$$\phi_x = -D\frac{\partial N}{\partial x}$$

where D is the diffusion coefficient. So, equation 4.2 may be re-written:

$$\frac{dN}{dt} = \frac{\partial}{\partial x}\left(D\frac{\partial N}{\partial x}\right) - \frac{\partial \phi_E}{\partial E} + q$$

At this point, the above equation can be easily generalised to:

$$\frac{dN}{dt} = \nabla\left(D \cdot \nabla N\right) - \frac{\partial \phi_E}{\partial E} + q$$

the flux of particles through dx which have energy E at some time in interval dt, is ϕ_E. Defining $b(E) = \frac{dE}{dt}$ as the loss rate of particles of energy E, then the number of particles passing through E per unit of time is:

$$N(E)\frac{dE}{dt} = \phi_E = b(E)N(E)$$

Therefore, the diffusion equation is obtained:

$$\frac{dN}{dt} = \overrightarrow{\nabla}\left(D \cdot \overrightarrow{\nabla} N\right) - \frac{\partial}{\partial E}\left(b \cdot N\right) + q \tag{4.3}$$

New terms can be added to this equation if other processes are taken into account. For instance, in order to reproduce the general transfer equation, terms describing spallation gain and losses, catastrophic loss of particles, and radioactive decay, have to be included. So, the final diffusion transfer equation for cosmic rays is [Gin64]:

$$\frac{\partial N_i}{\partial t} - \overrightarrow{\nabla} \cdot (D_i \overrightarrow{\nabla} N_i) + \frac{\partial}{\partial E}(b_i N_i) - \frac{1}{2}\frac{\partial^2}{\partial E^2}(d_i N_i) = \tag{4.4}$$

$$= q_i(E, \overrightarrow{r}, t) - P_i N_i + \sum_{j \neq i} \int P_i^j(E', E) N_j(E', \overrightarrow{r}, t) dE'$$

where the subscript i characterises the type of nucleus considered. The term on the left hand side of equation 4.4 allows for fluctuation in the continuous variation in energy, coefficient $d_i \equiv \frac{d}{dt}\left(\overline{\Delta E}\right)^2$ is the mean square of the energy increment per unit of time. Second and third terms on the right hand side account for "catastrophic" processes such as energy losses or gains and formation of new particles when the considered particles interact with the ISM gas. P_i is the probability per unit of time of such a catastrophic processes for particles of type i, so that $P_i N_i$ is the number of disappeared particles. The last term, describes the incoming flux of particles resulting of catastrophic processes. $P_i^j(E', E)$ is the probability per unit of time and unit of energy of formation of a particles of type i with an energy E in a catastrophic process of particle of type j with energy E'.

4.2.2. The Leaky Box model

In order to "reach" the leaky box transport equation, several simplifying assumptions have to be imposed to the above equation 4.4 for the diffusion model. Such assumptions, together with its corresponding effect may are summarised below (see chapter 3 for a detailed description):

(*i*) There is no systematic motion of the medium, such as expansion and compression.

(*ii*) Spatial and temporal dependence of all coefficients is neglected.

(*iii*) Coefficients D_i, b_i, d_i do not depend on the type of particle considered.

(*iv*) Conservation of the energy per nucleon in catastrophic processes causes that the energy dependence of the equation is better described in terms of the energy per nucleon, $\varepsilon \equiv \frac{E}{A}$ rather than energy E, in consequence, $P_i^j(\varepsilon', \varepsilon) = p_i^j \delta(\varepsilon' - \varepsilon)$.

(*v*) Re-acceleration mechanism during propagation is neglected, thus, the term $\frac{1}{2}\frac{\partial^2}{\partial E^2}(d_i N_i)$ is removed.

(*vi*) Only spallation and disintegration processes are considered as catastrophic processes, so that, left hand terms have to be replaced by the corresponding terms on the right hand:

$$\begin{aligned} P_i N_i &\longrightarrow nv\sigma_i N_i + \frac{1}{\tau_i} N_i \\ \sum_{j>i} p_i^j N_j &\longrightarrow \sum_{j>i} nv\sigma_{ij} N_j + \sum_{j>i} \frac{1}{\tau_{ij}} N_j \end{aligned}$$

being σ_i and σ_{ij} the total and partial inelastic spallation cross sections respectively, τ_i the disintegration lifetime, v the velocity of particle and n the ISM density.

(*vii*) A rapid diffusion process causes a constant density of cosmic rays over the propagation region, thus the diffusion coefficient vanishes, and consequently the escape from the propagation volume, leaking through its boundaries is allowed. So, τ_{esc} is the parameter, having dimensions of time, which characterises the escape of cosmic rays from the confinement region.

(*viii*) All quantities in the transport equation are averaged over the propagation volume, $q_i \longrightarrow \overline{Q_i}$.

(*ix*) Energy is kept constant during propagation and thus any energy variation is neglected removing the term $\frac{\partial}{\partial E}(b_i N_i)$.

(*x*) Production rate of particles is balanced with destruction rate of such particles inside the transport region, so $\frac{\partial N_i}{\partial t} = 0$, corresponding to the stationary case.

The resulting simplified equation is the transport equation for the LBM and can be expressed as follows:

$$N_i \left(\frac{1}{\lambda_{esc}} + \frac{1}{\lambda_{int}^i} + \frac{1}{\lambda_{dec}^i} \right) = \overline{Q}_i + \sum_{j<i} N_j \left(\frac{1}{\lambda_{spall}^{j \to i}} + \frac{1}{\lambda_{dec}^{j \to i}} \right) \tag{4.5}$$

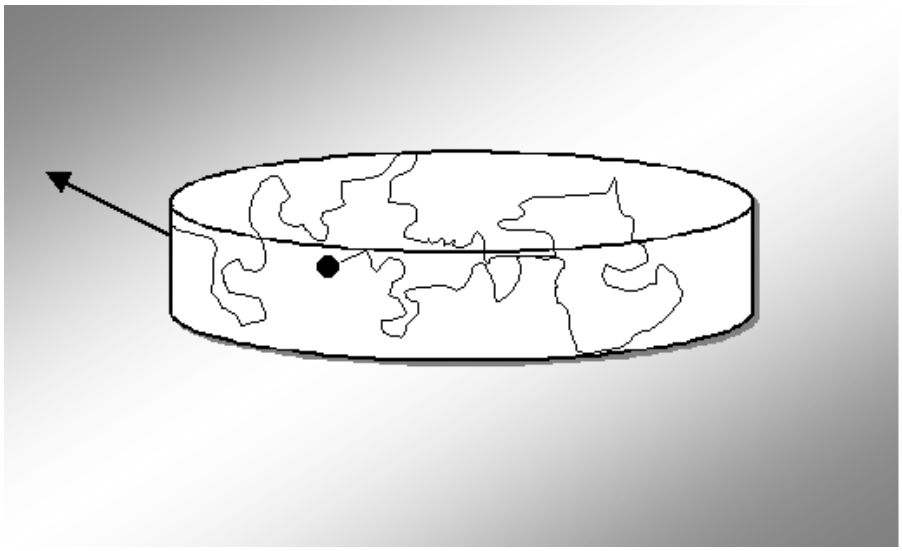

Figure 4.3. The confinement region modelled by the LBM. The path followed by a generic cosmic ray particle escaping from the box is also drawn.

where the magnitudes labelled with λ are the mean free paths for the different processes taken into consideration. Subscripts have the following meanings: "*esc*" refers to escape of cosmic rays from the confinement region, "*dec*" accounts for disintegration processes, "*int*" is related to inelastic nuclear interactions of cosmic rays particles with ISM gas atoms, and "*spall*" refers to spallation process of cosmic rays colliding with ISM gas atoms. Note that equation 4.5 consists in an equilibrium equation which balances the production and losses of particles inside the confinement region.

The two models of cosmic ray propagation mostly referred in the literature are the *Leaky Box model* (LBM) and the *Halo Diffusion model* (HDM). Both models are able to explain the cosmic ray data surprisingly well although the physical framework of them differs significantly.

According to the LBM, cosmic rays nuclei (primary and secondary nuclei) are homogeneously distributed in the confinement region (box) and its density is constant in time neglecting any gradient into any direction. Sources of cosmic rays are also considered to be homogeneously distributed into the box. Therefore, an equilibrium scenario is described in the LBM framework. The motion of cosmic rays is not governed by diffusion processes but a leakage mechanism et the boundaries of the box is allowed, which is paremetrised by the escape time, τ_{esc}, or the escape mean free path, λ_{esc}. Figure 4.3 illustrates the path which follows an hypothetical cosmic ray nucleus escaping from the propagation region after some reflections at the boundaries. In this case, the confinement region is simply the disc of our galaxy which can be modelled by a flattened cylinder.

Although LBM has often been used in propagation studies due to its simplicity,

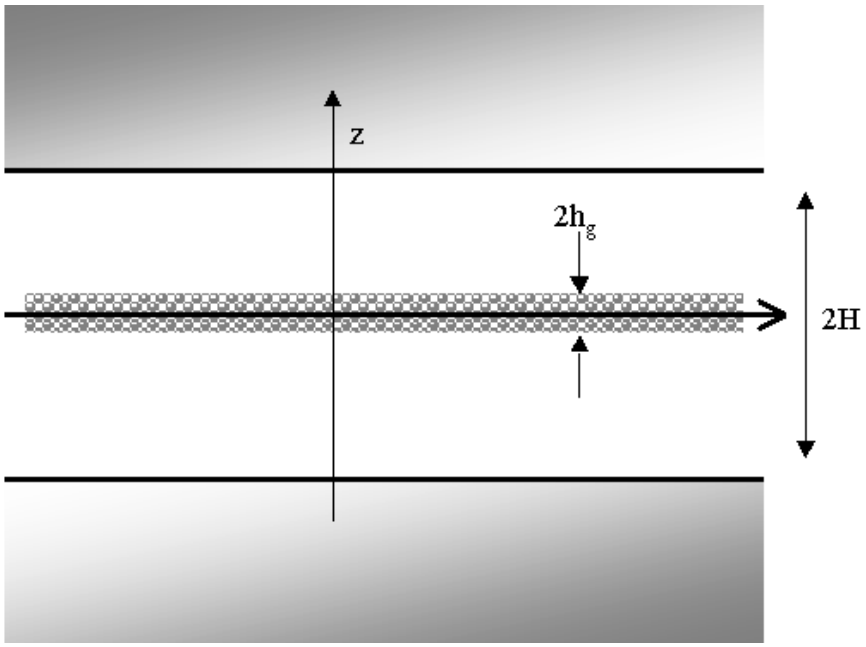

Figure 4.4. Schematic view of the geometry associated to HDM. The shaded area symbolises the thin galactic disc (of thickness $2h_g$ and H accounts for the halo size.

the model displays some drawbacks which are not straightforward solved, such as: (*i*) the mechanism which keeps the particles homogeneously distributed within the box. (*ii*) The motion described by cosmic ray particles (drawn in figure 4.3). (*iii*) The size of the region inside which cosmic ray particles are confined before escaping into intergalactic space. (*iv*) The mechanism of leakage in the boundaries of the box.

On the other hand, the HDM points to a more realistic physical propagation mechanism, as it takes more observational constraints into consideration [Ber90]. Figure 4.4 schematically illustrates the confinement region assumed in the HDM. According to this model, sources of cosmic rays are distributed in the thin disc and the escape into the halo and finally into the intergalactic space is controlled by diffusion. Therefore, a constant streaming of cosmic rays particles away from the galactic disc into the halo is produced by a gradient of cosmic ray density. The streaming mechanism is parametrised by the diffusion coefficient (D) and the halo size (H).

Physically, the HDM can be reduced to the LBM if a rapid diffusion is assumed. It can be also demonstrated that the LBM transport equation represents a mathematical approximation of the HDM [Sim02] as both can reproduce the same mathematical result for stable cosmic ray nuclei. In this context, the LBM cannot be considered a realistic physical propagation model of cosmic rays: it is a mathematical approximation and only works for stable nuclei and fails when radioactive nuclei are taken into account in the

propagation calculation. Taking this fact into consideration, propagation calculations using experimental data may be performed obtaining good results as it has been done in former works [Sch72], [Bre83], [Bre85], [Let84], [Gil85], [Mar85], [Mar86], ,[Bin89], [Cli93], [Wad96], [Wad97] [Wad98]. Therefore, LBM will be applied in present work with UHCRE results necessarily working with stable nuclei belonging to the charge region $Z \gtrsim 65$.

4.2.3. Solving the Leaky Box transport equation: The Weighted Slab Technique

In order to obtain propagation results of cosmic rays using the LBM, the following generic equation for each stable nucleus of type i has to be solved:

$$N_i \left(\frac{1}{\lambda_{esc}} + \frac{1}{\lambda_{int}^i} \right) = \overline{Q}_i + \sum_{j<i} N_j \left(\frac{1}{\lambda_{spall}^{j \to i}} \right) \tag{4.6}$$

Here the subscript $i = 1, 2, \ldots$ characterises the type of nucleus starting from the heaviest one ($i = 1$) and ending with the lightest one in the charge region where propagation is studied. Note that the terms related to disintegration processes have been removed from equation 4.5 according to the discussion above by which only stable nuclei can be worked with the LBM.

Due to the nature of the transport equation 4.6 it is not possible to calculate the source composition from the measured abundances in the Earth neightbourhood N_i. In consequence, it is necessary to assume a given source abundances, perform the transport calculation to near the Earth, and then to compare the results with experimental data. Therefore, a "trial and error" procedure has to be applied until the source abundances giving the best agreement between the calculated and measured abundances are found.

Although exact numerical solutions to the LB propagation equation can be determined, an alternative method of tackling the problem, known as *Weighted Slab Technique* (WST) has been adopted. It has been shown that WST results are consistent with numerical solutions for energies over $\backsimeq$ 1 GeV/n [Ste98].

The WST consists on a very flexible procedure that can be applied to any propagation model based on the diffusion model [Ptu90], [Ptu97], [Ptu03], [Jon01], [Str97], [Str98], [Str01], [Mau01], [Mau02a], [Mau02b], [Mau02c] & [Tai03]. Furthermore, after some appropriate modifications, the WST can also be used when the energy loss term is re-introduced to the corresponding transport equation [Hei95], [Ptu96] & [Wad98]. In particular, the WST has been applied to the LBM model with ultra heavy cosmic rays [Ber90], [Cli93], [Wad96], [Wad97] [Wad98],& [Font00], obtaining successful results for lighter nuclei [Gar87] & [DuV96b].

Solving a propagation equation using the WST allows to split the problem in two parts: one concerning only its astrophysical nature and another dealing only with its nuclear physics essence. The nuclear fragmentation problem is solved in the Slab model transport equation in which all propagating particles traverse the same grammage x in units of g/cm^2.

According to the LBM, the corresponding slab transport equation concerning the nuclear physics of the problem, can be written as:

$$\frac{dF_i(x)}{dx} + \frac{F_i}{\lambda_{int}^i} - \sum_{j<i} F_j \left(\frac{1}{\lambda_{spall}^{j \to i}} \right) = 0 \tag{4.7}$$

being $F_i(x)$ the composition function for the particles of type i, x is the matter traversed by cosmic ray nuclei from their sources, thus, $x = 0.0$ g/cm^2 characterises the source of such nuclei, therefore $F_i(x = 0)$ is the source abundance of the nucleus of type i.

The composition functions $F_i(x)$, which are determined by solving the slab transport equation 4.7, are then integrated over all values of grammage x weighted with a Path Length Distribution function $G(x)$ that must be obtained from an astrophysical model. Therefore,

$$N_i = \int_0^\infty F_i(x) \cdot G(x) dx \tag{4.8}$$

The *Path Length Distribution* (PLD) function, can be derived by means of the following equation:

$$\overline{m} \cdot \overline{n} \cdot v \cdot \frac{\partial G(x)}{\partial x} + \frac{G(x)}{\tau_{esc}} = \delta(x) \tag{4.9}$$

where the function $G(x)$ satisfies the condition $G = 0$ for $x < 0$, $\overline{m}$ is the average mass of an atom of the ISM, $\overline{n}$ is the particle density of the ISM gas averaged over the volume of the galaxy, v is the velocity of cosmic rays and τ_{esc} is the parameter with dimensions of time that characterises the escape of cosmic rays from the confinement region. In this way, $\overline{m} \cdot \overline{n} \cdot v$ has dimensions of density (g/cm^2).

An expression of $G(x)$ is obtained by solving equation 4.9:

$$G(x) = \exp\left\{ -\frac{x}{\overline{m} \cdot \overline{n} \cdot v \cdot \tau_{esc}} \right\} = \exp\left\{ -\frac{x}{\lambda_{esc}} \right\}$$

The PLD function based on the LBM is, thus, an exponential as a function of the matter traversed and does not depend on the position of the observer inside the propagation volume.

As the nuclear physics governing the propagation of cosmic rays is exactly the same for the LBM than for the diffusion model, the composition functions determined by solving equation 4.7 are fully shared by both propagation models when the WST is used. Contrarily, the PLD function $G(x)$ for the diffusion model and for LBM are different because these two propagation models respond to different astrophysical assumptions. In order to determine the PLD function for diffusion model, equation 4.9 has to be replaced by [Ber90]:

$$\rho \cdot v \cdot \frac{\partial G}{\partial x} + \frac{\partial G}{\partial t} - \nabla(D \cdot \nabla G) = v \cdot S(\overrightarrow{r}, t) \cdot \delta(x) \tag{4.10}$$

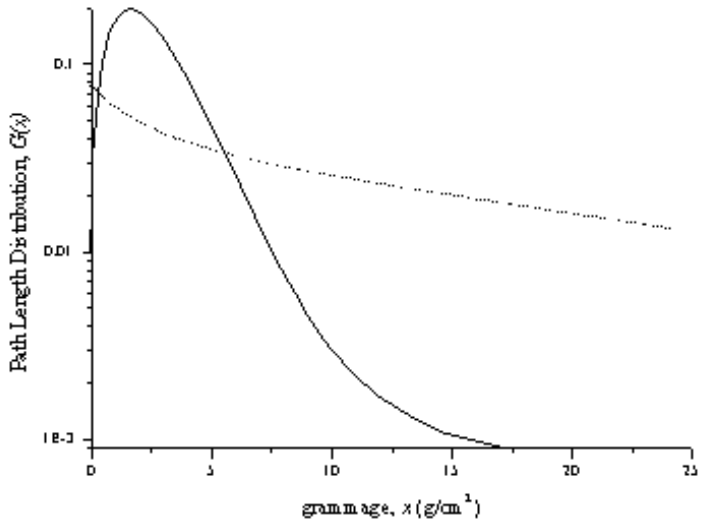

Figure 4.5. The PLD function of the particles in the diffusion model. Dotted line corresponds to the case in which the sources are distributed uniformly in the galactic disc, while for solid line sources are concentrated in the central region of the galaxy.

where $S(\overrightarrow{r}, t)$ is the distribution of the cosmic rays sources. Although equation 4.9 and 4.10 are clearly different giving, thus, different solutions, a PLD function close to an exponential is also obtained for the diffusion model when the sources of cosmic rays are taken uniformly distributed over the galactic disc [Ber90]. In figure 4.5, the PLD function for the diffusion model is plotted. As it can be seen, when sources are uniformly distributed (dotted line), an exponential type function is obtained, but if sources are concentrated in the central region of the galaxy a very different curve is deduced (solid line). In consequence, the LBM and the diffusion model with uniformly distributed sources are equivalent for describing the transformation of the chemical composition of cosmic rays in the galaxy.

4.3. Propagation parameters on Leaky Box model

One of the goals to reach in this chapter is the evaluation of the effects of the different parameters that have been assumed on the propagation results, in order to estimate the best fit to the experimental data from UHCRE. In this section, several available expressions of the propagation parameters are given.

4.3.1. Assumed cosmic ray particles

Although the LBM provides correct results only when the corresponding transport equation is set out for stable particles, as discussed in the previous section, unstable secondary or fragment nuclei have been included in propagation studies with the LBM [Wad96]. One criterion to consider a given nucleus as stable may be established by comparing its mean lifetime, τ_{dec}, with the confinement time of cosmic rays into the galaxy, also called the age of cosmic rays, τ_{CR}. Therefore, all particles having a τ_{dec} which exceeds τ_{CR} are treated as stable.

In the present work the propagation has been carried out for all isotopes as well as elements having charge comprised between 65 and 92. So, the application of the above stability criterion to the considered charge region has lead a total of 80 stable isotopes, which leads to a system of 80 transport equations of type 4.6, or of type 4.7 if WST is used. The set of equations can be reduced if the propagation is realised for elements instead of isotopes. In this case a total of 23 stable nuclei corresponding to the most abundant isotope are selected according to the stability criteria.

4.3.2. Assumed total interaction cross sections

The interaction mean free path, λ_{int}, is calculated from:

$$\lambda_{int}^{i} = \frac{\sigma_i}{m}$$

where σ_{int}^{i} is the total interaction cross section of nuclei of type i colliding with an atom of the ISM gas. Different expression for σ_{int}^{i}, can be found in literature.

Semiempirical fits

One of the most commonly used formula for the mass-changing cross section, σ_{int}^{i}, has been obtained by means of semiempirical fit techniques [Let83]:

$$\sigma_i(\varepsilon) = \sigma_i(\varepsilon \to \infty) \cdot \left[1 - 0.62 \exp\left(-\frac{\varepsilon}{200}\right) \sin\left(10.9\varepsilon^{-0.28}\right)\right] \tag{4.11}$$

with,

$$\sigma_i(\varepsilon \to \infty) = 45 \cdot A_P^{0.7} \cdot [1 + 0.016 \sin(5.3 - 2.63 \ln A_P)] \tag{4.12}$$

being A_P the mass number of the projectile nucleus, and ε its energy per nucleon in units of MeV/n. This empirical expression is only valid for an hydrogen target with a weak energy dependence as it is elucidated in figure 4.6 in which the total interaction cross section for the platinum nuclei is plotted as a function of the energy from 80 MeV/n to 5.0 GeV/n.

A more recent semiempirical formula of the total interaction cross section for proton-nucleus reactions has been proposed [Shi93]:

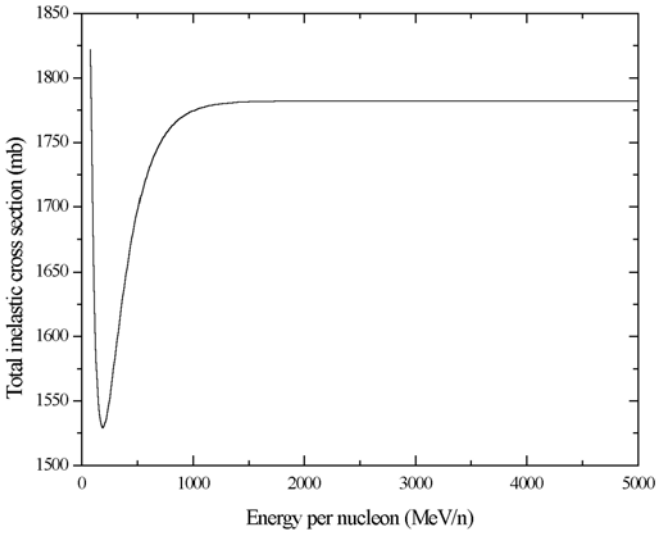

Figure 4.6. Total interaction cross section for a projectile platinum nuclei as a function of energy according to semiempirical fit expressions 4.11 & 4.12.

$$\sigma_i = \pi \cdot r_0^2 \cdot \left[1 + A_P^{1/3} - b_0 \left(1 + A_P^{-1/3}\right)\right]^2$$

with $b_o = 2.247 - 0.915 \left(1 + A_P^{-1/3}\right)$, and $r_0 = 1.36$ fm. Alternative expressions for such cross sections are also given by [Well96].

Parametric fits

A new expression was established fitting experimental data with an overlap model which was dependant on both the target and the particle nuclei [Bin87]:

$$\sigma_i = 10\pi \cdot r_0^2 \cdot \left[A_P^{1/3} + A_T^{1/3} - 0.209 \left(A_P + A_T\right)^{1/3}\right]^2 \tag{4.13}$$

where A_T is the mass number of the target nucleus which in the case of an hydrogen target has to be 0.089 for a best fit to experimental data. Note that equation 4.13 is independent of energy, although an energy dependence of these cross sections has been suggested et energies below $\simeq 1.5$ GeV/n [Wad91].

Factorised semiempirical fits

The analysis of new measurements of the mass changing cross sections has allowed to deduce a new expression [Web90a], also based on an overlap model:

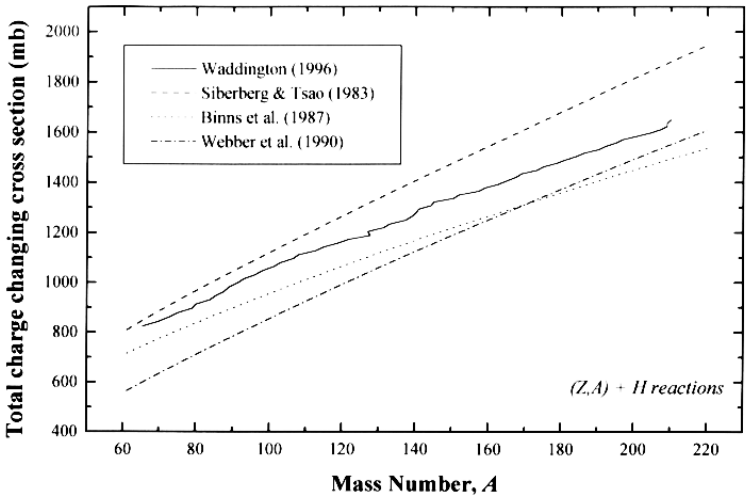

Figure 4.7. Calculated values of the total interaction cross section as a function of the projectile mass number according to different expressions.

$$\sigma_i = C \cdot \left[A_P^{1/3} + A_T^{1/3} - (t + t_0 \cdot A_T) + \left(b' A_P^{1/3} A_T^{1/3} \right) \right]^2 \tag{4.14}$$

the best fit is reached, taking $C = 57.3$, $t_0 = 1.36$, $t = 0.018$, and $b' = 0.065$, which may be modified if updated measurements of these cross sections are considered [Web98a].

Scaling treatment

In this case, the total cross section for charge-changing interaction were assumed to be independent of energy. For a nuclei of charge Z, the cross sections were scaled from the measured values for gold nuclei [Wad96], so that:

$$\sigma_i = \sigma_i^{Au} \cdot \left(\frac{Z}{79} \right)^{2/3} \tag{4.15}$$

In figure 4.7, the total interaction cross sections evaluated using the four different treatments described above are plotted as a function of the projectile mass number, in order to evidence the different results obtained from the expressions 4.11, 4.12, 4.13, 4.14 & 4.15.

In the present work only semiempirical and parametric fits expression for the total interaction cross sections have been used.

4.3.3. Assumed partial inelastic cross sections

One of main parameters in propagation calculations are the partial inelastic cross sections which account for the break up of a traveling nuclei (Z_P, A_P) when it collides

with the ISM atoms producing a fragment new nuclei (Z_F, A_F). Several expressions to calculate these cross sections have been proposed depending on the treatment applied to the experimental data, as in the case of the total cross sections.

Semiempirical fits

The basic equation of the spallation cross sections for a hydrogen target is [Sil73] & [Sil90]:

$$\sigma_{spall}^{P\to F} = \sigma_0 \cdot f(A_F) \cdot f(E) \cdot e^{-P\Delta A} \cdot e^{-\left(R\cdot\left|Z_F - SA_F + TA_F^2 + UA_F^3\right|^{\nu}\right)} \cdot \Omega \cdot \eta \cdot \xi \tag{4.16}$$

where ΔA is the difference between the parent and the fragment atomic masses. σ_0, $f(A_F)$, $f(E)$, P, R, S, T, U, ν, Ω, η, ξ are all functions depending on the particular situation in which the spallation takes place, given by the energy, the atomic masses of both projectile and fragment nuclei and other parameters, as described in [Sil73] & [Sil90] (for instance see section 3.3 of chapter 3). Continuous updates of the values of the parameters appearing in equation 4.16 are reported [Sil98].

In order to show the energy dependence of the calculated cross sections according to equation 4.16, the fragmentation cross section of the $^{208}_{82}$Pb nuclei producing $^{205}_{81}$Tl nuclei (reaction with $\Delta Z = 1$) has been plotted in figure 4.8 for an energy range 0.1-10000 MeV/n, and in figure 4.9 for the $^{208}_{82}$Pb+p$\longrightarrow^{195}_{78}$Pt reaction (with $\Delta Z > 1$).

Figure 4.9 evidences that the spallation cross section formula is not well defined when a wide range of energies is considered, so, more experimental data is needed in order to improve the corresponding formula. This feature may cause some drawbacks in propagation studies, specially for the heaviest cosmic ray nuclei having energies over $\simeq 1$ GeV/n.

Parametric fits

Alternatively, the parametric fits offer alternative expressions for the break up cross sections on heavy and hydrogen targets [Cum90]:

$$\sigma_{spall}^{P\to F} = \begin{cases} q_1 A_P^{q_2} E^{q_3} \exp\left\{-\frac{|\Delta Z|}{q_5 E^{q_6}}\right\} & |\Delta Z| \le q_7 \\ q_1 A_P^{q_2} E^{q_3} \exp\left\{-\frac{q_7}{q_5 E^{q_6}}\right\} \exp\left\{-\frac{\Delta Z - q_7}{q_8 E^{q_6}}\right\} & |\Delta Z| > q_7 \end{cases} \tag{4.17}$$

with E in units of GeV/n. The best fit values for the q_i parameters are: $q_1 = 15.53$, $q_2 = 0.51$, $q_3 = 1.28$, $q_5 = 6.87$, $q_6 = 1.43$, $q_7 = 7.91$, $q_8 = 4.15$, and $\Delta Z = Z_F - Z_P$. The above formula is only valid for $|\Delta Z| \le 20$.

Factorised semiempirical fits

The systematics of the experimental cross sections allow to write the cross section formula for the production of secondary fragments with energy over 200 MeV/n in hydrogen

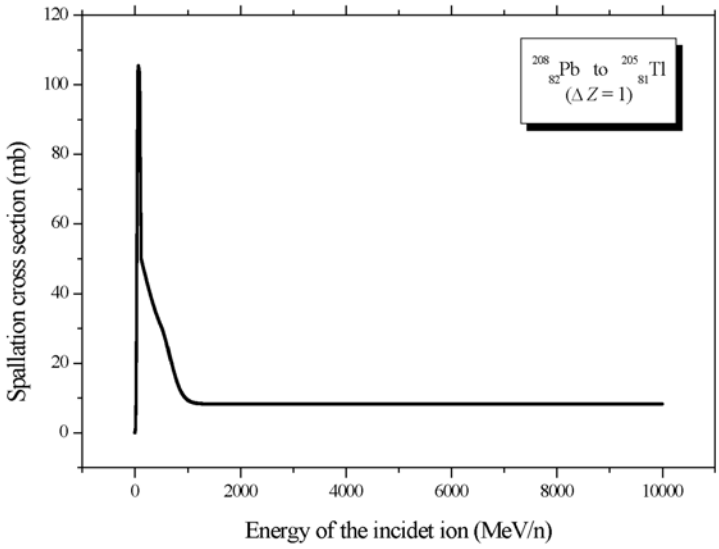

Figure 4.8. Spallation cross section for the reaction $^{208}_{82}$Pb+p$\longrightarrow^{205}_{81}$Tl ($\Delta Z = 1$) as a function of energy.

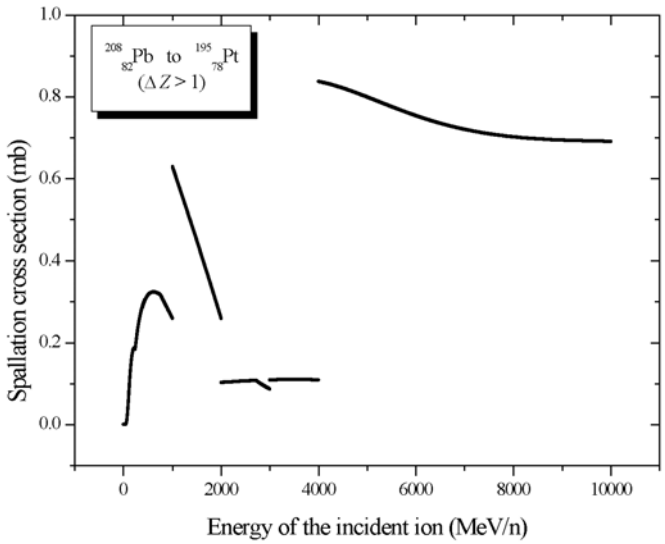

Figure 4.9. Spallation cross section for the reaction $^{208}_{82}$Pb+p$\longrightarrow^{195}_{78}$Pt ($\Delta Z > 1$) as a function of energy.

targets [Web90b]:

$$\sigma_{spall}^{P\rightarrow F} = \sigma_0(Z_F, Z_P) \cdot f_1(Z_F, A_F, Z_P, A_P) \cdot f_2(\varepsilon, Z_F, Z_P) \tag{4.18}$$

the formula is expressed as a product of three independent terms, one, $\sigma_0(Z_F, Z_T)$, describing the elemental cross section, another, $f_1(Z_F, A_F, Z_P, A_P)$ the isotopic cross section, and a third term, $f_2(\varepsilon, Z_F, Z_P)$ accounting for the energy dependence. Expression for all these terms can be found in [Web90b]. Furthermore, an expanded version of equation 4.18 based on new experimental cross sections [Web98b] has been given [Web03].

Scaling treatment

In this case, partial cross sections for the production of fragments over a range of ΔZ are calculated as a function of energy by making linear interpolations between measured values. For high energy interpolations, it has generally assumed that limiting fragmentation over which the cross sections becomes constant, is reached et an energy $\backsimeq 5GeV/n$. As for the total cross section, the partial cross section are scaled fir its charge, so that [Wad96] & [Wad98]:

$$\sigma_{spall}^{T\rightarrow F} = \sigma_{spall}^{Au\rightarrow F} \cdot \left(\frac{Z_P}{79}\right)^{2/3}$$

Among all the partial inelastic cross sections formulae given in this section, only those provided by semiempirical fits [Sil98] and parametric fits [Cum90] have been used in order to compare their effect on the propagation results.

4.3.4. Assumed source abundances

One of the main objectives in propagation studies is the determination of the source composition of cosmic rays by propagating the observed abundances near the Earth back through the travelled path. Nevertheless, due to the nature of transport equations, it is necessary to assume a source composition as initial abundance, propagate it forward to near the Earth and compare the resulting abundances with experimental measurements. According to the WST, source abundances are an input parameter which play the role of initial value of the composition function $F_i(x)$.

As described in Chapter 3, elements with charge over 65 are synthesised in the Universe predominantly by neutron capture processes, which are classified as slow (s-process) or rapid (r-process) according to the ratio between the time elapsed between two consecutive neutron captures and the half lifetime of the originated nuclei (see references in chapter 3).

Each of such formation processes occurs in distinct scenarios in which specific astrophysical conditions and seed material are given. The nuclei created according to these processes are accelerated by SNR shock waves (see discussion in section 4.1), cosmic ray composition at this point (*i.e.* after its production and acceleration) is what it is understood

as source compositions in terms of propagation. It is considered that the acceleration mechanism does not introduce any modification to the cosmic ray chemical composition and therefore one can consider that the nucleosynthesis processes are somehow responsible to the source abundances. In consequence, it is reasonable to assume source abundances by taking into account the formation processes (mainly r and s).

Assuming that the abundances in the primitive solar nebula were the same that in the sun, elemental abundances in the Solar System (SS), the so-called SS abundances, are referred to those in the sun. In practice, meteoritic abundances have been chosen as a practical standard for the compilation of the abundances of most of the elements. Therefore, SS abundances are based upon the abundances of elements relative to Silicon in C1 carbonaceous meteorites [Cam82] & [And82]. SS abundances are periodically updated according to improved measurements [And89] & [Gre98]

The SS abundances of heavy nuclides, are considered to be predominantly a result of mixture of material built up by both, the r- and s-neutron capture processes. As the physics of the s-process is better understood than that for the r-process, it is possible to calculate rather straightforward the contribution of the s-process (N_s^i) to the SS abundances (N_{SS}^i), so the contribution of the r-process (N_r^i) can be estimated by substracting both abundances ($N_r^i = N_{SS}^i - N_s^i$) [Bin85].

In the present work, two different source abundances have been assumed, the SS abundances [And89] and a pure r-process abundances [Bin85]. Both abundances are normalised to silicon (Si=10^6) as given in references.

The First Ionisation Potential correction

When Solar System abundances are compared to galactic cosmic ray source (GCRS) composition which is obtained de-propagating experimentally measured abundances at the Earth, significant deviations can be detected, in particular a certain enhancement of the heaviest element abundances. The interpretation of the difference between both abundances can be addressed to the nuclear physics associated to the nucleosynthesis processes, and/or to atomic properties of the traveling elements. In figure 4.10 the ratio between GCRS and SS abundances are plotted versus the First Ionisation Potential (FIP) of the elements considered, evidencing a definite pattern which is known as FIP effect [Cas78] & [Mey98]. Alternatively, volatility characterised by the condensation temperature, and mass-to-charge ratio have been pointed to the atomic property which best organise the GCRS composition [Mey97], [Mey98] & [Dru99].

As is can be seen, in figure 4.10, heavy elements with low FIP values ($\lesssim 8.5$ eV) are enhanced relative to those with high FIP values ($\gtrsim 11$ eV). This fact may be interpreted as preferential acceleration mechanism which can take place at the sources before acceleration by SNR shock waves or during injection, as already described in section 4.1.1.

In order to parametrise the FIP effect a fractionation function for the source material has been proposed [Let84].which have to multiply the assumed initial abundances if

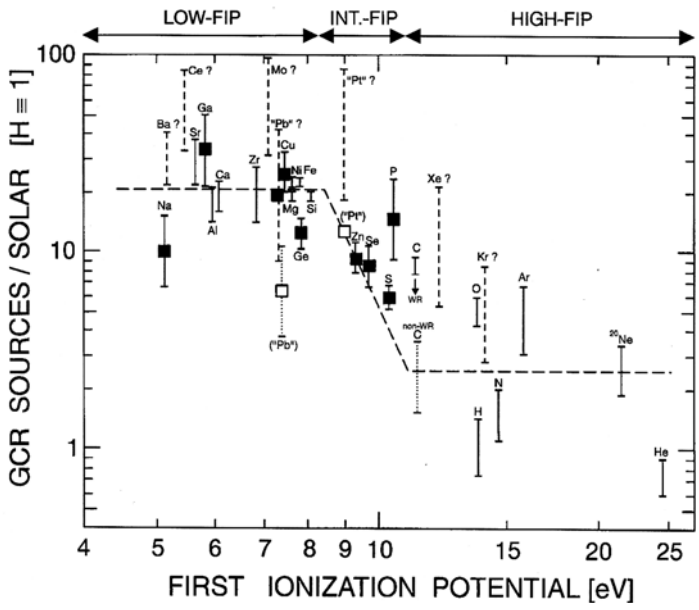

Figure 4.10. Standard GCRS to SS abundace ratio versus FIP [Mey97]

FIP effect is taken into account:

$$f(FIP) = \begin{cases} 1 & FIP < 7 \text{ eV} \\ \exp\{-0.27\,(FIP - 7)\} & 7 \text{ eV} \leq FIP \leq 13.6 \text{ eV} \\ 0.168 & FIP > 13.6 \text{ eV} \end{cases} \tag{4.19}$$

So, the input source abundances of cosmic ray are modified by this function, reducing the abundances of high FIP elements. In this work the effect of including the FIP correction ha been studied.

4.3.5. Assumed Path Length Distribution

According to the WST for the LBM, the equation describing the astrophysics of the propagation mechanism of cosmic rays, equation 4.9, leads to an exponential type function solution:

$$G(x) = \frac{1}{\lambda_{esc}} \exp\left\{-\frac{x}{\lambda_{esc}}\right\} \tag{4.20}$$

where the integral of this function over the traversed matter x is normalised to unity, thus, obtaining a real Path Length Distribution (PLD) function.

Alternatively, a truncated exponential function has been more commonly used as PLD function for the LBM [Pro81], [Cli93], [Wad96] & [Wad98]:

$$G(x) = \begin{cases} \frac{1}{\lambda_{esc}} \exp\left\{-\frac{(x-T)}{\lambda_{esc}}\right\} & x \geq T \\ 0 & x < T \end{cases} \tag{4.21}$$

This PLD function forces any particle to traverse at least some finite amount of matter from the source, T (in g/cm^2), before reaching the observer.

If the Nested Leaky Box model (NLBM) is used for propagation calculations instead of the LBM, only the PLD function must be changed as nuclear physics for both models is the same. A double exponential function is proposed for the NLBM [Cow75]:

$$G(x) = \frac{1}{x_1 - x_2} \cdot \left[\exp\left\{-\frac{x}{x_1}\right\} - \exp\left\{-\frac{x}{x_2}\right\}\right] \tag{4.22}$$

where x_1 is the escape mean free path of cosmic rays in the ISM region and x_2 is the mean free path characterising the source region. Both parameters can be calculated with:

$$\begin{aligned} x_1 &= \lambda_{esc} \\ x_2 &= 1.9 \exp\left\{-\frac{\varepsilon}{7.85}\right\} \end{aligned}$$

being ε the energy of the propagating particle.

The escape probability

The escape probability characterised by the escape mean free path, which is the main free parameter in the LBM, determines how easily a given cosmic ray nuclei can escape from the confining magnetic field of the galaxy. So that, the larger the escape length, the lower the probability of a particle to escape from observation. Several attempts have been realised in order to introduce an energy dependence on the escape mean free path, λ_{esc}. One of the most commonly used expressions for this parameter is [Orm78], [Cli93]:

$$\lambda_{esc} = \begin{cases} \lambda_{esc,0} & R \leq 7.6 \text{ GV} \\ \lambda_{esc,0} \left(\frac{7.6}{R}\right)^{\delta} & R > 7.6 \text{ GV} \end{cases} \tag{4.23}$$

with R, the rigidity of the particle (in units of GV), $\lambda_{esc,0}$ and δ are adjustable parameters which have been found to be $\lambda_{esc,0} = 5.5$ g/cm^2 and $\delta = 0.4$ [Orm78]. An alternative expression for the escape length is [Bre85] & [Wad85]:

$$\lambda_{esc} = \begin{cases} 26.9 \left[1 + \left(\frac{1.88}{R}\right)^2\right]^{3/2} & R \leq 11.4 \text{ GV} \\ 25.8 R^{-0.7} & R > 11.4 \text{ GV} \end{cases}$$

Once the PLD function has been chosen (single exponential, truncated exponential or double exponential), the associated mean free path can be taken as constant or as rigidity dependent according to expression 4.23.

4.3.6. Other assumed parameters

Despite the energy spectrum of cosmic rays is not taken into account in the LBM transport equation, the energy of cosmic rays plays a significant role due to the dependence on it of several parameters such as total and partial inelastic cross sections and the escape probability. Most of such parameters have an energy threshold beyond which constant values of these parameters are achieved. Calculations have been performed at several energy values which have been taken constant during the propagation process because energy loss and gain are neglected. The selected energies which are compatible with those having cosmic ray nuclei recorded in the UHCRE are: 0.5 GeV/n, 1.0 GeV/n, 2.0 GeV/n, 3.0 GeV/n, 5.0 GeV/n.

The composition of ISM gas has been assumed to be formed by pure hydrogen, neglecting thus the contributions of helium atoms ($\backsimeq 10\%$). This assumption allows to take the proton mass (m_p) as the mean interstellar atomic mass ($\overline{m}$). On the other hand, the calculated interaction and spallation mean free paths values may be significantly modified if helium atoms are assumed to be present in ISM, affecting thus propagation results.

In addition, the ISM atomic mean density ($\overline{n}$) has been taken constant along the trajectory of cosmic ray particles, fixing its value at 0.3 atoms/cm^3 [Wie80] & [Gar81].

4.4. Propagation results

4.4.1. Test of verification

In the present work, the WST has been adopted to solve the LBM transport equations. According to the WST, an equation of type 4.7 is assigned to every considered cosmic ray particle. The resulting system of differential equations can be solved either analytically or numerically. Numerical solutions are easily determined using the Runge-Kutta-Fehlberg method which allows to control several mathematical parameters such as the grammage step, dx, and the number of iterations. Analytical solutions can be laborious to obtain, specially for the lightest considered particles which have the contribution of all heavier particles. However, the solution is straightforward for some specific cases.

Therefore, in order to verify that our numerical method gives results consistent with those obtained from the analytical solution, a simple example is considered. Assuming a pure $^{208}_{82}$Pb source, the study is stressed to the $^{205}_{81}$Tl nuclei, in order to minimise the sum over spallation products. With such conditions, the system of two differential equations for the composition functions is:

$$\frac{dF_{82}}{dx} = -\frac{F_{82}}{\lambda_{int}^{82}} \tag{4.24}$$

$$\frac{dF_{81}}{dx} = -\frac{F_{81}}{\lambda_{int}^{81}} + \frac{F_{82}}{\lambda_{spall}^{82\rightarrow 81}} \tag{4.25}$$

Equation 4.24 can be very easily solved analytically, obtaining, thus, the exact solution for $F_{82}(x)$ which is required to determine $F_{81}(x)$:

$$F_{82}(x) = F_{82}(x=0)\exp\left\{-\frac{x}{\lambda_{int}^{82}}\right\}$$

$$F_{81}(x) = \frac{1}{\lambda_{spall}^{82\to 81}} \cdot \left(\frac{1}{\frac{1}{\lambda_{int}^{81}} - \frac{1}{\lambda_{int}^{82}}}\right) F_{82}(x=0) \cdot \left[\exp\left\{-\frac{x}{\lambda_{int}^{82}}\right\} - \exp\left\{-\frac{x}{\lambda_{int}^{81}}\right\}\right] \qquad (4.26)$$

being $F_{82}(x=0)$ the source abundance of $^{208}_{82}$Pb element ($F_{81}(x=0)$=0, as a pure lead source is assumed).

The numerical solution for the composition function $F_{81}(x)$ is generated by solving the system of equations 4.24 & 4.25 by means of the Runge-Kutta-Fehlberg method taking a grammage step of 0.001 g/cm^2 which ensures the requirements of accuracy. The number of iterations has been chosen to be 10000 leading a total path length traversed of 10.0 g/cm^2. Parametric fit expressions for interaction and spallation cross sections (see equation 4.13 & 4.17) have been evaluated at an energy of 3.0 GeV/n, obtaining:

$$\frac{1}{\lambda_{int}^{81}} = 0.880\ (\text{g/cm}^2)^{-1} \qquad \frac{1}{\lambda_{int}^{82}} = 0.888\ (\text{g/cm}^2)^{-1} \qquad \frac{1}{\lambda_{spall}^{82\to 81}} = 0.059\ (\text{g/cm}^2)^{-1}$$

The analytical solution from equation 4.25 and the numerical solution are compared in figure 4.11, in which the composition function for the $^{205}_{81}$Tl nuclei is plotted as a function of the grammage x (in g/cm^2), taking an initial lead abundance to be $F_{82}(x=0) = 10^3$ nuclei/s.

Actually, the curve obtained from the numerical solution and that obtained from the analytical solution overlap, evidencing an excellent agreement between both solutions. Nevertheless, in order to distinguish both solutions, the peak of each curve can be determined. Analytically, the peak position is obtained optimizing the composition function $F_{81}(x)$:

$$x_{peak} = \left(\frac{1}{\frac{1}{\lambda_{int}^{81}} - \frac{1}{\lambda_{int}^{82}}}\right) \ln\left(\frac{\lambda_{int}^{82}}{\lambda_{int}^{81}}\right)$$

Taking the above values for the mean free paths, the peak is found to be located at $x_{peak} = 1.1312$ g/cm^2 with a peak value of 24.39 particles/s, while the numerical solutions shows a peak at $x_{peak} = 1.1314$ and a peak value of 24.41. According to these results, the peak position agree to within 0.02% and the peak value differs by less than 0.08%.

The last step is to determine the abundance of the $^{205}_{81}$Tl nuclei, N_{81}, by integrating the composition function $F_{81}(x)$ weighted by a PLD function, since it represents an estimation of the measurable abundance. A truncated PLD function given in equation

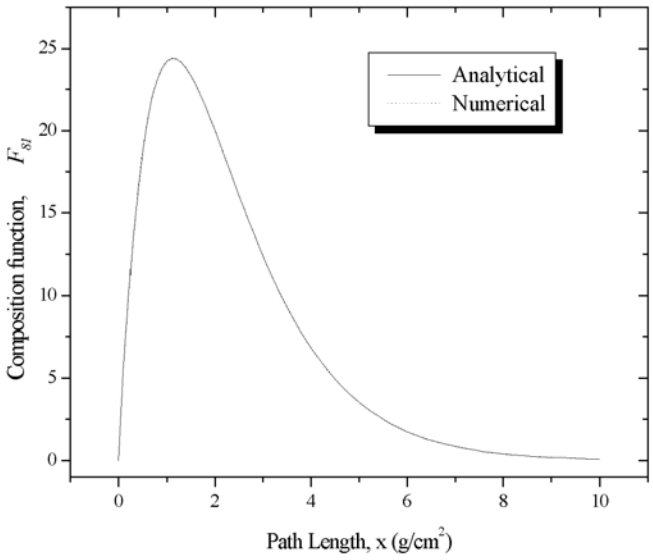

Figure 4.11. Comparison between analitycal (solid line) and numerical (dotted line) solutions to the $^{205}_{81}$Tl as a function of the path length.

4.21 with $\lambda_{esc} = 5.5$ g/cm^2 and $T = 1.0$ g/cm^2 has been assumed and multiplied by the composition function $F_{81}(x)$ according to equation 4.8, and finally integrated from zero, corresponding to a very close source, to infinity, corresponding to a very long path length traversed by cosmic ray nuclei. Taking expression 4.26 and 4.21, the analytical solution can be determined:

$$N_{81} = \frac{1}{\lambda_{esc}} \cdot \frac{1}{\lambda_{spall}^{82\rightarrow 81}} \cdot \left(\frac{1}{\frac{1}{\lambda_{int}^{81}} - \frac{1}{\lambda_{int}^{82}}} \right) F_{82}(x=0) \cdot \left[\left(\frac{1}{\frac{1}{\lambda_{int}^{82}} - \frac{1}{\lambda_{esc}}} \right) \exp\left\{ -\frac{T}{\lambda_{int}^{82}} \right\} - \left(\frac{1}{\frac{1}{\lambda_{int}^{81}} - \frac{1}{\lambda_{esc}}} \right) \exp\left\{ -\frac{T}{\lambda_{int}^{81}} \right\} \right] \tag{4.27}$$

On the other hand, numerical integration is also straightforward using the trapezoid's rule. Although the integration should be done from zero to infinity, in the numerical treatment a finite upper limit has adopted. As figure 4.11 shows, the composition function drops to near zero for $x \gtrsim 9$ g/cm^2, so that, extending the integration upper limit beyond 10 g/cm^2 will not introduce a significant variation to the final result. The abundance value, N_{81}, provided by both treatments are, 8.00649 for the numerical integration and 8.01265 using equation 4.27. The numerical integration result differs from the analytical exact solution by less than 0.08%.

4.4.2. Effects of varying parameters

As described in the previous section, there are several parameters, appearing in the propagation model, which can be varied, such as the cross sections expressions, the source abundances, the PLD function and the nature of propagating particles (i.e. elements or isotopes). The WST allows to study the effects introduced by the variation of these parameters into propagation results. For such purposes, two different kinds of plots are provided depending on if the variation of the parameter would be numerically significant. So, by default, the final abundances resulting of the propagation calculation will be plotted as a function of the charge. In the case that such plots would be overlapped, then the fractional difference will be given. The fractional difference between two sets of abundances (n_i, n_j) is defined by [Cli93]:

$$FD(i;j) \equiv \frac{n_i - n_j}{n_i + n_j}$$

Obviously $FD(i;j) = 0$ if $n_i = n_j$ and $FD(i;j) = +1$ or -1 if one of the set of abundances is zero. In order to calculate the fractional differences, normalised sets of results (n_i, n_j) are required.

A fixed set of parameter will be taken by default as a standard configuration, thus, all propagation results will be calculated taking this standard configuration unless otherwise indicated. The parameter values which have been chosen for the standard configuration are:

- Solar system source abundances [And89].
- FIP correction is included (equation 4.19).
- Semiempirical fit formulae for all cross sections (equations 4.11, 4.12 & 4.16).
- Propagation energy value of 3.0 GeV/n.
- Truncated exponential PLD with $\lambda_{esc} = 5.5$ g/cm^2 and $T = 1.0$ g/cm^2 (equation 4.21).
- Propagation performed by elements having charge comprised between 65 and 92.

Varying cross sections

Among all available treatments which have provided expressions for the total and partial cross sections, only parametric fits and semiempirical fits formulae have been considered. Energy has been the first parameter under study as all expressions display an energy dependence.

Figure 4.12 shows the different set of propagated abundances relative to lead, which has been obtained at energies 0.5 GeV/n, 1.0 GeV/n, 2.0 GeV/n, 3.0 GeV/n and 5.0 GeV/n using parametric fit expressions for the cross sections. As it can be seen, for energies

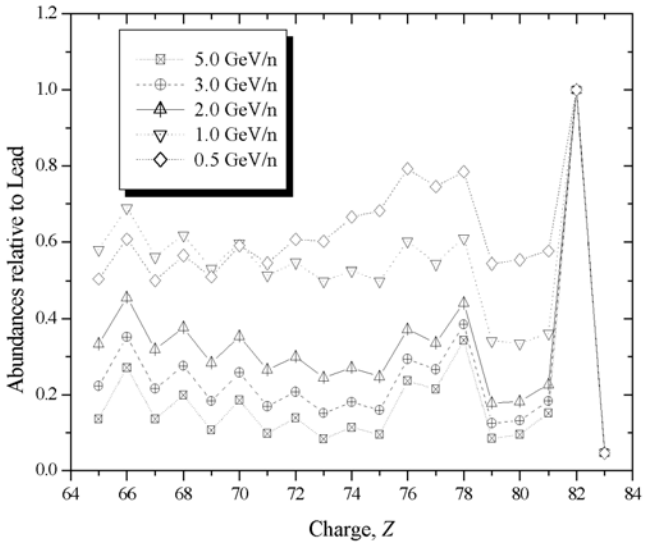

Figure 4.12. Propagated abundances relative to lead calculated using parametric fit expressions for fragmentation cross sections for several considered energies.

over 1.0 GeV/n, all the resulting abundances follow the same pattern, whereas a different behaviour is observed for the lowest energy. Furthermore, the abundance distribution at 0.5 GeV/n shows an enhancement for those elements belonging to the platinum peak with charge $74 \leq Z \leq 79$. In addition, this distribution crosses the abundance distribution corresponding to 1.0 GeV/n at $Z = 70$ indicating that at lower energies the parametric cross sections contribute significantly to the fragmentation of lead group elements to platinum group elements (*i.e.* low ΔZ), while cross section values for large ΔZ are underestimated with respect to the reference ones.

If semiempirical fit expressions are used instead of parametric ones, the resulting abundances at different energies overlap when they are drawn. So that, only propagated abundances et 0.5 GeV/n and 5.0 GeV/n are plotted in figure 4.13 in which it is stressed that energy is not a very significant parameter in semiempirical cross sections.

In order to compare between the effects of semiempirical and parametric cross section formulae, propagation results using both expressions at a fixed energy of 2.0 GeV/n are plotted in figure 4.14. From the figure it is inferred that although both distributions display the same behaviour, the parametric results are clearly overabundant with respect to semiempirical ones, evidencing that fragmentation of cosmic ray nuclei is overestimated by the semiempirical expressions.

Fractional differences between the semiempirical and the parametric set of propagated abundances at 0.5 GeV/n and 5.0 GeV/n are plotted in figure 4.15, which shows

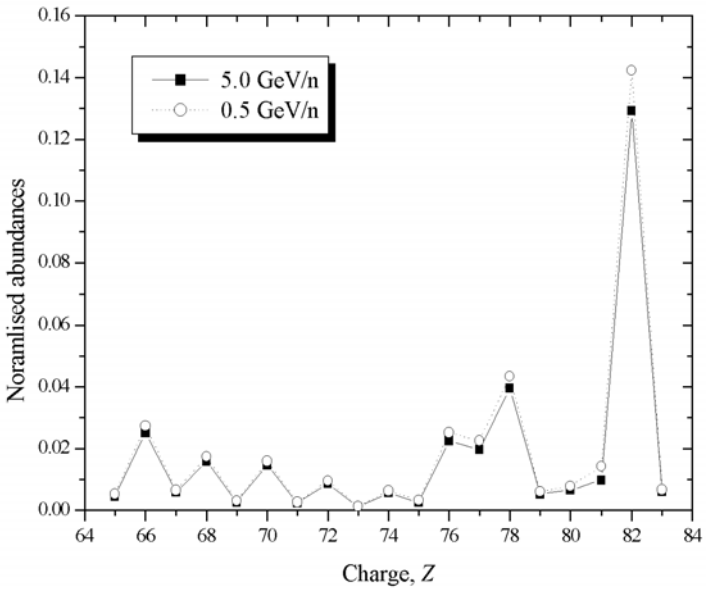

Figure 4.13. Propagated abundances relative to lead calculated using semiempirical fit expressions for fragmentation cross sections for two different energies.

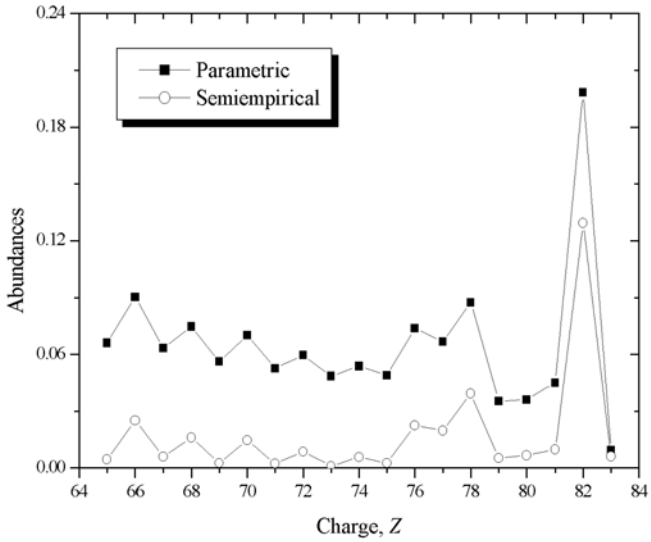

Figure 4.14. Propagated abundances in arbitrary units calculated using parametric and semiempirical fit expressions for fragmentation cross sections at 2.0 GeV/n.

that maximum discrepancies between both distributions are achieved for low energy values. Particularly critical is the case of $Z = 73$ in which a FD value close to -1 (at 0.5 GeV/n) is obtained indicating that N_{73} evaluated with semiempirical cross sections is near to zero due to its overestimated fragmentation together with low spallation contribution of heavier elements.

Varying source abundances

In order to evidence the effects of propagation on the assumed source abundances (SS_0), the fractional difference between them and the resulting propagated abundances is plotted in figure 4.16. which shows that final abundances (SS_P) are significantly distorted due to the propagation mechanism. The fact that for those nuclei with $Z \leq 76$, the FD value is positive, indicates that heavier nuclei have broken up during their eventful travel from sources, thus contributing to increase the abundance of lighter nuclei. In other words, figure 4.16 elucidates fragmentation effects of propagation.

There are two different source compositions available, the SS abundances and the r-process abundances. Figure 4.17 illustrates the propagated abundances relative to lead when both types of sources are considered. The enhancement of the platinum peak elements for an r-process source is inferred from figure 4.17. This feature can be also stressed in figure 4.18 in which the lower negative values of FD between propagated SS and r-process

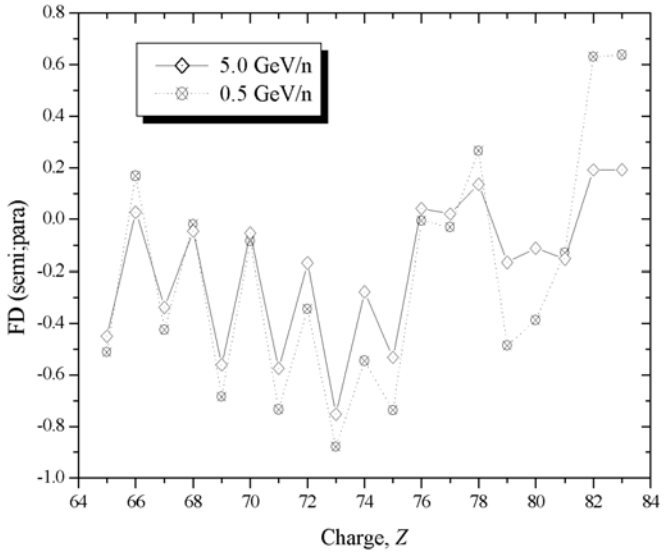

Figure 4.15. Fractional differences between propagated abundances as predicted by semiempirical and parametric fits at 0.5 GeV/n and 5.0 GeV/n.

abundances are achieved for platinum peak elements having charge $75 \leq Z \leq 79$ and higher positive FD values are obtained the lead peak elements.

Figure 4.18 also evidences that the FIP correction to the source composition has no significant effect on the propagation results as no distortion to the FD curve is introduced when the FIP correction is removed.

Varying the path length distribution

As depicted in previous section, the PLD function characterises the propagation model. In the case of LBM a single exponential (equation 4.20) or a truncated exponential (equation 4.21) are obtained, while a double exponential PLD function corresponds to the NLBM (equation 4.22).

Results of the propagation using a LBM are compared to those obtained by applying a NLBM in figure 4.19 in which the fractional differences between both abundance sets are plotted. As it can be seen, NLBM has favored the abundances of the heaviest nuclei (those with $Z \gtrsim 76$) since in this charge region, negative FD values are obtained, whereas abundances of lower charge region nuclei (having $Z \lesssim 76$) has been enhanced by the LBM.

The associated PLD function to the LBM allows to control several parameters such as $\lambda_{esc,0}$ and/or δ depending on if the escape mean free path is considered rigidity dependent or not according to equation 4.23. Figure 4.20 shows the FD between the propagated SS

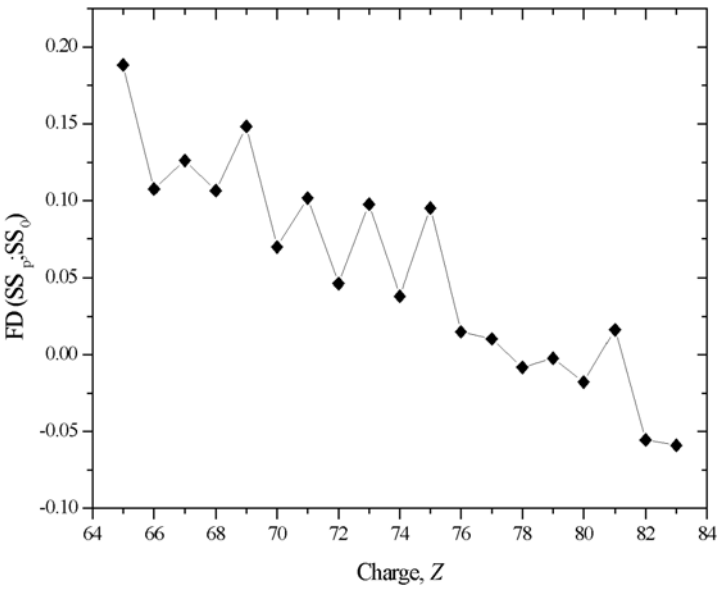

Figure 4.16. Fractional differences between the propagated and the source abundances of SS type.

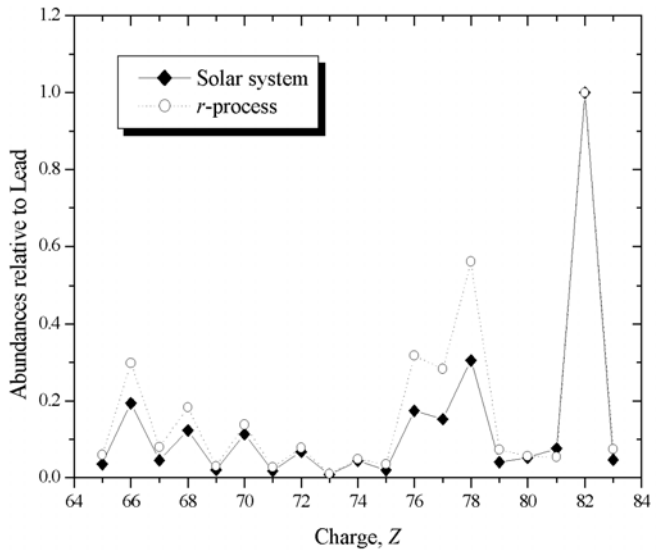

Figure 4.17. Propagated abundances relative to lead assuming a SS and r-process source composition .

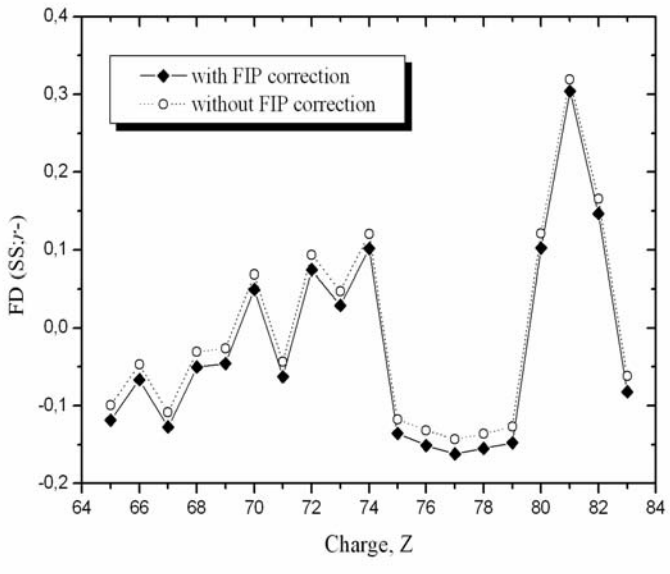

Figure 4.18. Fractional differences between propagated SS abundances and propagated r-process abundances with and without the FIP correction.

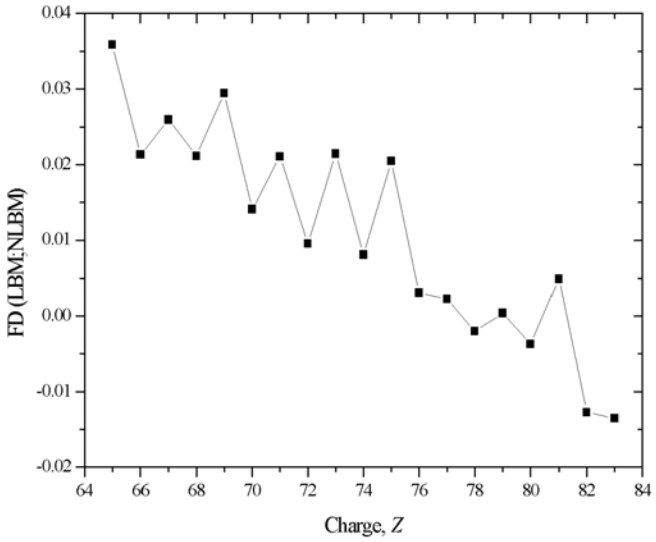

Figure 4.19. Fractional differences between propagated abundances under LBM and NLBM

abundances taking two different values of $\lambda_{esc,0}$: the standard value of 5.5 g/cm^2 and a larger value $\lambda_{esc,0} = 8.0$ g/cm^2. From the figure it is inferred that propagation is not very sensitive to this parameter, indicating, hence, that the escape length can not be reliably determined.

The effect of the variation of the truncation value, T, is illustrated in figures 4.21 and 4.22 in which semiempirical and parametric predicted cross sections are respectively used to determine the propagated abundances.

Comparing both figures, it can be seen that propagation with parametric fit cross sections are more sensitive to the truncation value than if semiempirical cross sections are used. Although, in both cases, the variation of the truncation T seems to introduce no significant distortion to final results, a couple of features can be addressed:

(i) The abundances of nuclei in the lowest charge region ($65 \leq Z \leq 75$) are increased when larger T values are considered.

(ii) The abundances of Pt and Pb nuclei drop for higher T values but at different rate, so that, the relative abundance between these elements becomes significantly modified for different truncations of the PLD function.

Figure 4.23 illustrates the effects of propagation at 1.0 GeV/n and 5.0 GeV/n using the energy dependent PLD function for the NLBM (according to equation 4.22). It can be seen that for the bulk propagated elements, FD is positive indicating an overabundance for low energy compared to higher energies. Actually the low values of FD shows that energy does not play a significant role in the propagation using NLBM.

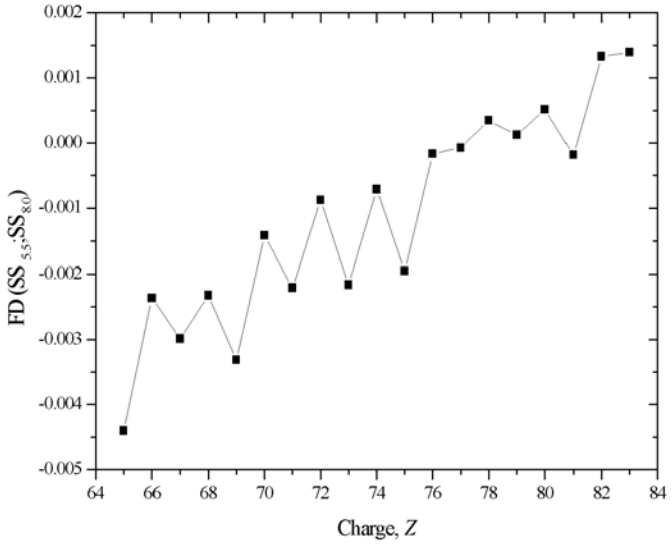

Figure 4.20. Fractional differences of propagated abundances calculated with an escape length of 5.5 g/cm^2 and 8.0 g/cm^2.

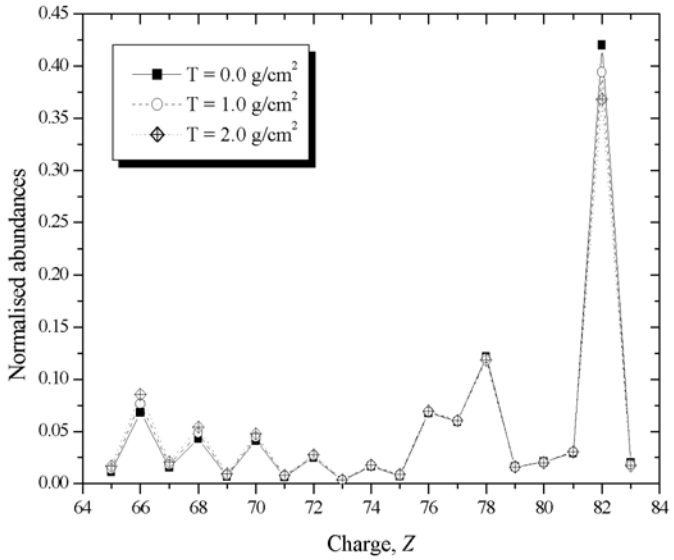

Figure 4.21. Normalised abundances calculated at several truncation values of the PLD function using the spallation cross sections predicted by semiempirical fits.

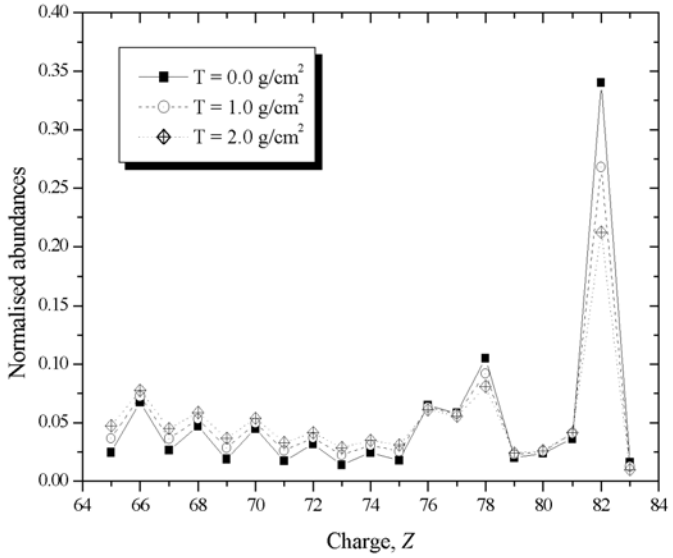

Figure 4.22. Normalised abundances calculated at several truncation values of the PLD function using the spallation cross sections predicted by parametric fits.

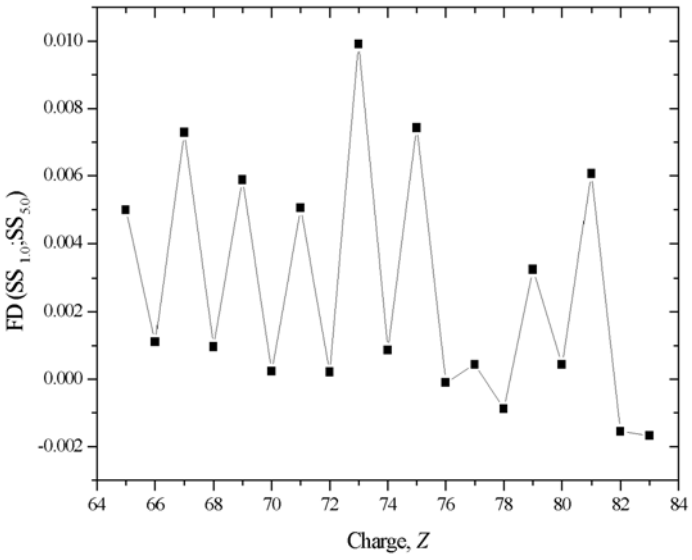

Figure 4.23. Fractional differences between propagated abundaces under NLBM at 1.0 GeV/n and 5.0 GeV/N.

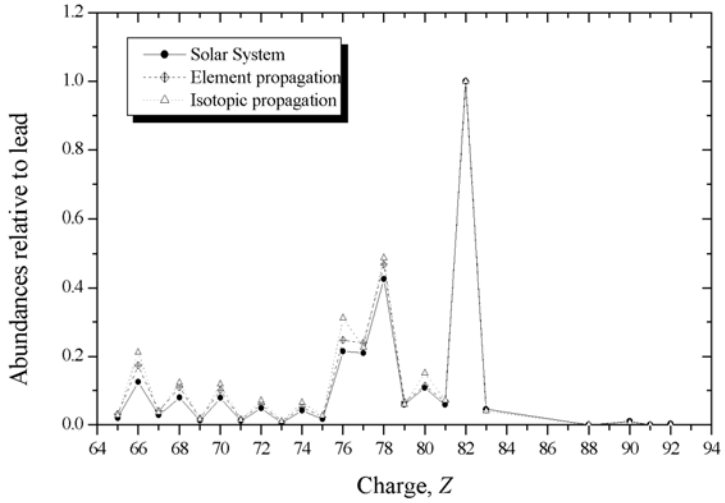

Figure 4.24. Elemental and isotopic propagated abundances relative to lead calculated from SS source abundances which are also plotted.

Assumed propagating particles

The transport of ultra heavy cosmic rays with charge over 65 can be carried out considering only those elements belonging to this charge region, leading, thus, a total of 19 traveling particles. The set of particles involved on the propagation can be enlarged to a total of 80 if all isotopes of the same charge region are taken into account.

The unique formula which allows to calculate isotopic fragmentation cross sections comes from semiempirical fits. For that reason, only cross sections predicted by semiempirical fits will be used for element and isotopic propagation.

Figure 4.24 illustrates the differences between element propagation and isotopic propagation at 10.0 GeV/n, SS source composition is also plotted. Alternatively, in figure 4.25 propagated abundances relative to lead at 2.0 GeV/n with an r-process source for both sets of traveling particles are plotted. An enhancement of the platinum group elements, specially for $Z = 76$, can be seen when the propagation is performed taking all 80 isotopes.

In order to confirm that the effects of varying the energy and the truncation value performing an isotopic propagation are similar to those concerning element propagation, figures 4.26 and 4.27 are supplied. In figure 4.26 isotopic propagation results at 0.8 GeV/n and 5.0 GeV/n are compared by means of fractional difference. Except for $Z = 91$, the FD values for the remaining elements are very close to zero indicating that isotopic spallation cross sections are not sensitive to variations of energy. Propagated abundances calculated

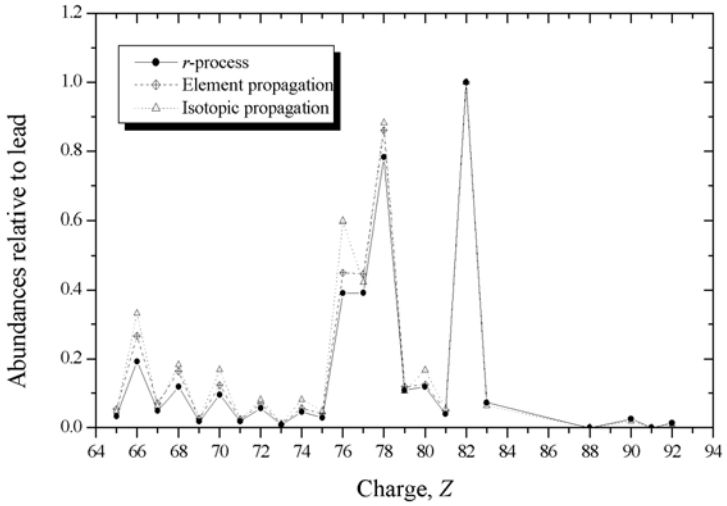

Figure 4.25. Elemental and isotopic propagated abundances relative to lead calculated from r-process source abundances which are also plotted.

with a truncated PLD function at 3.0 GeV/n are plotted in figure 4.27. The behaviour of such abundances for different truncation values are the same of that observed in figures 4.21 and 4.22.

4.4.3. Comparison with observations from UHCRE

In order to make a reliable comparison between the propagated abundances with the LBM and the measured abundances from UHCRE, intrinsic charge uncertainty achieved in experimental results has to be taken into account. Therefore, for each element, the resulting abundance N_i is distorted by a gaussian function which is centered to the corresponding charge value, Z_i, with an standard deviation equals to the assumed charge uncertainty, σ_Z. Each of such gaussian functions are extended from $-3\ \sigma_Z$ to $+3\ \sigma_Z$ containing, thus, the 99.73% of the total area. Then, gaussian functions for each element are summed, obtaining a continuous curve which becomes a distribution curve after a proper normalisation. Figure 4.28 elucidates the aspect of one of such distribution curve which has been obtained by propagating all isotopes assuming a SS source abundances, using semiempirical cross sections at 2.0 GeV/n with a truncated PLD function at $T = 1.0$ g/cm^2 applying a fixed charge uncertainty $\sigma_Z = 1.5$.

The abundance distribution effected by a charge uncertainty can, then, be compared to the experimental results from UHCRE by estimating the χ^2 statistical parameter

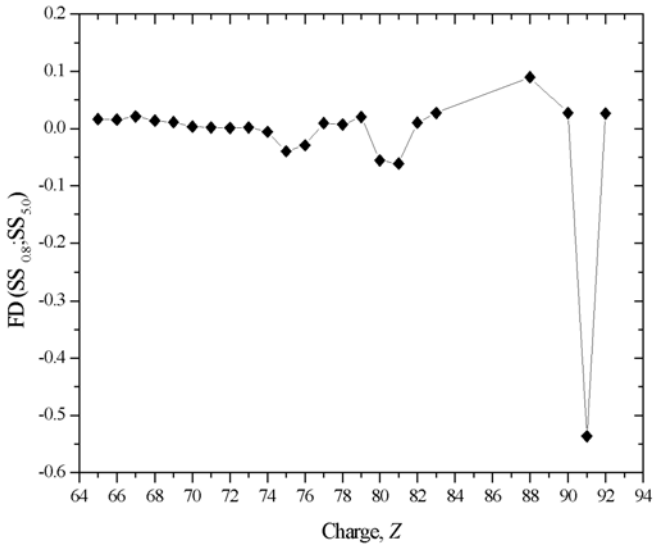

Figure 4.26. Fractional differences between isotopic propagation results using cross sections predicted by semiempirical fits at 0.8 GeV/n and 5.0 GeV/n.

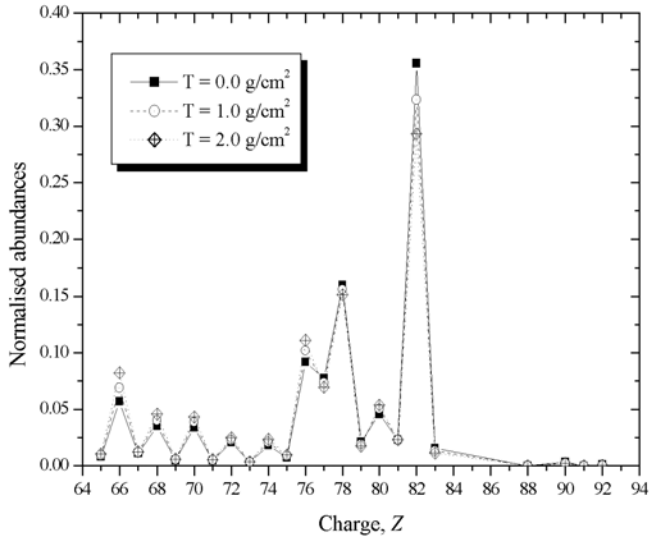

Figure 4.27. Normalised abundances calculated at several truncation values of the PLD function using the spallation cross sections predicted by semiempirical fits taking all isotopes with carge over 65 as propagating particles.

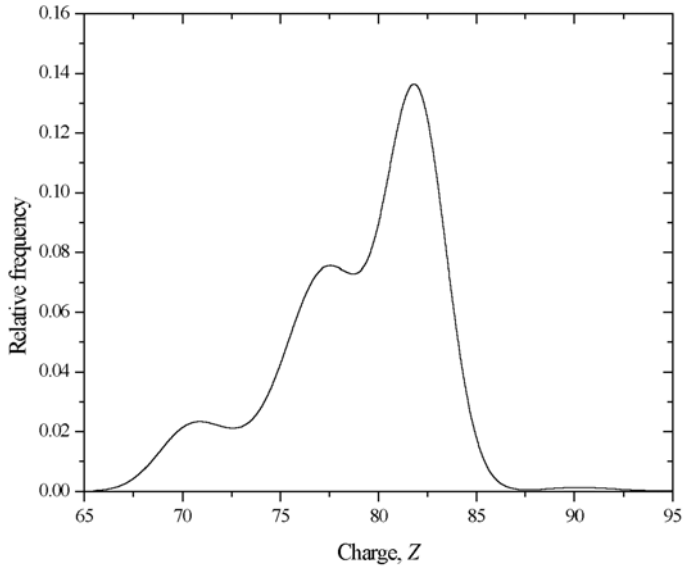

Figure 4.28. Abundance distribution obtained by modifying the propagated abundances by a charge uncertainty of 1.5.

which accounts for the goodness of the fit between the observed frequencies provided by the UHCRE measured abundances and the expected frequencies obtained from propagation calculation. The statistical parameter χ^2 is defined by:

$$\chi^2 = \sum_{i=1}^{k} \frac{(o_i - e_i)^2}{e_i} \tag{4.28}$$

where o_i are the observed frequencies, which in our case are the measured abundances given by UHCRE, and e_i are the expected frequencies which can be determined from the propagated abundances affected by σ_Z. In order to evaluate properly the χ^2 parameter according to expression 4.28, the number of degrees of freedom, ν, has to be known. The number of degrees of freedom can be determined by $\nu = k - 1$, being k the number of observed frequencies.

A study of χ^2 taking different sets of transport parameters will allow to select a candidate configuration which best describes the propagation of ultra heavy cosmic rays nuclei with charge over 65 according to the measured abundances in UHCRE and, thus, determine the source composition of such elements.

The propagated abundance distribution may be affected by several charge uncertainties values, leading, thus, different χ^2 values. In order to evidence the effect of varying the charge uncertainty, σ_Z, on χ^2, three distinct configurations for the propagation have

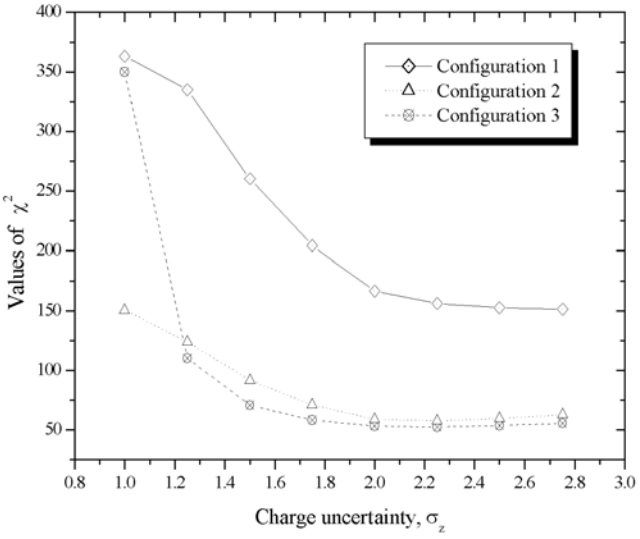

Figure 4.29. The variation of the statistical parameter χ^2 as a function of the charge uncertainty introduced to the propagated abundances using the LBM, for three different configurations of the propagation parameters (see text for details).

been adopted and the resulting abundances are contaminated by the following values of σ_Z: 1.0, 1.25, 1.5, 1.75, 2.0, 2.25, 2.5, 2.75. The first configuration assumes: only elements with $Z \geq 65$, an r-process source type with FIP correction, parametric cross sections at 1.0 GeV/n and a truncated PLD function at $T = 1.0$ g/cm^2, while the second configuration coincides with the first one but taking semiempirical cross sections at 2.0 GeV/n with a truncation value of $T = 1.5$ g/cm^2. The third configuration considers all isotopes with $Z \geq 65$, a SS initial abundances without FIP correction, cross sections predicted by semiempirical fits at 3.0 GeV/n and an exponential PLD function without truncation. Figure 4.29 illustrates the results of the estimated χ^2 values as a function of the assumed charge uncertainty for the three configurations. From this figure, two main features can be derived:

(i) When propagation calculation is performed either for elements as well as for isotopes using semiempirical cross sections, a χ^2 minimum value indicating a best fit is achieved for a charge uncertainty $\sigma_Z = 2.25$ which is consistent with the charge uncertainty assigned to the UHCRE measurements.

(ii) If propagation is carried out taking parametric cross sections, not only no relative minimum χ^2 value is observed (the higher the σ_Z, the lower the χ^2), but also worst values of the statistical parameter are obtained [Font97] & [Font99a].

According to the second feature, expressions of parametric cross sections may be excluded in those propagation calculations which are compared to UHCRE results. For

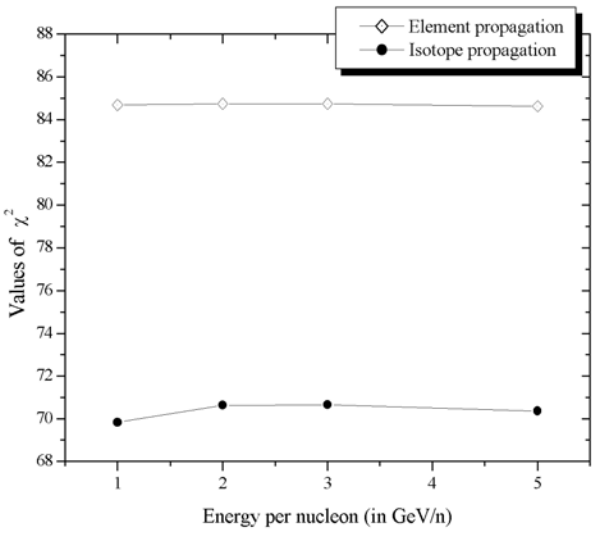

Figure 4.30. Variations of the χ^2 parameter as a function of the energy of cosmic ray particles. Transport has been performed taking two different sets of propagating particles, the elements and isotopes having charge over 65.

other propagation configurations, the minimum χ^2 value is shifted to $\sigma_Z = 2.0$ or $\sigma_Z = 2.5$, so hereinafter, χ^2 values are only calculated for a charge uncertainty comprised between 2.0 and 2.5 depending on which of them provides the best fit.

In order to study the effects of varying the energy by means of the χ^2 parameter, the standard configuration of the propagation parameters has been assumed, and transport calculations have been carried out by elements as well as by isotopes at different energy values which are compatibles with those of cosmic ray nuclei recorded in UHCRE (1.0 GeV/n, 2.0 GeV/n, 3.0 GeV/n and 5.0 GeV/n). Results are illustrated in figure 4.30.

As can be seen in figure 4.30, χ^2 values for an isotopic propagation are significantly lower than those for an element propagation. This difference is also observed when other propagation parameters are modified. In consequence, hereinafter, all propagations are performed by considering all isotopes as traveling particles, excluding, thus, any propagation by elements. Figure 4.30 also shows that χ^2 parameter has not varied remarkably in the chosen energy range, stressing, thus, that propagation results are not sensitive to the variations of energy.

Source composition is another parameter which can be changed in the transport equations. It is possible to differentiate four kinds of source abundances: SS and r-process abundances, both can be modified by the FIP correction. Performing the propagation for isotopes at 3.0 GeV/N with a truncation $T = 1.0$ g/cm^2 for the PLD function, the resulting χ^2 values are given in table 4.1.

Table 4.1. Values of the χ^2 statistical parameter calculated by different assumed source composition.

χ^2	SS	r-process
FIP	70.66	37.89
No FIP	49.64	27.23

Table 4.2. Values of the χ^2 statistical parameter calculated by several values of the scape length.

λ_{esc}	χ^2
3.0	27.19
5.5	27.21
8.0	27.23
10.0	27.23

The calculated χ^2 values in table 4.1 shoe that an r-process source type always gives best fits than the standard SS source composition, even if FIP correction is included. Furthermore, the inclusion of the FIP effect produce a worse fit for any kind of assumed source abundances. Although this result seems not to be in agreement with what has been shown in section 4.2.2 where FIP has been found not to be a significant parameter, it has to be taken into account that χ^2 is a more sensitive parameter than the used fractional differences (see figure 4.18). According to this result, an r-process source type without FIP correction will be taken in the following calculations.

Propagation can be realised by means of the LBM or the NLBM. In order to differentiate between both models, an r-process source at 2.0 GeV/n without truncation has been assumed, leading a $\chi^2 = 27.70$ for the LBM, while a $\chi^2 = 27.20$ has been obtained for the NLBM. These results point to that LBM and NLBM are nearly indistinguishable when propagated abundances are compared to UHCRE composition measurements.

The variation of the escape length parameter appearing in the PLD function, does not introduce any significative modification to the calculated χ^2, as can be observed in table in which several values of λ_{esc} with the corresponding χ^2 value are given for a propagation energy of 2.0 GeV/n with a truncation at $T = 1.0$ g/cm^2. This result seems to confirm those which has been found in section 4.2.3 (see figure 4.20), stressing that the propagation mechanism according to the LBM is not sensitive to the escape length in the range of 3.0 g/cm^2-10.0 g/cm^2.

In order to know which truncation value gives the best fit to experimental data, figure 4.31 has been built up, in which the estimated χ^2 values are plotted for different truncations ($T = 0.0$ g/cm^2, 0.5 g/cm^2,1.0 g/cm^2,1.5 g/cm^2, 2.0 g/cm^2 and 2.5 g/cm^2) at several energies ($\varepsilon = 1.0$ GeV/n, 2.0 GeV/n, 3.0 GeV/n and 5.0 GeV/n), describing a

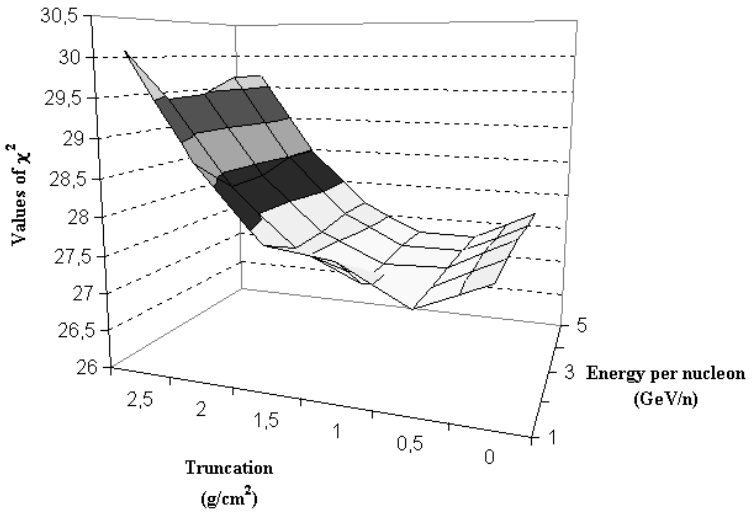

Figure 4.31. Surface drawn with the χ^2 values calculated from several combinations of values of the truncation and energy parameters.

surface in a (T, ε, χ^2) space.

As it can be seen, the minimum χ^2 value corresponds to an energy $\varepsilon = 2.0$ GeV/n and truncation at $T = 1.0$ g/cm^2, but differences between the χ^2 values obtained from all (T, ε) considered couples of parameters are small enough, not allowing to exclude any of such combinations, and consequently evidencing that both parameters (*i.e.*. truncation and energy) do not play a significant role in the propagation process when it is described by the LBM. It must be stressed that all χ^2 results on figure 4.31 are obtained taking a charge uncertainty of $\sigma_Z = 2.0$, improving the previous results [Font98a]

4.5. Discussion and Conclusions

In this chapter, propagation calculations have been performed by means of the so-called Weighted Slab Technique based on the Leaky Box Model, although the Nested Leaky Box model has also been used.

In order to establish the accuracy of the Runge-Kutta method used to solve numerically the differential equations for the compositions functions set out according to the WST, a comparison with analytical exact solutions has been done. Results of such comparison show an excellent agreement between both treatments which in the worst case they differ by less that 0.08%. An study has been effectuated accounting for the effects that have

on final integrated abundances by varying the propagations parameters such as spallation cross sections, the energy of the traveling cosmic rays, the source composition, and the path length distribution function (in terms of escape length and truncation). The main conclusions inferred from this discussion can be summarised as follows:

1. Cross sections.

a) Elements having charge lower than 76, which have been propagated using parametric cross sections are overabundant in comparison to those obtained with semiempirical cross sections. Therefore, this result indicates that predicted cross sections values from parametric fits for spallation reactions with large charge changing are slightly larger than those predicted with semiempirical fit expressions [Font97] & [Font99a]

b) Parametric fit expressions are more sensitive to the energy of the interacting cosmic ray particles than semiempirical fit formulae for which the energy in the range 0.5 GeV/n to 5.0 GeV/n does not play a significant role.

2. Source composition.

a) An enhancement of the platinum peak elements abundance is observed when a source consisting on r-process synthesised material is assumed, instead of taking an standard solar system source composition. This result is consistent with the measured abundances in the UHCRE which displays a dominant platinum peak and also a secondary less abundant lead peak [Font98b]

b) The FIP correction seems not to have a significative effect as its inclusion on the initial composition does not improve the agreement of the resulting abundances with the experimental data [Font98c].

3. Path Length Distribution.

a) Nested leaky box model with its corresponding double exponential PLD function provides rather the same results than the LBM with a truncated PLD. In addition, variation of the escape length does not modify considerably the calculated abundances.

b) Propagation results obtained using parametric cross sections seem to be more sensitive to the truncation value of the integrating PLD function.

4. Propagating particles.

a) When propagation is carried out considering all isotopes as propagating cosmic rays, an enhancement of the platinum peak group element abundances is observed with respect to the calculated abundances assuming only the most abundant isotope for a given charge as a traveling particles. This results allows to conclude that an isotopic propagation deals better with the experimental composition provided by the UHCRE measurements.

b) The effects of varying the energy and the truncation value is rather the same for element propagation than for isotopic propagation.

Once a set of parameters is fixed, transport equations are numerically solved obtaining a propagated composition which is infected by a fixed charge uncertainty, σ_Z, in order to be compared with experimental abundances measured in UHCRE. The statistical parameter, χ^2 offers an idea of the goodness of the fit. Therefore, varying the set of assumed

parameters, a different fit may be done and, consequently, a different χ^2 value is obtained. It has been found that taking semiempirical cross sections the minimum χ^2 value is always achieved for a charge uncertainty comprised between 2.0 and 2.5 which is compatible with the predicted charge uncertainty for the UHCRE measurements, in opposition to the χ^2 results for parametric cross sections with which the larger σ_Z, the lower χ^2, evidencing a meaningless physical behaviour and, thus, such expressions for the spallation cross sections may be excluded for our transport calculations.

The significance level, p, is estimated comparing the calculated χ^2 value with the corresponding χ^2_q value (with $q = 1-p$) which is provided by the χ^2 probability distribution. The χ^2_q value depends on the number of degrees of freedom, ν, which may be determined by $\nu = k - 1$ being k the number of experimental points. If propagation is carried out taking cosmic ray particles with charge comprised between 70 and 92, then $\nu = 22$, this gives a maximum χ^2_q value corresponding to $q = 0.995$ equals to 42.8. So that, all those sets of parameters which lead to a calculated χ^2 larger than $\chi^2_{0.995} = 42.8$ are not statistically significant, and, consequently, have been excluded. Only those parameters sets with which $\chi^2 < \chi^2_{0.995}$ have been taken into account. Furthermore, parameter configurations providing the lower χ^2 value will be the best fit to UHCRE measured abundances, because the lower the χ^2 value, the higher the confidence level.

According to this statistical criteria, propagation performed assuming elements as traveling cosmic rays has been excluded as well as when standard SS abundances have been taken as source composition of ultra heavy cosmic rays. In other words, only isotopes have been propagated from an r-process type source to a region near the Earth, because their corresponding χ^2 value is lower than $\chi^2_{0.995} = 42.8$. Furthermore, it has been found that if the FIP correction is not taken into account, the associated χ^2 value decreases.

The escape length, λ_{esc}, the truncation value T of the integrating PLD function and the energy are the three parameters producing a negligible impact on the propagation calculation results, as their variation does not introduce a significant modification on χ^2. The same behaviour is also observed when NLBM is applied instead of the LBM. In conclusion, the χ^2 parameter criterion does not allow to distinguish between sets of propagating parameters which differ on the energy, the PLD function (double exponential, truncated exponential) or the escape mean free path.

In that case, it would be useful to compare the abundance ratios R_1, R_2 and R_3 determined after the propagation procedure, with those calculated from UHCRE measurements. These abundances ratios are defined as [Bin88] & [Kla85]:

$$R_1 = \frac{\text{Actinide abundances } (87 \leq Z \leq 100)}{\text{Platinum \& lead group abundances } (74 \leq Z \leq 86)}$$

$$R_2 = \frac{\text{Platinum group abundances } (81 \leq Z \leq 86)}{\text{Lead group abundances } (74 \leq Z \leq 80)}$$

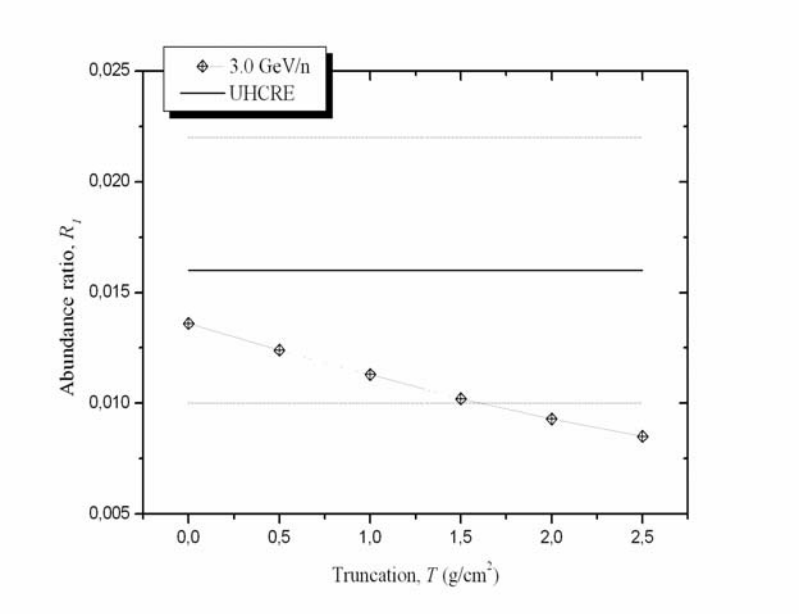

Figure 4.32. Values of R_1 abundance ratio calculated by propagating an isotopic r-process source composition at 3.0 GeV/n for several truncation values. UHCRE value is also plotted (solid line) as well as its error (dashed lines).

$$R_3 = \frac{\text{Abundances of elements with } (70 \leq Z \leq 73)}{\text{Platinum \& lead group abundances } (74 \leq Z \leq 86)}$$

Figures 4.32, 4.33 and 4.34 show, respectively, the values of the abundance ratios R_1, R_2 and R_3 estimated with propagated abundances at an energy of 3.0 GeV/n taking several truncation values. Abundance ratios calculated taking the UHCRE results are also plotted in the corresponding figure, associated errors are also included (dashed lines). Errors on R_1, R_2 and R_3 which are similar to those obtained in former experiments (mainly HEAO-3) [Bin88], have been determined assuming an uncertainty on N_i of 10%.

As an example, the calculated abundance ratios R_1, R_2 and R_3 at 1.0 GeV/n with a PLD truncated at $T = 1.0$ g/cm^2 are respectively, 0.011, 0.385 and 0.111 while at 3.0 GeV/n the corresponding values are 0.0113, 0.388 and 0.109. Therefore, the assumed energy of the propagating particles, being higher that 0.5 GeV/n, insists in not playing a significant role in propagation calculations according to the LBM.

As it can be seen in figure 4.32, the calculation results are consistent with the experimental ones for low values of truncation, $T \lesssim 1.5$ g/cm^2, while figure 4.33 shows that the ratio R_2 values coming from propagation are in agreement with those calculated from UHCRE data for $T \gtrsim 1.0$ g/cm^2. In consequence, the abundance ratios R_1 and R_2 allow to limit the truncation value, so that combining both figures, this parameter concerning to the

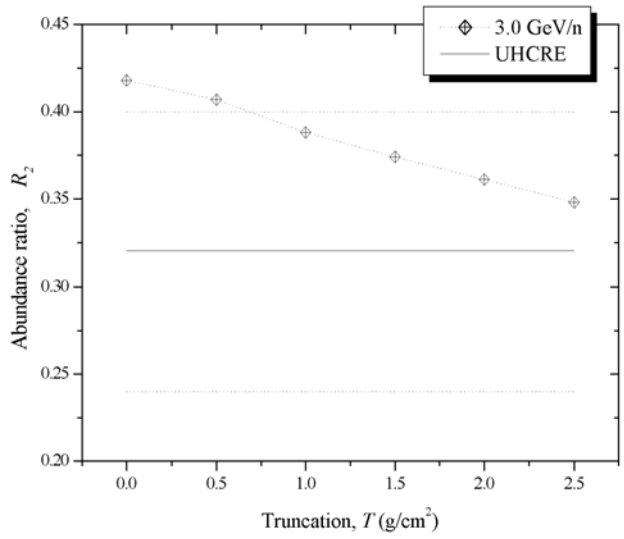

Figure 4.33. Values of R_2 abundance ratio calculated by propagating an isotopic r-process source composition at 3.0 GeV/n for several truncation values. UHCRE value is also plotted (solid line) as well as its error (dashed lines).

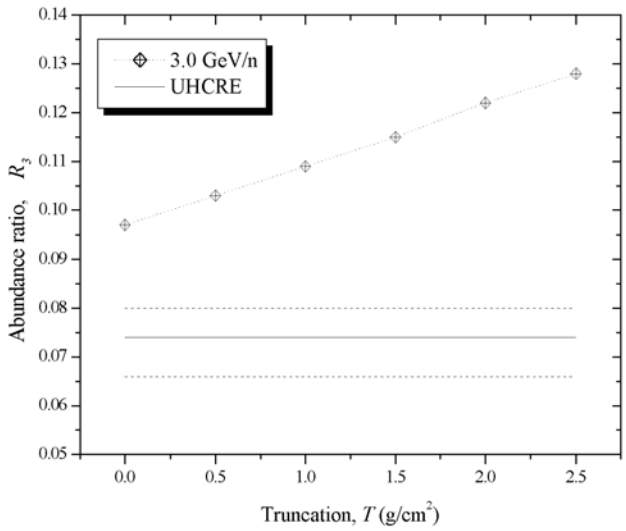

Figure 4.34. Values of R_3 abundance ratio calculated by propagating an isotopic r-process source composition at 3.0 GeV/n for several truncation values. UHCRE value is also plotted (solid line) as well as its error (dashed lines).

integrating PLD function its truncation should be comprised between 1.0 g/cm^2 $\lesssim T \lesssim$ 1.5 g/cm^2.

The values of the abundance ratio R_3 obtained from propagation results integrated at several truncated PLD functions, are not compatible with the experimental value estimated from UHCRE abundances, even if the associated uncertainty is taken into account, as clearly illustrated in figure 4.34. This discrepancy may be explained by considering that detectors utilised in the UHCRE experiment show a small detection efficiency in the lowest charge region, as this region is located very close to the threshold of registration, so that abundances of elements with charge between 70 and 73 are underestimated, leading, thus, a lower value of the abundance ratio R_3 according to its definition. This fact could be taken into account in order to enlarge the associated uncertainty to $R_3(UHCRE)$, allowing, then, a certain agreement with those calculated values of R_3 for low truncation values, confirming, thus, results from figure 4.32.

The abundance ratios do not provide a reliable resource in order to study the effect, and, hence determine a value giving the best fit, of the escape length propagation parameter, because of the three calculated abundance ratios taking $\lambda_{esc} = 8.0$ g/cm^2 are $R_1 = 0.0112$, $R_2 = 0.387$ and $R_3 = 0.110$, which do not differ to those obtained with $\lambda_{esc} = 5.5$ g/cm^2: $R_1 = 0.0113$, $R_2 = 0.388$ and $R_3 = 0.109$.

When propagation is performed by means of NLBM, the corresponding calculated abundance ratios are found to be: $R_1 = 0.0123$, $R_2 = 0.400$ and $R_3 = 0.104$ which are also consistent with UHCRE ratios.

In conclusion, it has not been found any clue that allows to differentiate between LBM with truncated PLD and NLBM as propagation models, as well as to evaluate the effects of varying the energy of the traveling cosmic rays and the escape mean free path, and, therefore, establish limits on their reliable values. On the other hand, one of the main conclusion of this propagation study is that it has been found that spallation cross sections (both total and partial) are the parameters which introduce more distortion to the final propagated abundances because the propagation mechanism is fundamentally governed by the fragmentation process according to the assumed LBM. Therefore, cross sections values calculated with greater accuracy will be required for reliable propagation calculations. It has been found that the configuration that best reproduces the UHCRE measured abundances near the Earth neighbourhood, consists on:

- A source composed by r-process synthesised material without FIP correction.
- Total and partial inelastic cross sections provided by semiempirical fit formulae.
- A truncated path length distribution function corresponding to the leaky box propagation model, with truncation comprised between 1.0 g/cm^2 $\lesssim T \lesssim$ 1.5 g/cm^2.
- All stable isotopes are considered as traveling cosmic ray particles.
- A charge uncertainty between 2.0 and 2.5.

This configuration leads to calculated χ^2 values below the maximum tabulated χ^2 value corresponding to 22 degrees of freedom. Furthermore, the minimum calculated χ^2 values which are comprised between 27.21 and 30.08 are obtained applying a charge uncertainty $\sigma_Z = 2.0$. Taking the tabulated values of χ^2, and by means of a linear interpolation, it has been found that the minimum calculated χ^2 value correspond to $\chi^2_{0.79}$. Therefore, the UHCRE experimental abundances are fitted by propagated results with a significance level of 21%, which means that the adjustment is statistically correct but not excellent.

It has to be emphasised that the R_2 abundance ratio describes the ratio between the two main peaks in the charge region of $Z \gtrsim 65$, i.e. the platinum abundance peak which is mainly synthesised following a rapid neutron capture process, and, on the other hand, the lead abundance peak mainly formed by s-process built up material. Each of such neutron capture processes have occurred in different astrophysical scenarios, so that, fundamentally, R_2 gives an idea of the relative importance of the r and s-processes. According to its definition, if $R_2 > 1$ means that the lead peak is dominant compared to the platinum peak, while if $R_2 < 1$, the opposite situation is described.

If standard SS abundances [And89] having an associated $R_2(SS) = 1.03$, are assumed as source abundances, the resulting abundance ratio calculated after performing the propagation procedure is $R_2(SS, prop) = 0.72$, indicating that the propagation mechanism is able to invert the dominant peak (Pb at source leading Pt at Earth neightbourhood). Nevertheless, this peak inversion is not enough to reproduce what is experimentally recorded near the Earth with UHCRE detectors which lead an $R_2(UHCRE) = 0.32$, in agreement with former experiments as Ariel VI and HEAO-3 [Font00]. In order to obtain a value of R_2 to be consistent with $R_2(UHCRE)$ an enhancement of the platinum peak element abundances is needed. The solution could arise by considering an r-process source type which has an $R_2(r) = 0.60$ instead of SS source. In this case, the propagated abundance ratio is found to be $R_2(r, prop) = 0.38$ which is closer to $R_2(UHCRE)$. Elements belonging to the platinum peak have an intermediate FIP value ($\backsim$ 9.0 eV), and those elements forming the lead peak have low FIP values ($\backsim$ 7.4 eV). The FIP correction (see equation 4.19) is another attempt to enhance those elements having low FIP value by reducing the abundance of those elements with large FIP values. Despite of FIP correction has been included, it has been found that experimental data are better reproduced without this correction as discussed above. For most elements, values of FIP and condensation temperature, T_C, are anticorrelated, so, it is not easy to distinguish which of these two parameters could better reproduce after propagation the measured composition. Condensation temperature which controls the ability of elements to condense into solid compounds, allows to classify elements into volatile (low T_C) and refractory (high T_C). It has been proposed that cosmic ray source composition is best ordered in terms of a general enhancement of the refractory elements relative to volatile ones and among the volatile elements an enhancement of heavier elements relative to lighter ones indicating a mass to charge dependence, together with a condensation temperature dependence, of the acceleration efficiency [Mey97] & [Mey98].

Only refractory elements are locked in grains of ISM which are accelerated by shock waves together with gas ions to an energy of $\backsim$ 100 KeV/n, then these grains sputter refractory ions which are simultaneously accelerated up tu GeV and TeV energies [Ell97], [Ell98] & [Ell99]. So that, according to this model, grains of ISM could supply to cosmic ray stream an extra-abundance of refractory elements and in particular platinum peak elements accounting for the enhancement needed to reproduce the measured ratio between platinum and lead peak abundances. The quantification of this contribution for dust grains becomes extremely complicated because of the number of factors which influences the final abundances. For that reason, this model will not be taken into account in the present work, but will be under consideration for a future work.

It should be stressed that in order to reproduce the charge distribution of the chemical elements recorded in the UHCRE experiment, an enhancement of the platinum peak abundances is required. There has been several attempts to account for this extra contribution, such as the FIP correction or an enhancement in the source composition by taking an r-process source type instead of SS source composition which in principle would seem more realistic, or alternatively, considers the contribution of the sputtered ions from accelerated dust grains. It has been found that FIP corrections does not help to enhance the platinum peak abundance, but better results are obtained if the source of cosmic rays with $Z \gtrsim 65$ is considered to be formed of material built up by means of rapid neutron capture process which are related with explosive scenarios such as type II-Supernovae sites modelled in terms of core collapse supernova models or neutron stars mergers models (see section 1 of chapter 3 for detailed information). In other words, the hand that rocks the cradle of such cosmic rays seems to feel rather excited so that it would be more adequate to say that this hand really shakes this cradle.

Propagation of ultra heavy cosmic rays having charge over 65, has been modelled by means of the leaky box model. Effects of varying all parameters involved in the propagation process has been studied and results of transport calculations have been compared with measured composition in UHCRE, but the following improvements can be studied in a future work in order to obtain propagation results more consistent with experimental results:

(i) Not only spallation cross sections are the main parameter that influences the propagation calculation (as they control the fragmentation processes), but also they are not well determined in the charge region and energies concerning to recorded ions in UHCRE. So that, partial inelastic cross sections with grater accuracy which are provided by updated expressions based on recent measurements [Web03] should be taken into account replacing the expressions used in this work.

(ii) The energy loss process by ionisation and also energy gain due to re-acceleration mechanism during propagation may be considered by re-introducing the energy loss term, $\frac{\partial}{\partial E}(b_i N_i)$, in the leaky box transport equation which can also be numerically solved by means of the WST [Wad98].

(*iii*) Instead of applying the WST to the LBM, this technique also may be used to solve the transport equations for the diffusion model which provide a more realistic description of the propagation mechanism of cosmic rays in the galaxy.

(*iv*) If source composition is ordered by the condensation temperature and mass to charge ratio rather than FIP, the enhancement of refractory elements such as platinum peak elements may be explained by the contribution of sputtered ions from dust grains during their acceleration. Depending on this contribution, the source composition of cosmic rays in the considered charge region have to be modified.

References

[Ach92] A. Achterberg & W.M. Krülls, Astron & Astrophys., **265** (1992) L13.

[And82] E. Anders & M. Ebihara, Geochim. Cosmochim.Acta, **46** (1982) 2363.

[And89] E. Anders & N. Grevesse, Geochim. Cosmochim.Acta, **53** (1989) 197.

[Axf77] W.I. Axford *et al.*, Proc. 15th ICRC (Plovdiv) **11**, (1978) 132.

[Bar95] M.G. Baring *et al.*, Adv. Spa. Res. **15** (1995) 397.

[Bar97] M.G. Baring, astro-ph/9711177

[Bel78] A.R. Bell, Mon. Rot. R. Astron. Soc., **182** (1978) 147.

[Ber90] V.S. Berezinskii *et al.*, Astrophysics of Cosmic Rays. V.L. Ginzburg ed. (North Holland, 1990) pg. 45.

[Ber94] E.G. Berezhko *et al.*, Astropart. Phys., **2** (1994) 215.

[Ber95] E.G. Berezhko *et al.*, Nuclear Phys. **B 39** (1995) 171.

[Ber96] E.G. Berezhko, Astropart. Phys., **5** (1996) 367.

[Ber99] E.G. Berezhko & D.C. Ellison, Astrophys. J., **526** (1999) 385.

[Ber00] E.G. Berezhko & H.J. Völk, Astron. & Astrophys., **357** (2000) 283.

[Bin81] W.R. Binns *et al.*, Astrophys. J., **247** (1981) L115.

[Bin85] W.R: Binns *et al.*, Astrophys. J., **297** (1985) 111.

[Bla78] R.D. Blanford & J.P. Ostriker, Astrophys J. **221** (1978) L29.

[Bin87] W.R. Binns *et al.*, Phys. Rev. C **36** (1987) 1870.

[Bin88] W.R. Binns, Genesis and propagation of cosmic rays. M.M. Shapiro & J.P: Wefel, eds. (D. Reidel publishing Co., 1988) p.71.

[Bin89] W.R. Binns *et al.*, Astrophys. J., **346** (1989) 997.

[Bla80a] R.D. Blanford & J.P. Ostriker, Astrophys J. **237** (1980) 793.

[Bla80b] R.D. Blanford, Astrophys J. **238** (1980) 410.

[Bla87] R.D. Blanford & D. Eichler, Phys. Rep. **154** (1987) 1.

[Bla94] R.D. Blanford, Astrophys J. Suppl. **90** (1994) 515.

[Blo93] J.B.G.M. Bloemen *et al.*, Astron. & Astrophys., **267** (1993) 372.

[Bre83] N.R. Brewster *et al.*, Astrophys. J., **264** (1983) 324.

[Bre85] N.R. Brewster *et al.*, Astrophys. J., **294** (1985) 419.

[Cas78] M. Cassé & P. Goret, Astrophys. J., **221** (1978) 703.

[Cow67] R. Cowsik *et al.*, Phys. Rev. **158** (1967) 1238.

[Cow73] R. Cowsik & L.W. Wilson, Proc. 13th ICRC (Denver) **1** (1973) 500.

[Cow75] R. Cowsik & L.W. Wilson, Proc. 14th ICRC (München) **2** (1975) 659.

[Cli93] R.R. Clinton & C.J. Waddington, Astrophys. J., **403** (1993) 644.

[Cam82] A.G.W. Cameron, Essays in nuclear Astrophysics, C.A. Barnes et al. eds. (Cambridge University press, 1982) p. 23.

[Cum90] J.R. Cummings *et al.*, Phys. Rev. C **42** (1990) 2530.

[Dor90] E. A. Dorfi, Astron. & Astrophys., **234** (1990) 419.

[DuV96a] M.A. Du Vernois *et al.*, Astron. & Astrophys., **316** (1996) 555.

[DuV96b] M.A. Du Vernois *et al.*, Astrophys. J., **466** (1996) 457.

[Dru83] L. O'C. Drury, Rep. Prog. Phys., **46** (1983) 973.

[Dru99] L. O'C. Drury *et al.*, astro-ph/9905008.

[Eich80] D. Eichler, Astrophys. J., **237** (1980) 809.

[Ell90] D.C. Ellison *et al.*, Astrophys J. **352** (1990) 376.

[Ell97] D.C: Ellison *et al.*, Astrophys. J., **487** (1997) 197.

[Ell98] D.C: Ellison *et al.*„ Spa. Sci. Rev., **86** (1998) 203.

[Ell99] D.C: Ellison & J.P. Meyer, astro-ph/9905038.

[Fie00] B.D. Fields *et al.*, astro-ph/0010121.

[Fic68] C.E. Fichtel & D.V. Reames, Phys. Rev., **175** (1968) 1564.

[Font97] J. Font *et al.*, Proc. Adavances in Nuclear Physics and related Areas (Thesalonikii, 1997) p. 718.

[Font98a] J. Font *et al.*, Rayos Cósmicos'98. Proc. 16th. European CR Symp. (Alacalá de Henares, 1998) 303.

[Font98b] J. Font & C. Domingo, Nuclear Astrophysics. Proc. Int. Workshop XXVI on Gross Properties of Nuclei and Nuclear Excitations (Hirschegg, 1998) p. 242.

[Font98c] J. Font & C. Domingo, Acta Physica Polonica B **29** (1998) 357.

[Font99a] J. Font et al., Proc 26th ICRC (Salt Lake, 1999) OG.3.2.49.

[Font00] J. Font, New vistas in Astrophysics, M.M. Shapiro et al. eds. (World Scientific, 2000) p.285.

[Fre80] I. Freedman *et al.*, Astron. & Astrophys., **82** (1980) 110.

[Gar81] M. Garcia-Muñoz *et al.*, Proc. 17th ICRC (Paris) **2** (1981) 72.

[Gar87] M. Garcia-muñoz *et al.*, Astrophys. J. Suppl., **64** (1987) 269.

[Gil85] M. Giler & T. Wibig, Proc. 19th ICRC (La Jolla) **3** (1985) 17.

[Gil87] M. Giler *et al.*, Proc. 20th ICRC (Moscow) **12**, (1987) 214.

[Gil88] M. Giler *et al.*, Astron. & Astrophys., **196** (1988) 44.

[Gil89] M. Giler *et al.*, Astron. & Astrophys., **217** (1989) 311.

[Gin64] V.L. Ginzburg & S.I Sirovatzkii, The Origin of cosmic rays (Pergamon press, 1964)

[Gin76] V.L. Ginzburg & V.S. Ptuskin, Rev. Mod. Phys., **48** (1976) 161.

[Glo69] G. Gloecker & J.R. Jokipii, Phys. Rev. Lett., **22** (1969) 1448.

[Gre98] N. Grevesse & A.J. Sauval, Spa. Sci. Rev., **85** (1998) 161.

[Hei95] U. Heinbach & M. Simon, Astrophys. J., **441** (1995) 209.

[Jok76] J.R. Jokipii, Astrophys. J., **208** (1976) 900.

[Jon79] F.C. Jones, Astrophys. J., **229** (1979) 747.

[Jon01] T.W. Jones, Cosmic Rays in the Universe: 7th Taipei astrophysics workshop. C. M. Ko. ed. (ASP conference series, Vol XX, 2001)

[Jon92] T.W. Jones & H. Kang, Astrophys. J., **396** (1992) 575.

[Jone01] F.C. Jones *et al.*, Astrophys. J., **547** (2001) 264.

[Kan01] H. Kang, Cosmic Rays in the Universe: 7th Taipei astrophysics workshop. C. M. Ko. ed. (ASP conference series, Vol XX, 2001)

[Kan02] H. Kang *et al.*, Astrophys. J. **579** (2002) 337.

[Kan03] H. Kang, Journal of Korean Astronomical Society, **36** (2003) 1.

[Kla85] J. Klarmann *et al.*, Proc. 19th ICRC (La Jolla) **2** (1985) 127.

[Kot80] J. Kota & A.J. Owens, Astrophys. J., **237** (1980) 814.

[Lag83] P.O. Lagage & C.J. Cesarsky, Astron. & Astrophys., **118** (1983) 223.

[Lem03] M. Lemoine & G. Pelletier, Astrophys. J., **589** (2003) L73.

[Let83] J.R. Letaw *et al.*, Astrophys. J. Suppl., **51** (1983) 271.

[Let84] J.R. Letaw *et al.*, Astrophys. J., **279** (1984) 144.

[Let87] J.R. Letaw *et al.*, Proc. 20th ICRC (Moscow) **2**, (1987) 222.

[Let93] J.R. Letaw *et al.*, Astrophys. J., **414** (1993) 601.

[Let95] J.R. Letaw *et al.*, Adv. Space Res. **15** (1995) 65.

[Mal98a] M.A. Malkov, Phys. Rev. E., **58** (1998) 4911

[Mal98b] M.A. Malkov & H.J. Völk, Adv. Space Res., **21** (1998) 551.

[Mal99] M.A. Malkov, Astrophys. J., **511** (1999) L53.

[Mar85] S.H. Margolis & J.B. Blake, Astrophys. J., **299** (1985) 334.

[Mar86] S.H. Margolis, Astrophys. J., **300** (1986) 20.

[Mau01] D. Maurin *et al.*, Astrophys. J., **555** (2001) 585.

[Mau02a] D. Maurin *et al.*, Astron. & Astrophys., **394** (2002) 1039.

[Mau02b] D. Maurin *et al.*, Astro-ph/0212111.

[Mau02c] D. Maurin *et al.*, astro-ph/0202334.

[Mel02] A. Meli & J.J. Quenby, astro-ph/0212329.

[Mey97] J. Meyer *et al.*, Astrophys. J., **487** (1997) 182.

[Mey98] J. Meyer *et al.*, Spa. Sci. Rev., **86** (1998) 179.

[Mor83] H. Moraal & W.I. Axford, Astron & Astrophys, **125** (1983) 204.

[Orm78] J.F. Ormes & P. Freier, Astrophys. J., **222** (1978) 471.

[Osb87] J.L. Osborne & V.S. Ptuskin, Proc. 20th ICRC (Moscow) **12**, (1987) 218.

[Ost96] M. Ostrowsky & G. Siemieniec-Ozieblo, astro-ph/9610247

[Ost02] M. Ostrwski & J. Bednarz, Astron. & Astrophys., **394** (2002) 1141.

[Owe77] A.J. Owens & J.R. Jokipii, Astrophys. J., **215** (1977) 677.

[Pet77] B. Peters & N.J. Westergaard, Astrophys. Spa. Sci., **48** (1977) 21.

[Pro81] R.J. Protheroe *et al.*, Astrophys. J., **247** (1981) 362.

[Ptu90] V.S. Ptuskin & A. Soutoul, Astron. & Astrophys., **237** (1990) 445.

[Ptu96] V.S. Ptuskin *et al.*, Astrophys. J., **465** (1996) 972.

[Ptu97] V.S. Ptuskin *et al.*, Adv. Space Res., **19** (1997) 787.

[Ptu03] V:S. Ptuskin *et al.*, astro-ph/0301420.

[Que88] K.B. Quest, J. Geophys. Res. **93** (1988) 9649.

[Ras75] I.L. Rasmussen & B. Peters, Nature, **258** (1975) 412.

[Sch72] D.N. Schramm, Astrophys. J., **177** (1972) 325.

[Sha92] M.M. Shapiro *et al.*, Ann. New York Academy of Sciences. Frontiers in cosmic physics: Symposium in memory of Serge Alexander Korff (1992) p. 138.

[Shi93] L. Shiver *et al.*, Phys. Rev. C **47** (1993) 1225.

[Sil73] R. Silberberg & C.H. Tsao, Astrophys. J. Suppl., **25** (1973) 316; Astrophys. J. Suppl., **25** (1973) 335.

[Sil83] R. Silberberg *et al.*, Phys. Rev. Lett., **51** (1983) 1217.

[Sil89] R. Silberberg *et al.*, Cosmic gamma rays, neutrinos and related astrophysics. Eds. M.M. Shapiro & J:P: Wefel (D. Reidel publishing company, 1989) p. 491.

[Sil90] R. Silberberg & C.H. Tsao, Phys. Rep., **191** (1990) 351.

[Sil98] R. Silberberg *et al.*, Astrophys. J., **501** (1998) 911.

[Sim77] M. Simon, Astron. & Astrophys., **61** (1977) 833.

[Sim86] M. Simon *et al.*, Astrophys. J., **300** (1986) 32.

[Sim02] M. Simon, Frascati Physics Series Vol. XXIV (2002) p. 119.

[Sla02] P. Slane, astro-ph/0205481

[Ste81] S.A. Stephens, Proc. 17th ICRC (Paris) **9** (1981) 199.

[Ste98] S.A. Stephens & R.E. Streitmatter, Astrophys. J., **505** (1998) 266.

[Str83] R.E. Streitmatter *et al.*, Proc. 18th ICRC (Bangalore) **2** (1983) 183.

[Str85] R.E. Streitmatter *et al.*, Astron. & Astrophys., **143** (1985) 249.

[Str97] A.W. Strong *et al.*, Proc. 25th ICRC (Durban) **4**, (1997) 257.

[Str98] A.W. Strong & I.V. Moskalenko, Astrophys. J., **509** (1998) 212.

[Str01] A.W. Strong & I.V. Moskalenko, Adv. Space Res., **27** (2001) 717.

[Tai03] R. Taillet & D. Maurin, Astron. & Astrophys., **402** (2003) 971.

[Vie03] M. Vietri, Astrophys. J., **591** (2003) 954.

[Vin03] J. Vink, astro-ph/0304176.

[Wad85] C.J. Waddington *et al.*, Proc. 19th ICRC (La Jolla) **3** (1985) 1.

[Wad91] C.J. Waddington *et al.*, 22nd ICRC (Dublin) **2** (1991) 288.

[Wad96] C.J. Waddington, Astrophys. J., **470** (1996) 1218.

[Wad97] C.J. Waddington, Adv. Space Res. **19** (1997) 759.

[Wad98] C.J. Waddington, New Astronomy Reviews **42** (1998) 277.

[Wan87] A. Wandel *et al.*, Astrophys. J., **316** (1987) 676.

[Web85] G.M. Webb *et al.*, Astrophys J. **298** (1985) 684.

[Web90a] W.R. Webber *et al.*, Phys. Rev. C **41** (1990) 520.

[Web90b] W.R: Webber *et al.*, Phys. Rev. C **41** (1990) 533; Phys. Rev. C **41** (1990) 547; Phys. Rev. C **41** (1990) 566.

[Web92] W.R. Webber *et al.*, Astrophys. J., **390** (1992) 96.

[Web98a] W.R. Webber *et al.*, Astrophys. J., **508** (1998) 940.

[Web98b] W.R. Webber *et al.*, Astrophys. J., **508** (1998) 949.

[Web03] W.R. Webber *et al.*, Astrophys. J. Suppl.Series, **144** (2003) 153.

[Well96] H.P. Wellish & D. Axen, Phys. Rev. C **54** (1996) 1329.

[Wib92] T. Wibig, Astrophys. J., **390** (1992) 105.

[Wie80] M.E. Wiedenbeck & D.E. Greiner, Astrophys. J., **239** (1980) L139.

5. Conclusions and perspectives

PHYSICS IS LIKE SEX
Sure, it may give some practical results,
but that's not why we do it

RICHARD FEYNMAN

The main conclusions inferred from the present work are given in a condensed format as follows:

- The Reduced Etch Rate Fractional Gradient identification method is fully applicable only for incident non-stopping ions having an energy over 50 MeV/n at any point of their path inside the detector.
- The parameters of the identification method have to be determined by means of an appropriate calibration at the same energy than the ions recorded in the UHCRE. Alternatively a peak calibration can be performed if an accelerator calibration is not available.
- The parameters of the identification method are found to be energy dependent and maybe charge dependent.
- The abundances of ultra heavy ions recorded in the UHCRE reproduce the two abundance peaks in this charge region: the Platinum group peak and the Lead group peak, respectively located at $Z = 78$ and $Z = 82$. A third peak corresponding to the actinide region can also be observed. This result is in agreement with all former works.
- The charge uncertainty introduced intrinsically by the application of the RERFG identification method leads to a value of $\sigma_Z \simeq 0.1$ e, whereas the charge resolution for the UHCRE detectors is estimated to be $\simeq 1.5 - 2.0$ e.

- The close collisions may contribute to the latent track formation of the incident ions into a solid state nuclear track detector.

- A strong correlation between the original REL model identification parameters and the close collision contribution parameter has been found.

- When a higher contribution of close collisions to track formation is considered, the model responds by decreasing the fraction of the total energy deposited by the penetrating ion responsible of the latent track formation.

- The inclusion of the modified REL model to the charge assignation procedure gives a limiting value for the close collision contribution parameter, $\kappa \lesssim 0.4$, when the UHCRE measurements are taken.

- The estimation of the close collision contribution parameter using experimental data from accelerator at an energy ~ 1 GeV/n leads to a value of $\kappa \sim 0.3$.

- A simple method of resolution of the Leaky Box propagation equations is a rather good approach to obtain a rough estimation of the source composition of ultra heavy cosmic rays.

- The main source of uncertainty in propagation calculations comes from the cross sections expressions for the fragmentation of cosmic ray ions colliding with interstellar atoms.

- An improvement of transport calculation results, when experimental abundances are taken, could be provided by performing the propagation for all isotopes of the considered charge range instead of only considering the elements.

- Source composition derived from UHCRE abundances using our simple method of resolution of the Leaky Box propagation equations shows a prominent abundance peak centered at $Z = 78$ and a secondary peak at $Z = 82$. This result is in agreement with former works from other authors.

- The relevance of the Pt-Pb abundance peaks is inverted in the Solar System abundances with respect to the calculated source composition, evidencing an enhancement of the r-process nucleosynthesis in the cosmic ray sources.

- Nucleosynthesis of ultra heavy cosmic rays with charge over 65 seems to take place in explosive environenments in which extreme conditions of temperature and neutron flux are achieved.

- Numerical solutions from the Runge-Kutta method for solving the Leaky Box transport equations using the Weighted Slab Technique differ from the analytical exact solutions by less than 0.08%.

- The propagation mechanism based on the Leaky Box model is able to invert the dominant peak (Pb at the source converting to Pt at the Earth neighbourhood). Nevertheless an enhancement of r-synthesised material is still needed to better reproduce the UHCRE abundances.
- Escape length and energy of the traveling particles are parameters that produce a negligible impact on the propagation calculation results.
- Propagated abundances and UHCRE measured ones are in agreement with a significance level of 21% when the propagation calculation is performed taking all stable isotopes, and the following combination of the propagation parameters:
  - A source composed by r-process synthesised material without First Ionisation Potential correction.
  - Total and partial inelastic cross section for fragmentation given by semiempirical fit formulae.
  - A truncated path length distribution function with a truncation value comprised between 1.0 g/cm^2 and 1.5 g/cm^2.
- The minimum values of the χ^2 parameter between propagated and measured UHCRE abundances are achieved when a charge uncertainty of $\sigma_Z = 2 - 2.5$ e is introduced to the calculated abundances. The result confirms the predicted charge uncertainty for this experiment.

Some of the results obtained in this work have raised some new questions which can be understood as perspectives for further work.

- In order to confirm the elimination of the energy dependence of the identification parameters a new modification of the Restricted Energy Loss model should be studied which consists on the inclusion of as many parameters as close collision terms considered to contribute to the formation of the latent track.
- Alternatively, a simpler latent track formation model can be tested using UHCRE measurements. According to this new model, all correction terms appearing in the corrected Bethe-Bloch formula are assumed to contribute to the fraction of the total energy deposited by the penetrating ion responsible to the track formation.
- Not only spallation cross sections are the main parameter that influences the propagation calculation results (as they control the fragmentation processes), but they are also not well determined in the charge region and energies concerning to the ions recorded in UHCRE. So that, partial inelastic cross sections with grater accuracy which are provided by updated expressions based on recent measurements should be taken into account replacing the expressions used in this work.

- The energy loss process by ionisation and also energy gain due to re-acceleration mechanism during propagation may be considered by re-introducing the energy loss term, $\frac{\partial}{\partial E}(b_i N_i)$, in the leaky box transport equation which can also be numerically solved by means of the WST.

- Instead of applying the WST to the LBM, this technique also may be used to solve the transport equations for the diffusion model which provide a more realistic description of the propagation mechanism of cosmic rays in the galaxy.

- If source composition is ordered by the condensation temperature and mass to charge ratio rather than FIP, the enhancement of refractory elements such as platinum peak elements may be explained by the contribution of sputtered ions from dust grains during their acceleration. Depending on this contribution, the source composition of cosmic rays in the considered charge region have to be modified.